MuCap Run8 Analysis Report

Steven M. Clayton

6th October 2006

Contents

1	Introduction	4
	1.1 Run Selection	4
	1.2 Notes	
Ι	Raw Data Analysis	6
2	Raw Analysis Software Modules	7
	2.1 Common Modules	7
	2.2 Illinois Modules	8
3	Electron Detector Analysis	ç
	3.1 Electron Detector Configuration	Ć
	3.2 Electron Proportional Chambers (ePC's)	Ć
	3.2.1 Hit Clustering	Ć
		1(
		11
		11
		15
		16
		16
	<u> </u>	29
	3.7 Electron Detector Efficiencies	29
4		31
	0	31
	/	31
		31
		31
	• /	34
	1	34
	4.7 Entrance Detector Efficiencies	44
5		48
	1	48
	5.2 Noisy Wires Suppression	50

6	Software Tree Structure	,
II	Tree Analysis Studies	
7	"Extra EL Pixels" in the TPC	
8	$\mu + p$ Scatters	
9	"Cosmics" Contribution to Background	(
10	Muon Lifetime Studies 10.1 Lifetime vs. eDetector Treatment 10.2 Lifetime vs. Muon-Electron Vertex Cut 10.3 Lifetime vs. TPC Fiducial Volume 10.4 Lifetime vs. eSC Segment ("Gondola") 10.5 Lifetime vs. MuPC Pileup Protection 10.6 Lifetime vs. MuSC Artificial Deadtime 10.7 Lifetime vs. ePC Artificial Deadtime 10.8 Fit Start Time Scans 10.9 Fit Stop Time Scans 10.10Lifetime vs. Run Group 10.11Lifetime vs. Rebinning Phase 10.12Lifetime vs. Rebinning Factor 10.13Fit Function Modified to Include Wall Stops	
11	Impurity Captures	
12	μp and μd Diffusion 12.1 Sensitivity of \tilde{c}^{-1} to Impact Parameter Distribution	
II	I Simulations	
13	Numerical Studies 13.1 χ^2 vs. Lifetime Histogram Binning Phase	
ΙV	Conclusions	
14	Results	1
15	Further Work	1

\mathbf{V}	Appendix	106
\mathbf{A}	UIUC Event Display	107
В	Description of ROOT Macros	108

Introduction

This report covers the analysis of μ Cap μ^- data from the fall, 2004 data run (Run8). The statistics of this data set are somewhat less than 2×10^9 , or 20% of the MuCap statistics goal. Considering systematic corrections and associated errors, we expect a result for the μ^- lifetime in 10 bar hydrogen gas of ≈ 30 ppm precision. Taking the difference with the world average μ^+ lifetime — or the anticipated μ Lan result — will give us the muon capture rate to 3% or better, determining g_P to around 20%.

The analysis is divided into two major stages. In the first, the raw data are processed into the higher-level physics objects: muon stops in the TPC and electron tracks. The physics objects are written into ROOT trees to be read in by the second analysis stage, which fills various histograms, in particular lifetime spectra, according to different cuts on the muons and electrons. These tree studies take much less CPU time than the raw data stage, usually less than 24 hours for all of the clean μ^- data, and therefore more passes over the complete Run8 statistics are possible.

The raw data analysis is the subject of part 1 of this report; A few sections are at the moment only placeholders, and other sections will benefit from more explanation in later revisions. Higher level analyses, including lifetime fits and systematics studies, are covered in part 2. Part 3 is devoted to simulations, or numerical studies, and is at the moment incomplete; regard this part as a placeholder to be filled in later. In part 4, which is titled "Conclusions," a preliminary recommendation for the lifetime result is given along with a few systematics corrections.

1.1 Run Selection

Run selection was done according to the "runs8" table in the Run8 MySQL database. Since most of the production data were taken with the TPC at 5.0 kV, and we have observed gain dependent effects (for example the topics of chapters 7 and 8), production data at other TPC voltages are not included in this analysis. The calibration runs, however, were taken at the end of Run8 and with the somewhat lower TPC voltage of 4.8 kV. Gain dependent effects are probably not important at the much lower statistics of these calibration data sets.

The MySQL commands to select the run groups are shown below. Also, file names of the generated run lists are indicated, and these files can be found in this document's source directories. • Production data (Prod50). RunLists/runlist_prod50_muminus.txt

```
use mucap;
SELECT run FROM runs8
WHERE condition='mu-'
AND LOCATE("Prod-50",production)>0
AND LOCATE("CHUPS",target)>0
AND shift_ok=1
AND tpc_voltage=5017;
```

• Natural hydrogen (NatH2).¹ RunLists/runlist_naturalH2_muminus.txt

```
SELECT run FROM runs8
WHERE condition='mu-'
AND LOCATE("CalibNat",production)>0
AND shift_ok=1;
```

• Deuterium-doped protium (CalibD2). RunLists/runlist_calibD2_muminus.txt

```
SELECT run FROM runs8
WHERE condition='mu-'
AND LOCATE("CalibD2",production)>0
AND shift_ok=1;
```

• Nitrogen-doped protium (CalibN2). RunLists/runlist_calibN2_muminus.txt

```
SELECT run FROM runs8
WHERE condition='mu-'
AND LOCATE("CalibN2",production)>0
AND shift_ok=1;
```

1.2 Notes

• Histogram time axes are generally in nanoseconds assuming a clock frequency of exactly 50 MHz. Likewise, rates derived from fits to lifetime spectra differ from the stated units, usually s⁻¹, by a factor $f_{actual}/50 \sim 10^{-3}$, where f_{actual} is the unblinded clock frequency in MHz.

¹Francoise's suggestion for naming the natural hydrogen data CalibNat was unfortunately not adhered to in the Illinois analysis, where I instead write NatH2 (perhaps a misnomer).

Part I Raw Data Analysis

Raw Analysis Software Modules

2.1 Common Modules

The Illinois raw data analysis procedures are called within the MIDAS analyzer framework developed at Berkeley for MuCap.¹ The first few of the MuCap Berkeley Analysis Software (MBAS) modules, those dealing with low-level data decompression, quality checks and sorting, are also used in the Illinois software. Also shared are the MBAS muon scintillator modules, MMuSCAnalysisMQL and MMuSCAnalysisC. A list of the MBAS common modules is below. More detailed information about these modules may be found in the MBAS user manual.

- MUnCompressRawData. Uncompresses raw data.
- MUnDuplicator. Deals with a particular DAQ disease in which an event block was occasionally written to file twice.
- MCaenCompProcessRaw. Sorts CAEN and Compressor data into a single, time-ordered "HITS" bank.
- MRolloverCheckMQL. Checks that the 2.5 kHz rollover clock is present in all CAENS.
- MRolloverCheckC. Actually does the block cut if the preceding module found a rollover clock discrepancy.
- MTDC400ProcessRaw. Sorts TDC400 raw data into a single, time-ordered array of C-structures.
- MMuSCAnalysisMQL. Combines multiple channels of muSC information into two banks: the intersection of different channels for muSC seed hits, and the union of all information to use for pileup protection of the seed hits. Also, this module vetoes muSC seed hits based on the muon scintillator hole counter (muSCA) signal, and the muSCA is included in the union bank used for pileup-protection.
- MMuSCAnalysisC. Cuts block if there are too many mismatches between the two copies of the muSC signal.

¹The user manual, "MuCap Berkeley Analysis Software User Manual," by Tom Banks and Fred Gray, which describes analyzer framework relevant for the Illinois analysis, can be downloaded from Tom's analysis page, http://weak0.physics.berkeley.edu/weakint/research/muons/private/tbanks_analysis.html.

Many of the data analysis passes, for both Berkeley and Illinois, were over a reduced ("skimmed") raw data set, in which only raw data $\pm 30~\mu s$ around pileup-protected (with itself) muSC hits were retained. The subsequent analysis of this data set then only required the MBAS modules MUnCompressRawData, MMuSCAnalysisMQL, and MMuSCAnalysisC, since the basic data quality checks and sorting were already done in the skimming pass. The CPU time saved is substantial due to the large reduction in input file size.

2.2 Illinois Modules

The MuCap Illinois Analysis Software (MIAS) has its own framework separate from the MBAS. Earlier MIAS versions were not part of a MIDAS analyzer; however, to take advantage of the Berkeley low-level data quality checks, the MIAS is linked into the MBAS structure via the module uiuc_analysis. A partial list of functional components within MIAS follows.

- SparkAnalysis. Rough "sparks" identification.
- Electron Analysis. Electron detector analysis.
- MuonAnalysis. Muon entrance detectors and TPC analysis.
- Lifetime Analysis. Lifetime with TPC not required, and lifetime using electron detector combinations that are not written to the output Tree.
- HotWiresAnalysis. Finds and kills excessively noisy ePC wires for the duration of the present data file.
- EventTreeAnalysis. Creates and fills the output tree with muon and electron objects for subsequent higher-level analysis.
- Display. Graphical event display.
- EfficienciesAnalysis. Special study of ePC1, ePC2, and eSC efficiencies.

Electron Detector Analysis

3.1 Electron Detector Configuration

detector geometry: diagram, some specifications, etc.

3.2 Electron Proportional Chambers (ePC's)

3.2.1 Hit Clustering

Since a particle traversing a multiwire proportional chamber (MWPC) plane can cause multiple wires to fire, the "singles hits" must be grouped together into one object, a "cluster," characterized by time, location in the plane, and size. The basic clustering algorithm is the following:

- 1. Effectively project singles hits in the plane onto the time axis and find time-coincident hits.
- 2. For time-coincident hits, sort by wire number.
- 3. Define clusters as groups of singles hits continuous in wire number, possibly allowing a small gap. The cluster time is taken to be the time of the first hit of each cluster; cluster location is the average of the wires in the cluster; and cluster size is the number of singles hits.

Details of the clustering algorithm are set by in the file Parameters.cpp. Each MWPC plane has a variable of type CLU_PARAM defined; the members of this structure are listed here along with their effects on the clustering behavior.

- TimeWindow. The clustering time width, its specific meaning depends on the value of the next setting.
- DiffClustering. If non-zero (TRUE), the time difference between successive singles hits in step 1 of the clustering algorithm are compared to the clustering time width. If zero (FALSE), the time with respect to the earliest singles hit in the potential cluster is used instead.

- DeadTime. As the singles are encountered in chronological order, individual wires are "killed" for this number of ns. That is, if a subsequent hit occurs on the same wire within this time, it is ignored.
- UpdatingDeadtime. If non-zero (TRUE), hits that fall within the deadtime of a previous hit on the same wire extend the deadtime. This is similar to how an updating discriminator extends the output pulse if an additional input signal falls within the output pulse width.
- AllowedGap. In step 3 of the clustering algorithm above, this is the maximum allowed wire number gap to be part of the same cluster. (1 means adjacent wires, 2 means one wire missing, etc.)

Clustering parameters are listed in table 3.1 for ePC1 and table 3.3 for ePC2; relavent clustering-related histograms are referenced in these tables.

3.2.2 Anode-Cathode Coincidences

For each anode cluster, an attempt is made to find coincident cathode clusters, and the result is stored in a C-structure:

An array of these structures will be referred to as "ePC hits" (as opposed to "ePC singles hits," "ePC anode cluster hits," etc.). The procedure to fill the ePC hit structure starts with an anode cluster, which gives the values for T and Phi, and then goes on to fill in the cathodes-based data as follows:

- 1. Search for inner and outer cathode clusters each time-coincident with the anode cluster, and the z-position from the anode×inner coincidence ($Z_{anode\times inner}$) near that of the anode×outer coincidence ($Z_{anode\times outer}$). This is referred to as an ePC "triple cluster" or "triple coincidence" in the analysis code and this document. The z-position is taken to be the average of $Z_{anode\times inner}$ and $Z_{anode\times outer}$.
- 2. If no triple coincidence is found, search for an inner cathode cluster time-coincident with the anode cluster and with $Z_{anode \times inner}$ within the active length of the detector.
- 3. If no anode×inner cathode cluster is found, search for an outer cathode cluster time-coincident with the anode cluster, and $Z_{anode \times outer}$ within the active length of the detector.

Anode×cathode coincidence cuts are listed in table 3.2 for ePC1 and table 3.4 for ePC2; some of these parameters are illustrated in figures 3.5, 3.6, 3.13, and 3.14. Figures 3.7 and 3.15 show the (ϕ, z) distibution of hits in the two ePC's, and figures 3.8 and 3.16 show autocorrelations.

3.2.3 ePC1

• Geometry Alignment: Describe procedure, show supporting hists.

CLU_PARAM	ePC1	ePC1 Inner	ePC1 Outer
Member	Anodes	Cathodes	Cathodes
TimeWindow	300:fig. 3.1(a)-left	300:fig. 3.1(b)-left	300:fig. 3.1(c)-left
DiffClustering	1	1	1
DeadTime	900:fig. 3.1(a)-middle	1000:fig. $3.1(b)-$ middle	1000: fig. 3.1(c) - middle
UpdatingDeadtime	1	1	1
AllowedGap	2:fig. 3.2-left	3:fig. 3.2-middle	3:fig. 3.2-right

Table 3.1: ePC1 Clustering Parameter Values. Histogram references are indicated by :fig.[figure label]-position in figure].

EPC_PARAM Member	Value
AnodeInner.tDiff_low	-200:fig. 3.5-left
AnodeInner.tDiff_high	170:fig. 3.5-left
AnodeOuter.tDiff_low	-200:fig. 3.5-right
AnodeOuter.tDiff_high	170:fig. 3.5-right
TripleClu.zDiff_low	-20:fig. 3.6
TripleClu.zDiff_high	20:fig. 3.6

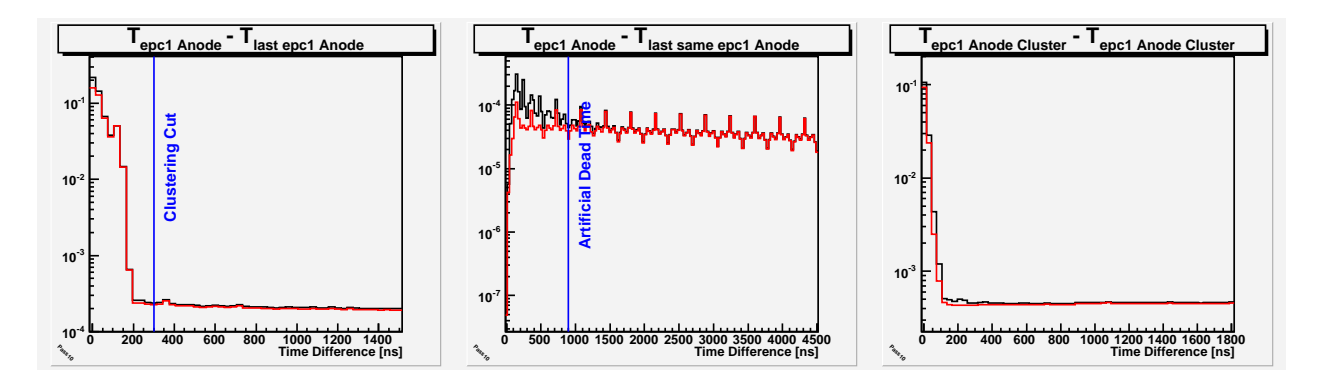
Table 3.2: ePC1 Triple Cluster Coincidence Parameter Values. Histogram references are indicated by :fig.[figure label]-[position in figure].

3.2.4 ePC2

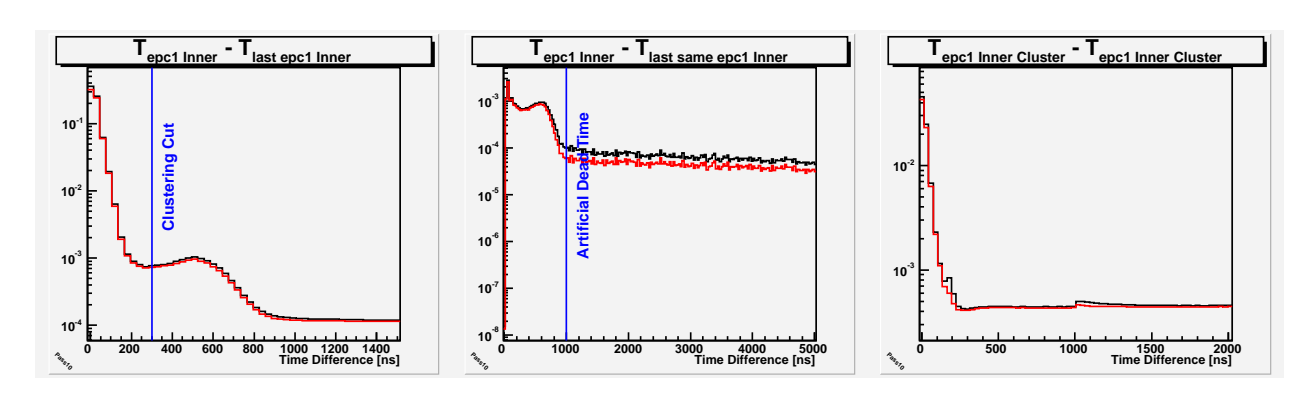
• Geometry Alignment: Describe procedure, show supporting hists.

CLU_PARAM	ePC2	ePC2 Inner	ePC2 Outer
Member	Anodes	Cathodes	Cathodes
TimeWindow	300:fig. 3.9(a)-left	300:fig. 3.9(b)-left	300:fig. 3.9(c)-left
DiffClustering	1	1	1
DeadTime	1000:fig. 3.9(a)-middle	1000: fig. 3.9(b) - middle	900:fig. $3.9(c)$ -middle
UpdatingDeadtime	1	1	1
AllowedGap	2:fig. 3.10-left	3:fig. $3.10-$ middle	3:fig. 3.10-right

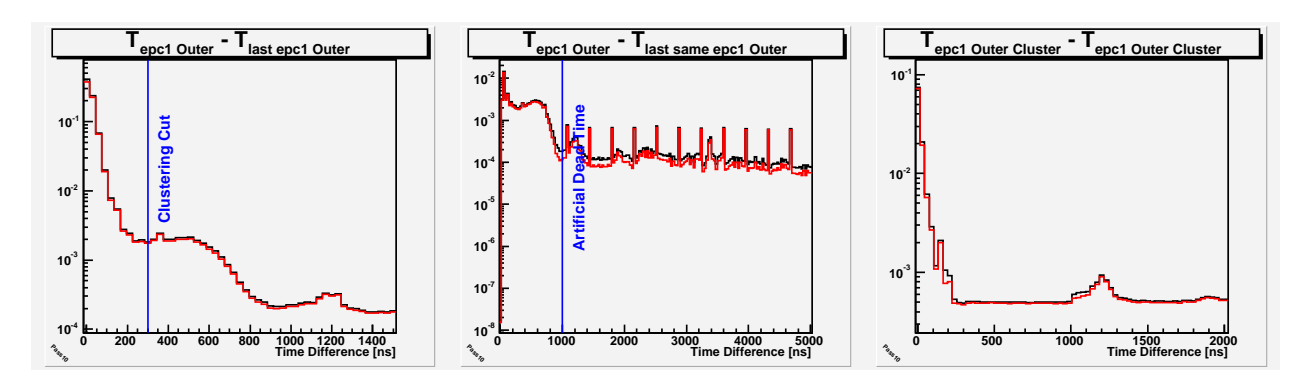
Table 3.3: ePC2 Clustering Parameter Values. Histogram references are indicated by :fig.[figure label]-[position in figure].



(a) ePC1 Anodes.



(b) ePC1 Inner Cathodes.



(c) ePC1 Outer Cathodes.

Figure 3.1: ePC1 Clustering Histograms. Left: time difference between successive singles hits in the same plane. Middle: time difference between successive singles hits on the same wire. Right: Autocorrelation of clusters. In each panel, the red line is after spark cuts and hot wires suppression.

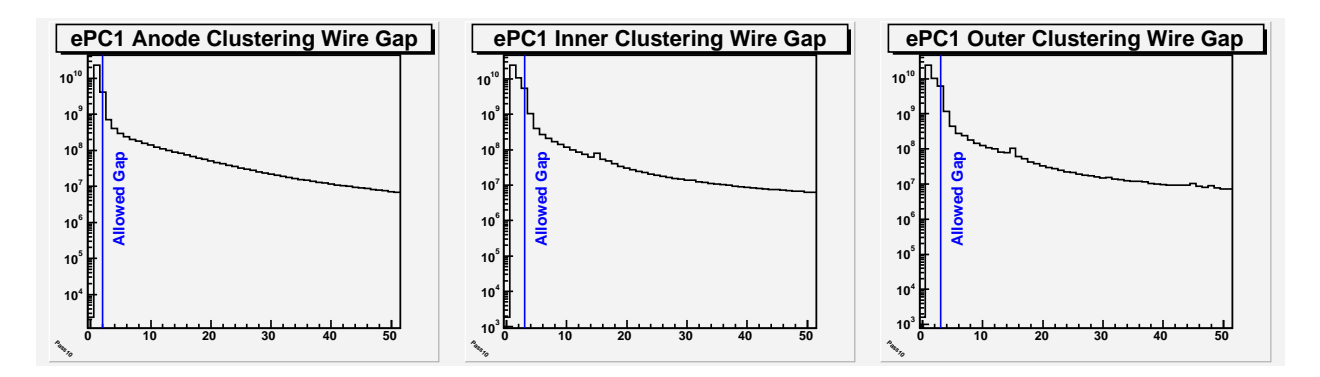


Figure 3.2: ePC1 Wire Gap Histograms. For time-coincident singles hits, the hits are sorted into wire number order, and the wire number differences between neighbors in the sorted list are histogrammed. Left: anode plane; middle: inner cathode plane; right: outer cathode plane.

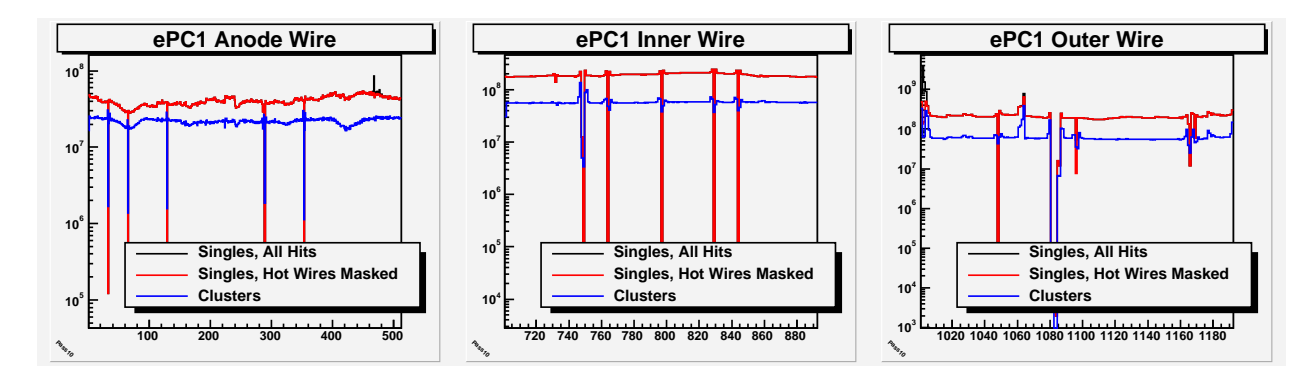


Figure 3.3: ePC1 Hits Spatial Distribution (parameter number). Singles, singles with hot wires removed (see section 5.2), and clusters distributions are shown. Left: anode plane; middle: inner cathode plane; right: outer cathode plane.

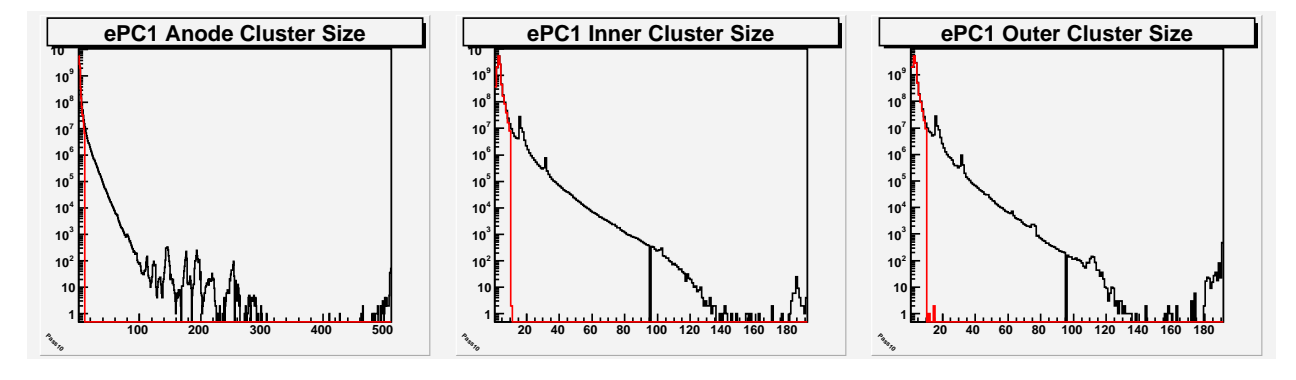


Figure 3.4: ePC1 Cluster Size Distribution (number of wires). The red curve is the distribution after "spark cuts" (see section 5.1). Left: anode plane; middle: inner cathode plane; right: outer cathode plane.

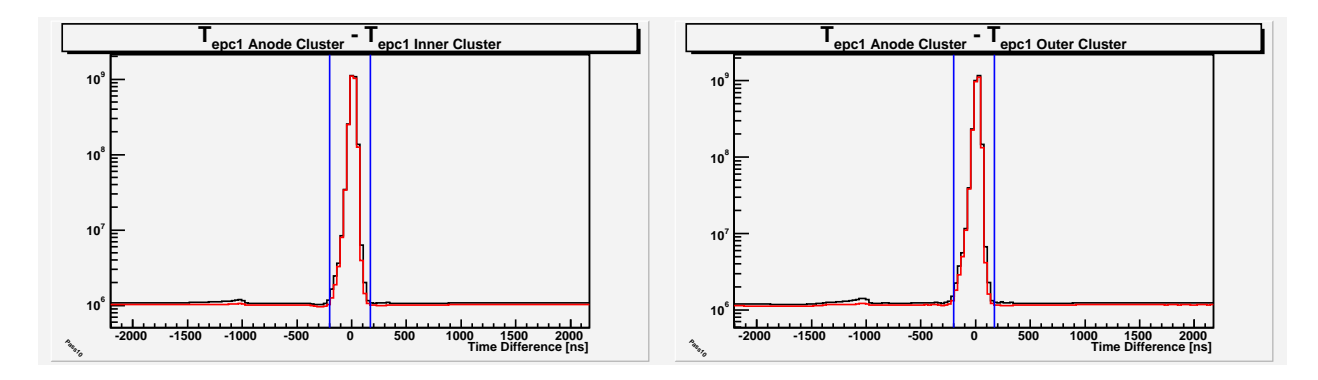


Figure 3.5: ePC1 Anode×Cathode Cluster Time Difference. Coincidence cuts are indicated by the vertical blue lines. The red curve is the distribution after "spark cuts" (see section 5.1). Left: anode×inner cathode; right: anode×outer cathode.

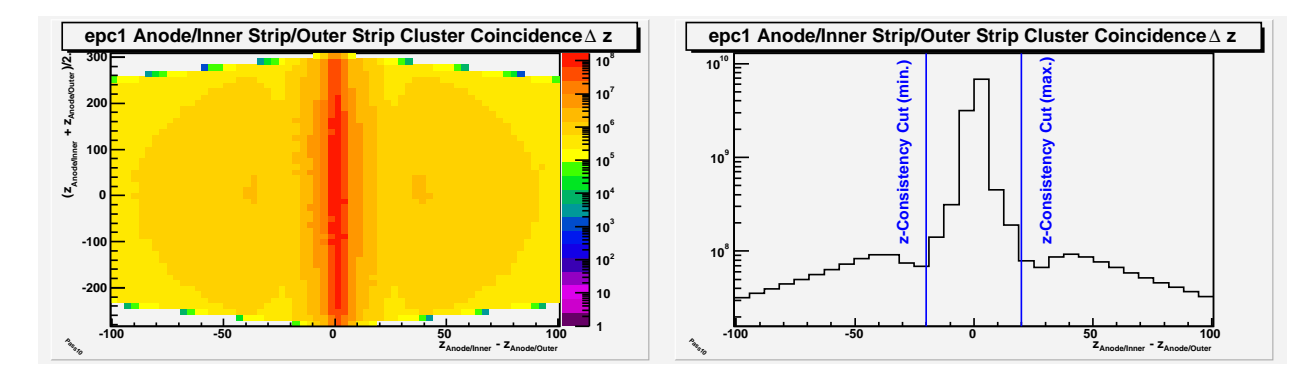


Figure 3.6: ePC1 $Z_{anode \times inner} - Z_{anode \times outer}$ of anode × inner clusters time-coincident with anode × outer clusters.

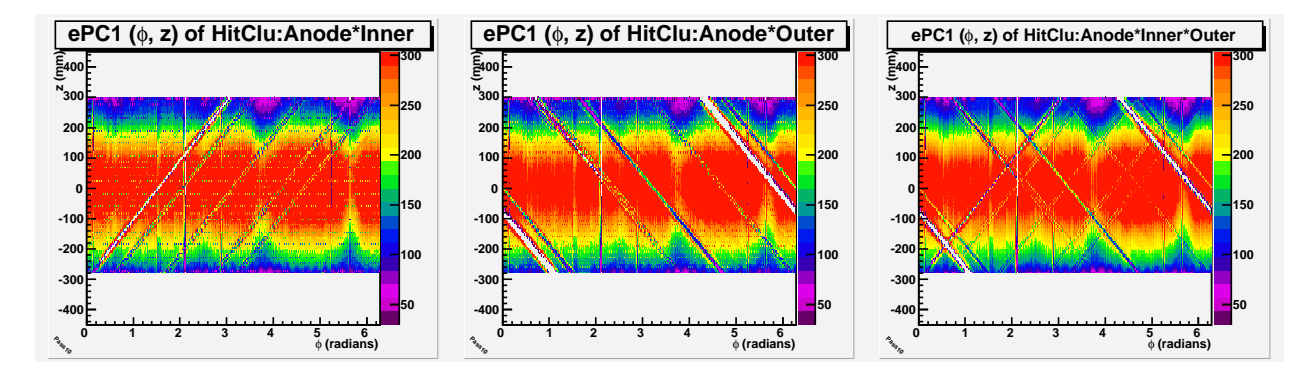


Figure 3.7: ePC1 Anode×Cathode Cluster (ϕ, z) Distribution. Left: anode×inner cathode; middle : anode×outer cathode; right: anode×inner cathode cathode.

EPC_PARAM Member	Value
AnodeInner.tDiff_low	-200:fig. 3.13-left
AnodeInner.tDiff_high	170:fig. 3.13-left
AnodeOuter.tDiff_low	-200:fig. 3.13-right
AnodeOuter.tDiff_high	170:fig. 3.13-right
TripleClu.zDiff_low	-13:fig. 3.14
TripleClu.zDiff_high	20:fig. 3.14

Table 3.4: ePC2 Triple Cluster Coincidence Parameter Values. Histogram references are indicated by :fig.[figure label]-[position in figure].

3.3 Electron Scintillator Hodoscope (eSC)

eSC clustering of singles (PMT) hits into "4-fold clusters" is performed separately on each segment. The algorithm is the following:

- 1. Loop over singles hits (in chronological order as usual). As each single is encountered, apply a fixed deadtime to that PMT channel of the amount specified in the parameters file (first row of table 3.5).
- 2. Adjust each singles hit time, by an amount specified in the parameters file, to account for slight variation in the timing with respect to the other PMT channels (from slightly different cable lengths, for example). In practice, the times are adjusted by up to ≈ 2 ns.
- 3. Find clusters of singles hits within the maximum time specified by the "tDiff" parameters in table 3.5, plus a few ns to account for the small relative timing offsets between the PMT channels. These clusters can be considered 4-fold candidates. The left panel of Figure 3.20 is a histogram of the number of singles hits per 4-fold candidate.
- 4. Check the candidates for good 4-fold hits. Each must contain exactly one hit from each of the four PMT's and have relative PMT timings within the cuts specified by the "tDiff" parameters (and shown by the vertical blue lines in figure 3.19). The time is taken to be the average of the four PMT times. The z-position is the time difference between the average of the upstream PMT times, minus the average of the downstream PMT times, and multiplied by a velocity factor (67 mm/ns, from a study placing a source along the length of one of the gondolas). Figure 3.21 shows per-eSC-segment autocorrelations of good 4-fold cluster times, and the right panel of figure 3.20 is the sum of these. Figure 3.22 shows the (ϕ, z) -distribution of good 4-fold clusters.

GOND_PARAM Member	Value
DeadTime	65:fig. 3.17
tDiff_IU_OU	15:fig. 3.19
tDiff_ID_OD	15:fig. 3.19
tDiff_IU_ID	25:fig. 3.19
tDiff_OU_OD	25:fig. 3.19
tDiff_IU_OD	25:fig. 3.19
tDiff_ID_OU	25:fig. 3.19

Table 3.5: eSC 4-Fold Clustering Parameter Values. Histogram references are indicated by :fig.[figure label]-[position in figure].

3.4 Electron Track Candidates: ePC1×ePC2

Coincident ePC1 and ePC2 hits are considered "electron track candidates," subject to later approval by the eSC. Different versions of the track candidates are considered separately:

- Anodes Only. Cathode information in the EpcHitClu_t is ignored.
- Either Cathode. At least one cathode is required to be coincident with the anode.
- Both Cathodes. Both inner and outer cathodes must be coincident with the anode.

All ePC1, ePC2 pairs that satisfy the cuts, listed in table 3.6 and shown in figure 3.23, constitute the electron track candidates for a given cathodes requirement (none, either, or both). The C-structure for each candidate is:

```
struct Epc1Epc2_t {
 double T1;
 float Phi1;
 float Z1;
 int iepc1; // index of epc1 fHitClu
 double T2;
 float Phi2;
 float Z2;
 int iepc2; // index of epc2 fHitClu
/**** calculated and used in TEpcTracks *****/
 float PhiGond; // phi of track extrapolated to gond radius
              // z of track extrapolated to gond radius
 char used;
               // to keep track of which epc1,epc2 pairs are already used
/***************/
 char multiple_choice; // 1 if same epc EpcHitClu_t is used
                       // in another epc1,epc2 pair
};
```

ΔT Min. [ns]	ΔT Max. [ns]	$\Delta \phi$ Min.	$\Delta \phi$ Max.	ΔZ Min. [mm]	ΔZ Max. [mm]
-125	180	-0.643	0.643	-750	750

Table 3.6: ePC1×ePC2 Coincidence Cuts.

3.5 Electron Detector Tracks: $ePC1 \times ePC2 \times eSC$

The electron track-finding procedure associates eSC 4-fold hits (section 3.3) with electron track "candidates" (ePC1×ePC2, section 3.4) to form complete electron detector track objects, which will be used directly in muon decay time spectra. Each eSC 4-fold hit and ePC1×ePC2 candidate is used at most once, though recall that, in ePC1×ePC2, a hit in one of the ePC's can be used more than once if there is more than one hit in the other ePC.

An important design decision of the UIUC analysis was to keep the electrons and muons logically separate until the last step of formation into lifetime spectra. This has immediate consequences in how the electron tracks are formed in the case of ambiguities, that is, when there is a choice in any of the detectors of which hit to associate with the others. One option is to retain all possible combinations until a later stage of the analysis, when the electron tracks are associated with muons, and then do some kind of "redundancy reduction" to avoid overcounting; that is the approach of the Berkeley analysis. Another option is to make a choice earlier on, even if it's wrong, of which e-Detector track candidates to use. As long as the choice is not somehow lifetime dependent or exaggerates deadtime effects, it should only amount to perhaps a difference in time-independent efficiency. The UIUC analysis indeed takes the latter option: eSC 4-fold hits are each paired with one and only one ePC1×ePC2 candidate.

If there is only one ePC1×ePC2 candidate that is T-, ϕ - and z-coincident with the eSC 4-fold hit, then the track is unambiguous and is considered a good e-Detector track; table 3.7 lists the coincidence parameters.

ETRACK_PARAM		
Member	Value	Description of Constraint
tDiff1_low	-15 ns	$T_{eSC} - T_{ePC1} \geq exttt{tDiff1_low}$
tDiff1_high	166 ns	$T_{eSC} - T_{ePC1} \leq exttt{tDiff1_high}$
tDiff2_low	-46 ns	$T_{eSC} - T_{ePC2} \geq exttt{tDiff2_low}$
tDiff2_high	131 ns	$T_{eSC} - T_{ePC2} \leq exttt{tDiff2_high}$
zDiff_low	-300 mm	$Z_{eSC} - Z_{ePC1 imes ePC2@eSC} \geq exttt{zDiff_low}$
zDiff_high	300 mm	$Z_{eSC} - Z_{ePC1 imes ePC2@eSC} \leq exttt{zDiff_high}$
phiDiff_low	-0.300 radians	$\phi_{eSC} - \phi_{ePC1 imes ePC2@eSC} \geq exttt{phiDiff_low}$
phiDiff_high	0.300 radians	$\phi_{eSC} - \phi_{ePC1 imes ePC2@eSC} \leq exttt{phiDiff_high}$

Table 3.7: eSC×ePC1×ePC2 Coincidence Cuts. The ϕ - and Z-cuts act on the ϕ and Z location of the ePC1×ePC2 track extrapolated to the radius of the eSC.

The situation is more interesting if there are more than one ePC1×ePC2 candidate for a given eSC 4-fold hit. The code tries to "optimize" the matching of eSC 4-fold hits to ePC1×ePC2 candidates based on some loose criteria explained below. First, lists of all eSC 4-fold hits and ePC1×ePC2 candidates linked by time and space coincidences are populated. Then all ways of associating the eSC 4-fold hits with the ePC1×ePC2 candidates are tried, and the "best" combination is chosen. The algorithm is roughly the following:

- 1. The index of the eSC 4-fold hit being considered is entered as the first and only item in an eSC 4-fold indices list.
- 2. A list of indices of all ePC1×ePC2 candidates that are (T, ϕ, Z) -acceptable for the eSC 4-fold hit is populated.
- 3. A list of indices of additional eSC 4-fold hits that are (T, ϕ, Z) -acceptable, for at least one member of the ePC1×ePC2 indices list, is added to the eSC 4-fold indices list.
- 4. Steps 2 and 3 are repeated until no more hits are added.
- 5. If there are too many ways of associating the two lists, go to the next step. Otherwise, try each way, calculating a fitness function for each way. Basically, the fitness function

favors a higher number of successful pairings of the eSC with the ePC's. The fitness of a way of pairing them is initially zero (best), and points are added for each pair:

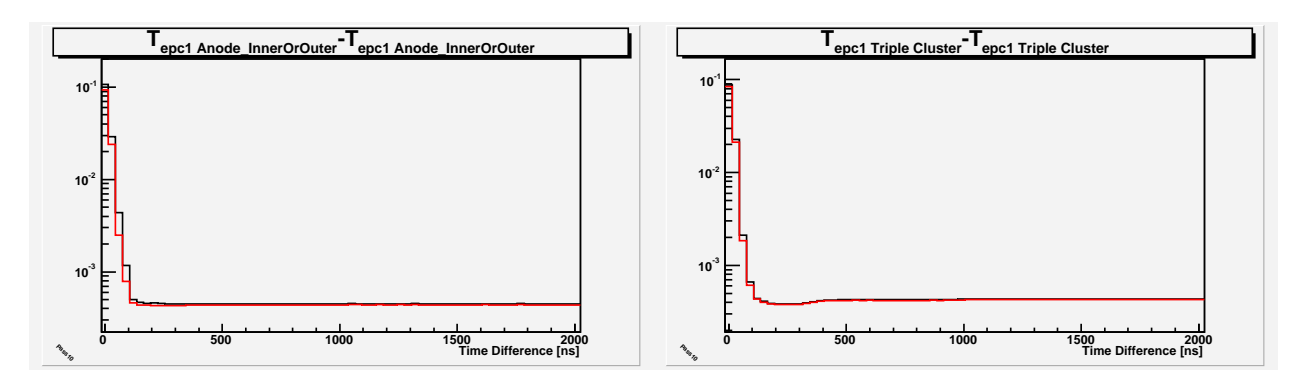
- Check for time-coincidence. If the eSC 4-fold hit and ePC1×ePC2 are not time-coincident, give a 10-point penalty.
- Check for ϕ -coincidence. If not ϕ -coincident then add 10 points to the overall fitness; if it is ϕ -coincident but the ePC1×ePC2 does not point directly at the eSC segment, then add to the fitness an amount ≤ 1 , increasing the further away from the eSC segment the candidate track points.
- Check for z-coincidence. If not z-coincident then add 10 points; otherwise, add an amount ≤ 1 , increasing the further away from Z_{eSC} the track candidate points.

Once all ways of pairing are evaluated, choose the one with the lowest penalty and make complete e-Detector track objects from the valid $((T, \phi, Z)$ -coincident) pairs. Fin.

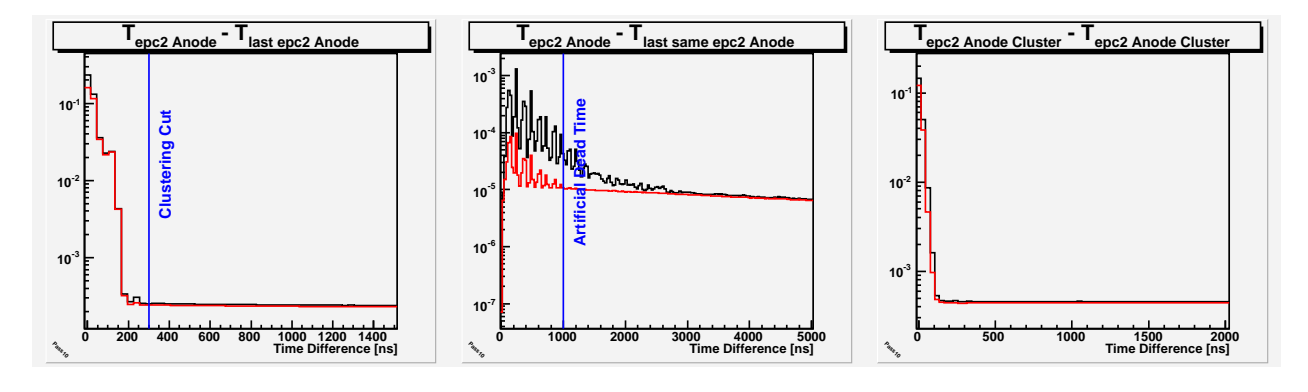
6. In the very rare case there are so many ways of associating the two lists that computation time would be prohibitive, then, rather than throwing out all or just picking the first one, the ϕ -coincidence cut is made more restrictive: the ePC1×ePC2 candidate must point directly at the eSC segment. The more restrictive cut applies only to this group. Then the whole procedure of associating eSC with the ePC track candidates is repeated. If there are still too many combinations, only then is the group thrown out; It is likely these are some kind of spark of weird shower event anyway, not something we want.

The good e-Detector tracks are stored in an array of objects of type TElectron. Data members of this class are:

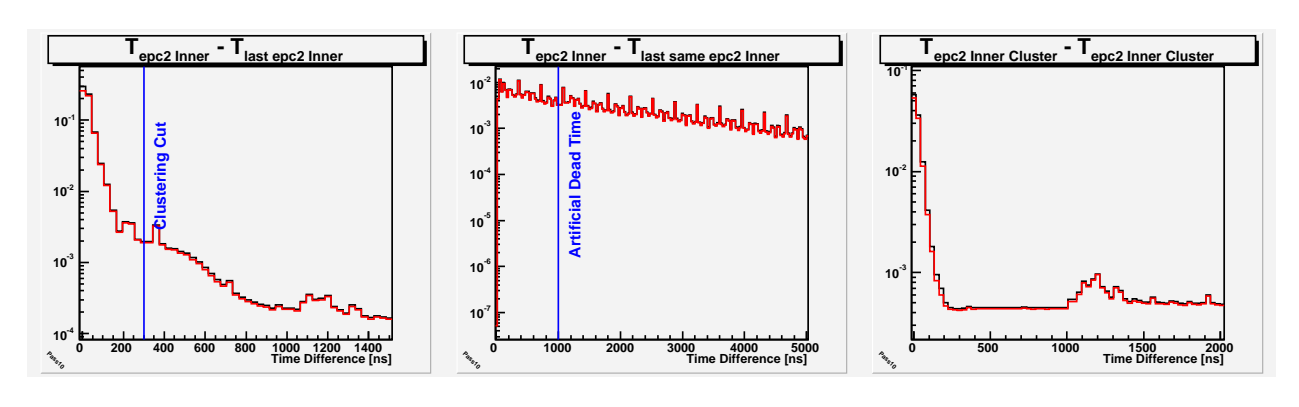
```
Double_t
           fT:
              // Gondola time [ns] of electron
                    // Phi-coordinate of track at ePC1
Float_t
                  // Z-coordinate [mm] of track at ePC1
           fZ1;
Float_t
                    // Phi-coordinate of track at ePC2
Float_t
           fPhi2;
Float_t
           fZ2;
                  // Z-coordinate [mm] of track at ePC2
           fGondID;
                    // Gondola ID of track [1-16]
UChar_t
           fGondZ; // Z-coordinate [mm] from Gondola U/D time diff.
Short_t
UShort_t
           fCluSize1; // anodes cluster size of ePC1 hit [0-512]
UShort_t
           fCluSize2; // anodes cluster size of ePC2 hit [0-1024]
UChar t fFlags; //bit1: multiple ways to combine eSC with ePC1*ePC2
                //bit2: ePC1 or ePC2 used more than once in ePC1*ePC2
```



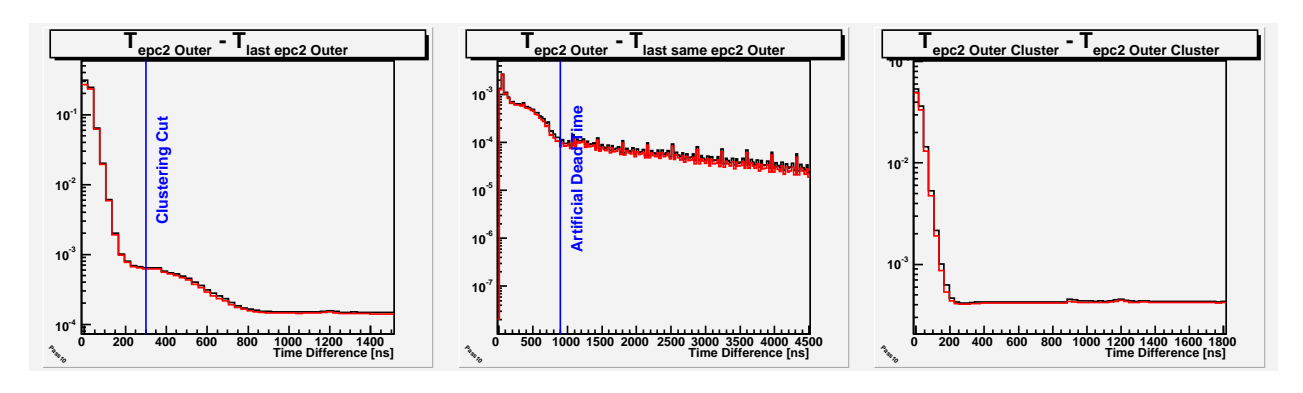
 $\label{eq:control_control_control} Figure~3.8:~ePC1~Anode\times Cathode~Cluster~Autocorrelation.~Left:~anode\times either~cathode;~right:~anode\times inner~cathode\times outer~cathode~("triple~coincidence").$



(a) ePC2 Anodes.



(b) ePC2 Inner Cathodes.



(c) ePC2 Outer Cathodes.

Figure 3.9: ePC2 Clustering Histograms. Left: time difference between successive singles hits in the same plane. Middle: time difference between successive singles hits on the same wire. Right: Autocorrelation of clusters. In each panel, the red line is after spark cuts and hot wires suppression.

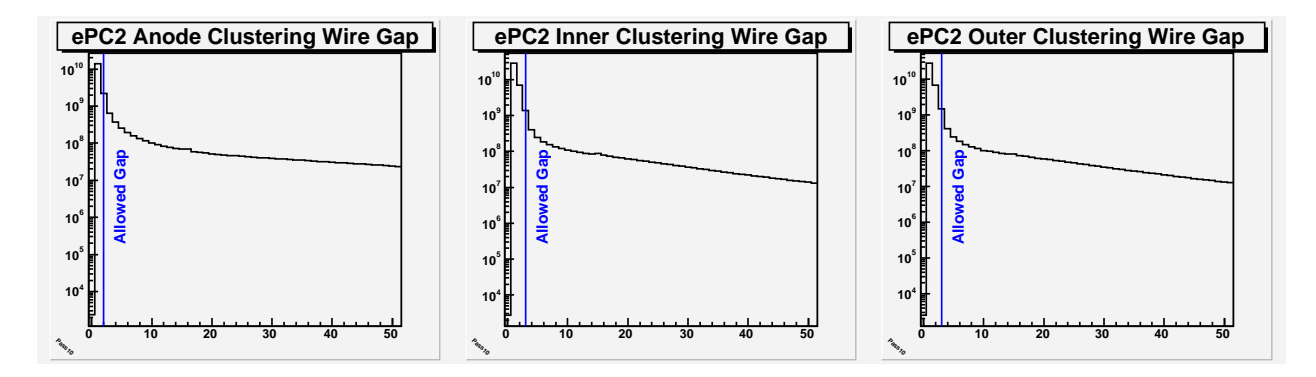


Figure 3.10: ePC2 Wire Gap Histograms. For time-coincident singles hits, the hits are sorted into wire number order, and the wire number differences between neighbors in the sorted list are histogrammed. Left: anode plane; middle: inner cathode plane; right: outer cathode plane.

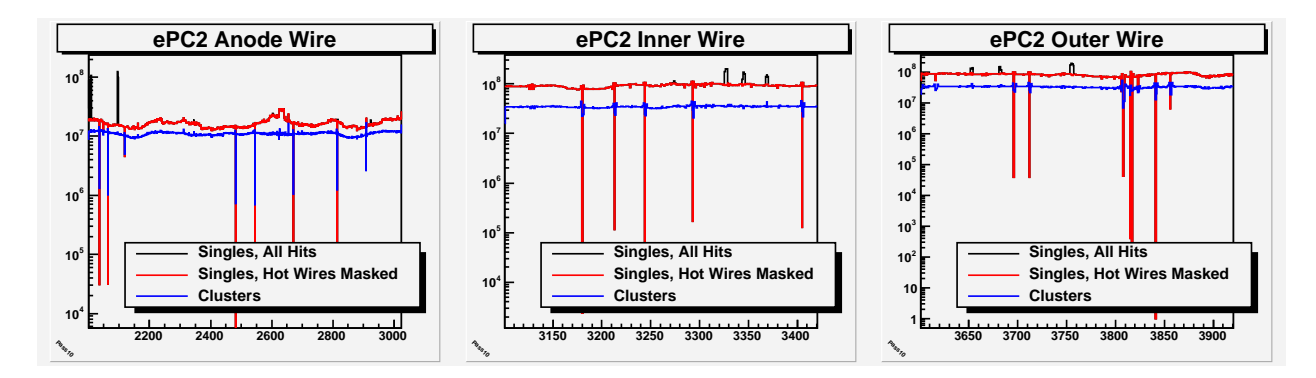


Figure 3.11: ePC2 Hits Spatial Distribution (parameter number). Singles, singles with hot wires removed (see section 5.2), and clusters distributions are shown. Left: anode plane; middle: inner cathode plane; right: outer cathode plane.

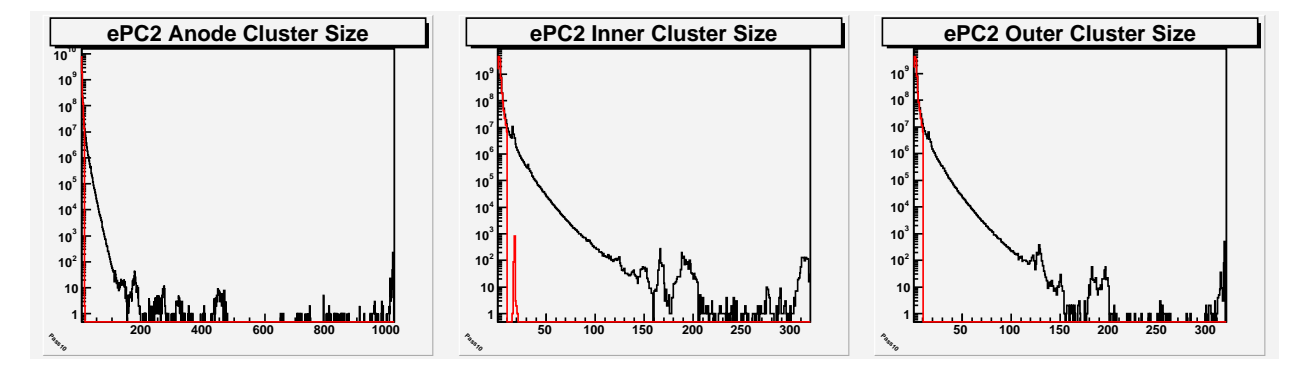


Figure 3.12: ePC2 Cluster Size Distribution (number of wires). The red curve is the distribution after "spark cuts" (see section 5.1). Left: anode plane; middle: inner cathode plane; right: outer cathode plane.

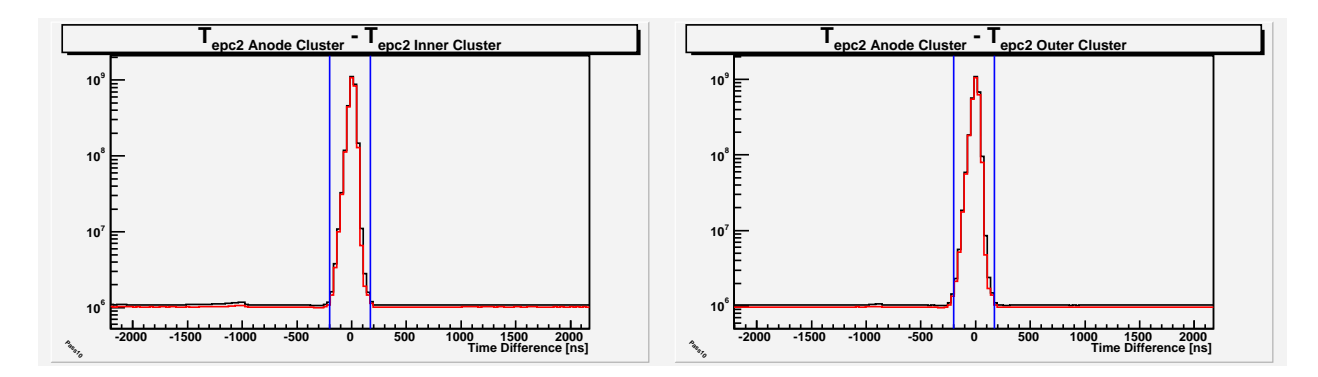


Figure 3.13: ePC2 Anode×Cathode Cluster Time Difference. Coincidence cuts are indicated by the vertical blue lines. The red curve is the distribution after "spark cuts" (see section 5.1). Left: anode×inner cathode; right: anode×outer cathode.

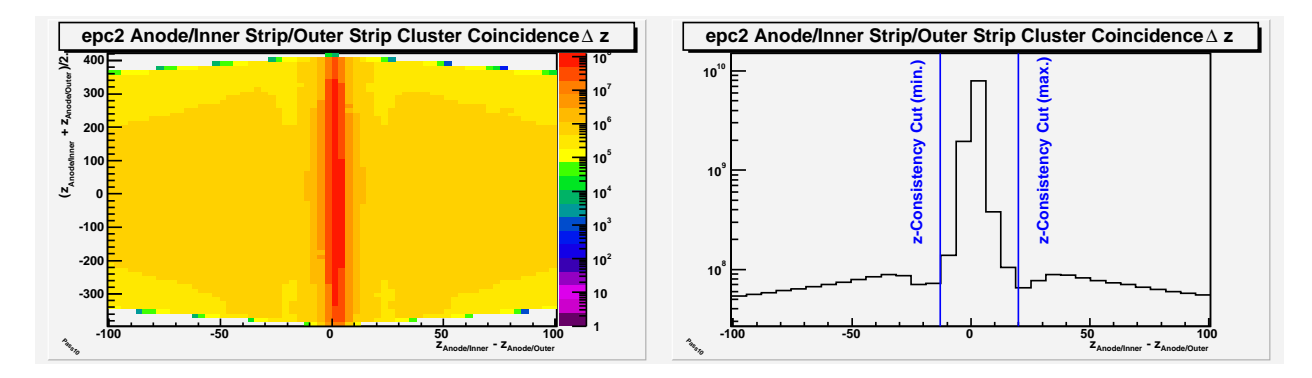


Figure 3.14: ePC2 $Z_{anode \times inner} - Z_{anode \times outer}$ of anode × inner clusters time-coincident with anode × outer clusters.

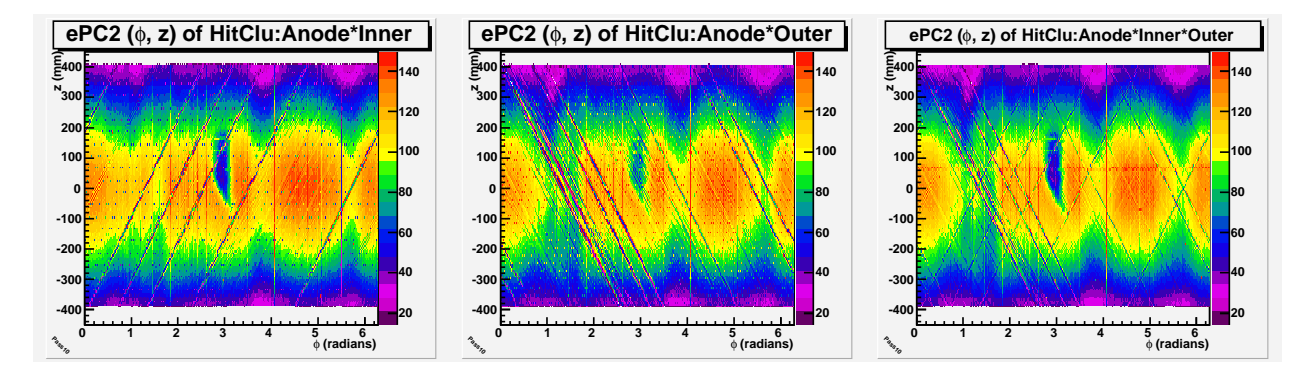


Figure 3.15: ePC2 Anode×Cathode Cluster (ϕ, z) Distribution. Left: anode×inner cathode; middle : anode×outer cathode; right: anode×inner cathode cathode.

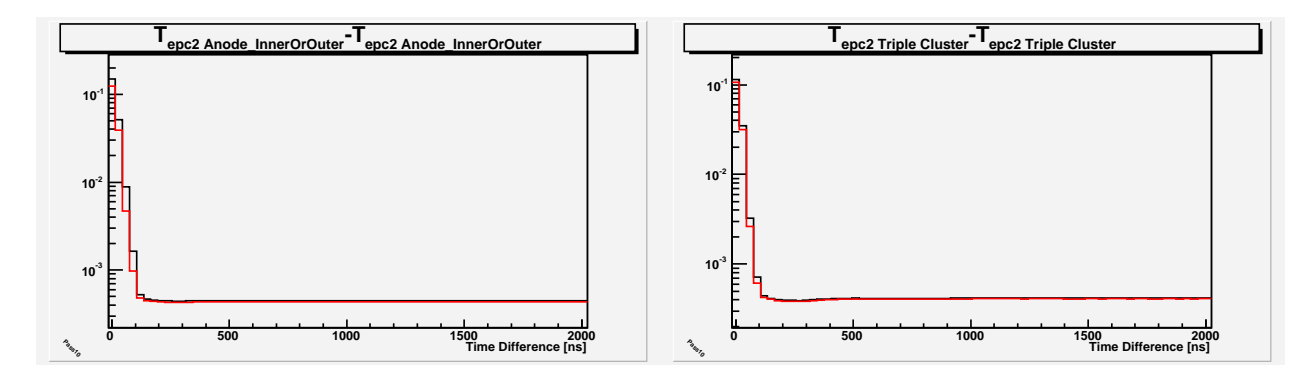


Figure 3.16: ePC2 Anode×Cathode Cluster Autocorrelation. Left: anode×either cathode; right: anode×inner cathode vouter cathode ("triple coincidence").

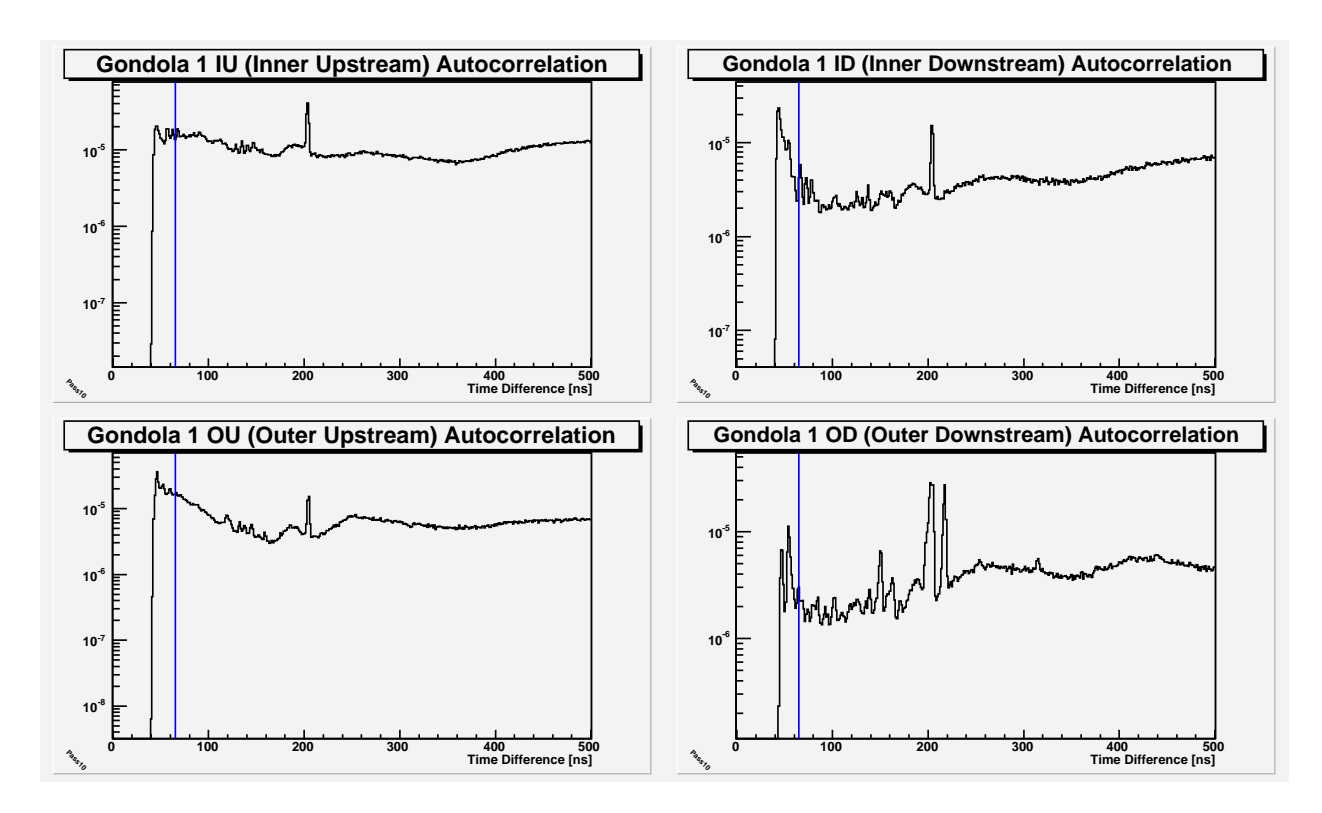


Figure 3.17: eSC Segment 1 ("Gondola 1") Autocorrelation of Individual Photomultiplier Channels. The other eSC segments exhibit similar behavior. The artificial deadtime imposed in the analysis is indicated by the vertical blue lines.

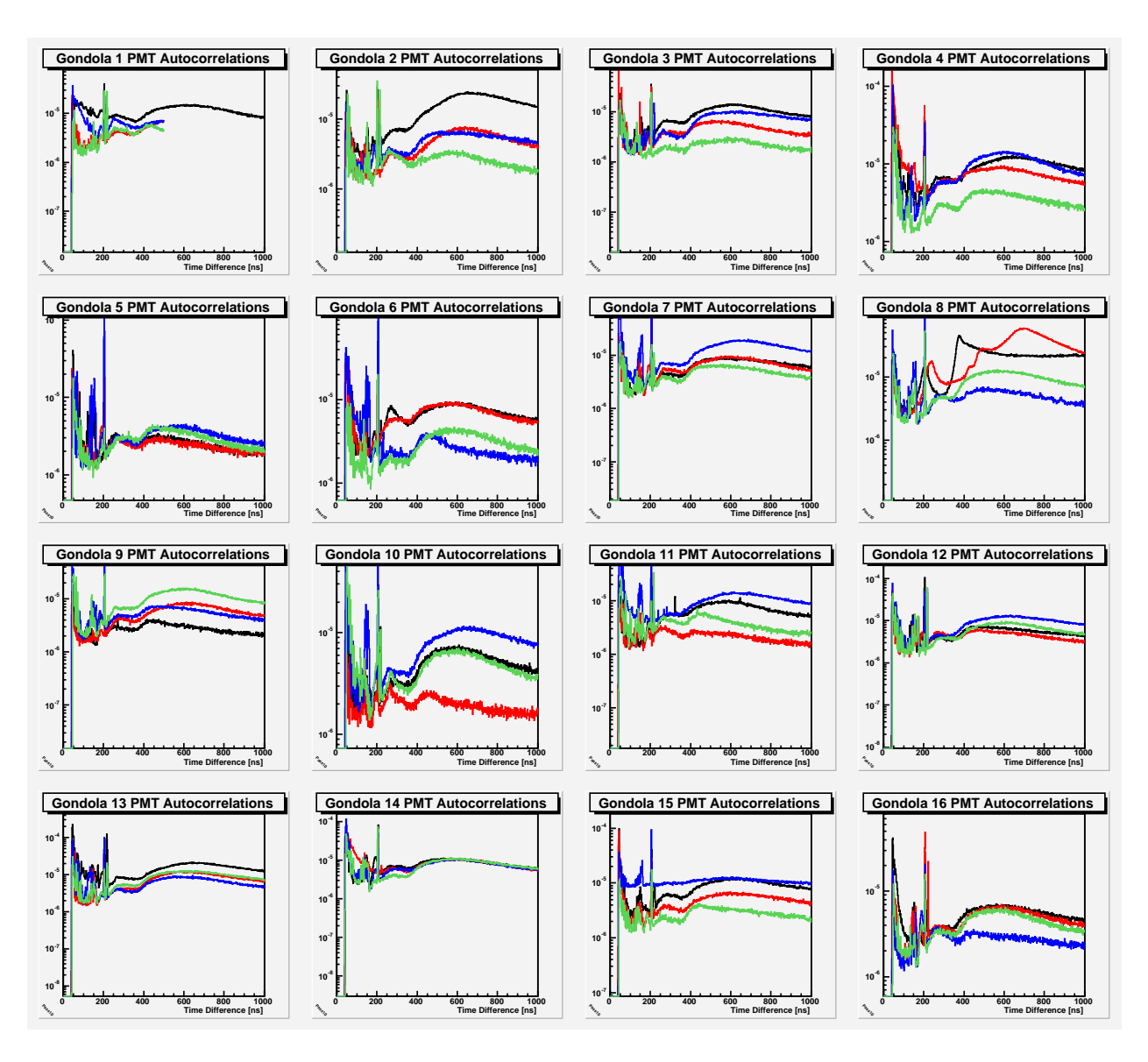


Figure 3.18: Autocorrelation of Individual Photomultiplier Channels. Black: Inner Upstream (IU); Red: Inner Downstream (ID); Blue: Outer Upstream (OU); Green: Outer Downstream (OD).

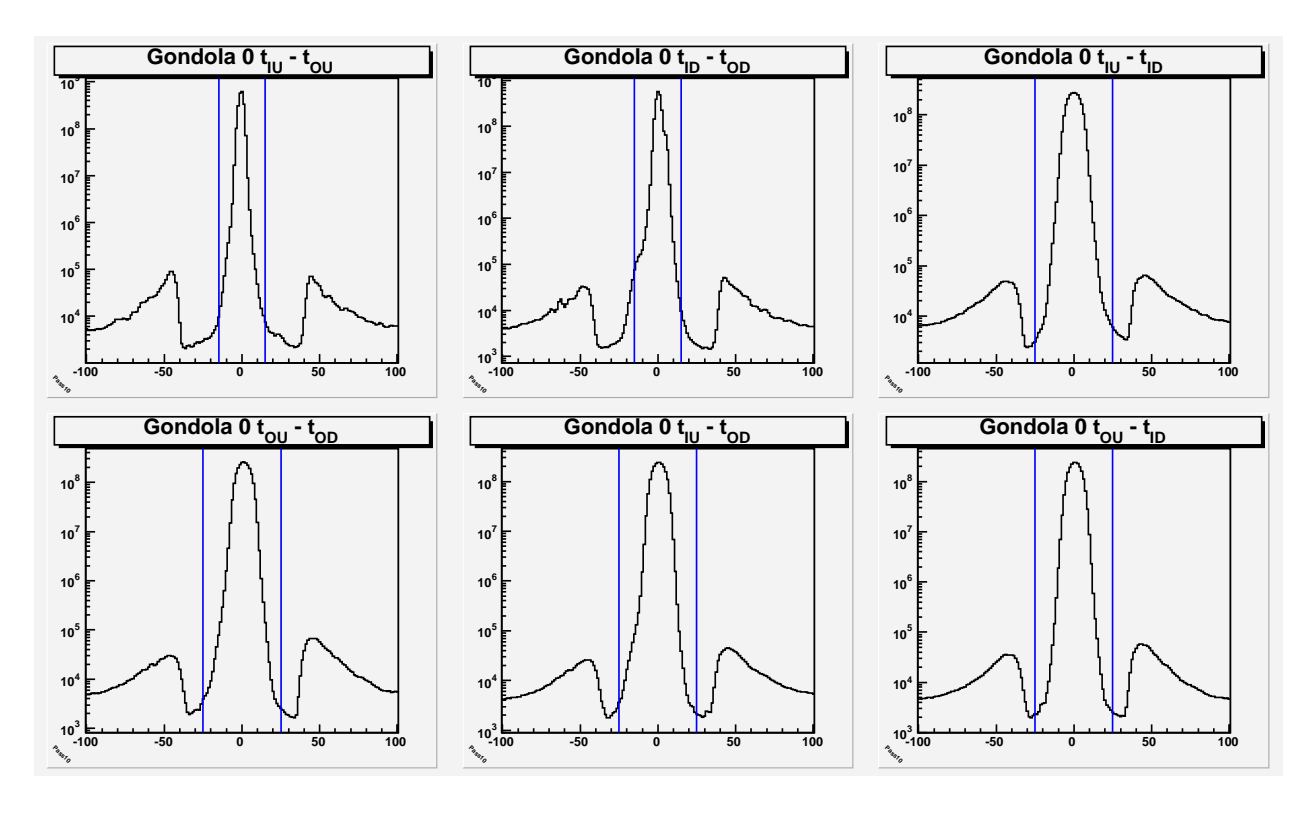


Figure 3.19: Time Differences of PMT Channels on the Same eSC Segment. The sum of these spectra for all eSC segments are shown. The clustering coincidence cuts are indicated by the vertical blue lines.

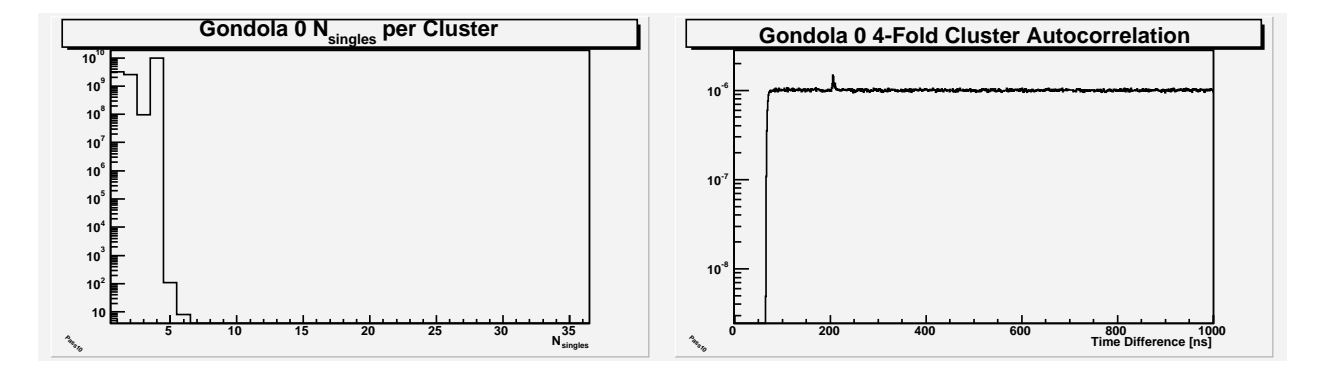


Figure 3.20: Left: Number of Time-Coincident PMT Channels on a Given eSC Segment; The sum of this distribution for each eSC segment is shown. Right: Autocorrelation of eSC 4-Fold Cluster. The autocorrelation is done on each eSC segment individually, and shown here is the sum of these for all 16 segments.

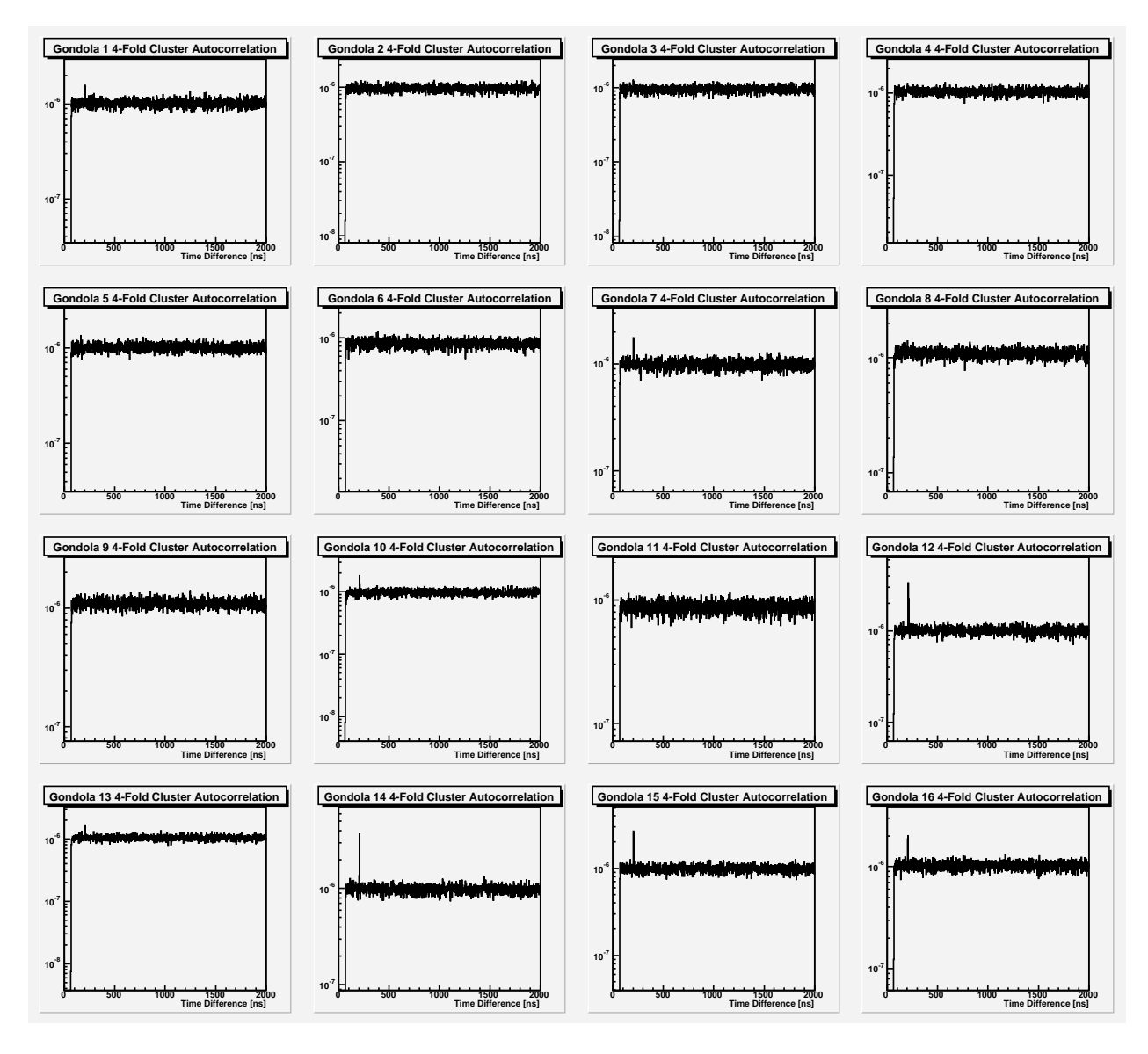


Figure 3.21: Autocorrelation of eSC 4-Fold Clusters, Segments 1 – 16.

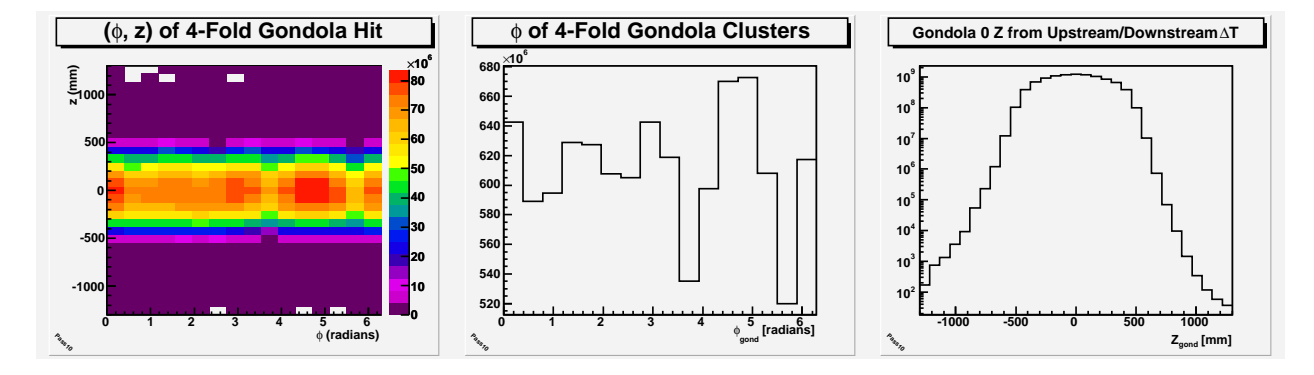
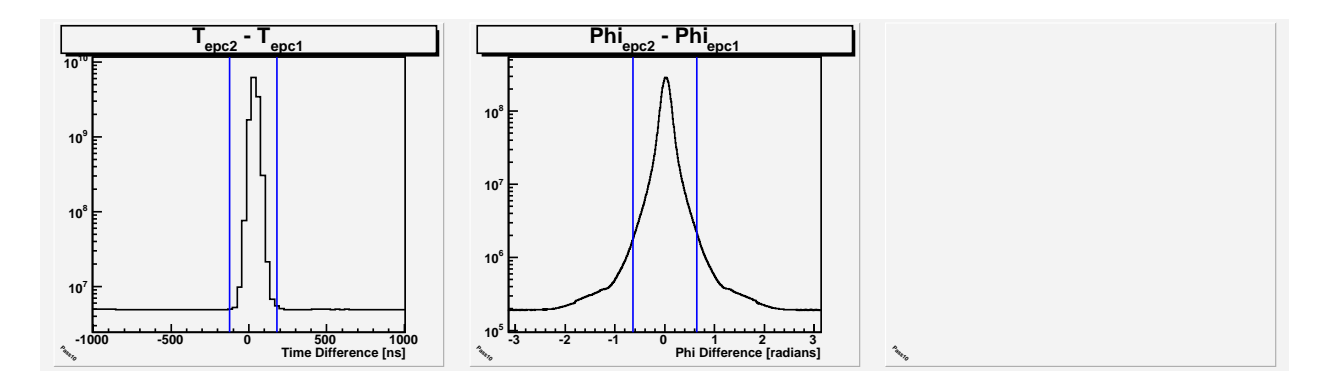
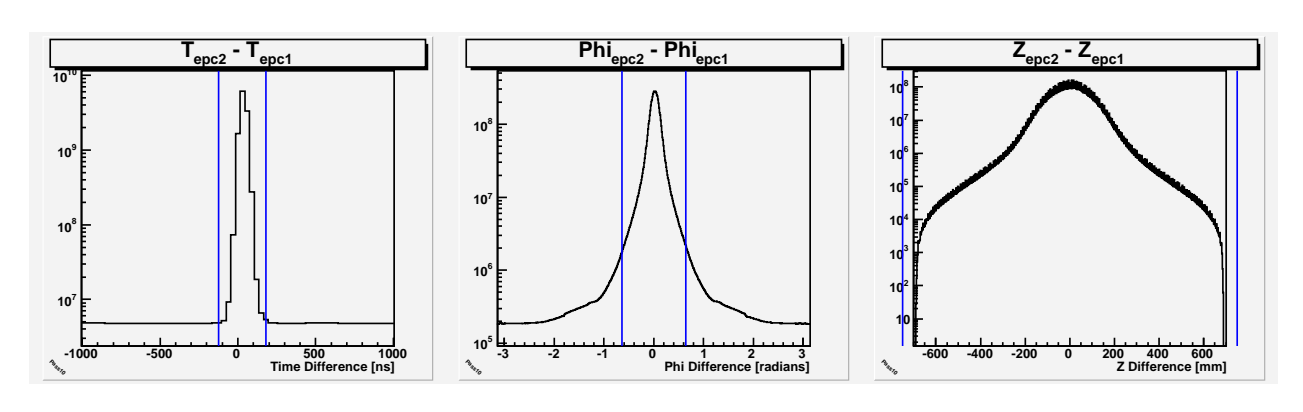


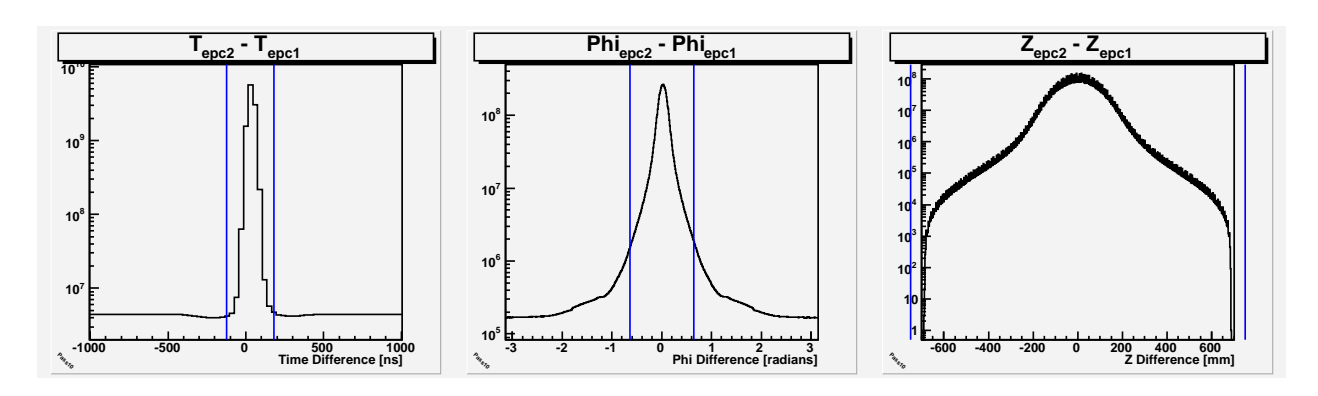
Figure 3.22: Left: (ϕ, z) Distribution Based Only on eSC Information; Middle: ϕ -Projection the the leftmost histogram; Right: z-Projection the the leftmost histogram. ϕ is taken at the center line of each eSC segment, and z is based on the time difference between upstream and downstream detectors of a 4-fold cluster.



(a) ePC1×ePC2, Anode Only



(b) ePC1 \times ePC2, Anode, Either Cathode



(c) ePC1×ePC2, Anode, Inner and Outer Cathode

Figure 3.23: ePC1×ePC2 Coincidence Histograms. Left: time differences, with coincidence cuts shown by the vertical blue lines. Middle: ϕ -differences of time-coincidences. $\Delta \phi$ -cuts are shown by the blue lines. Right: Z-differences of time-coincidences. ΔZ -cuts are shown by the blue lines.

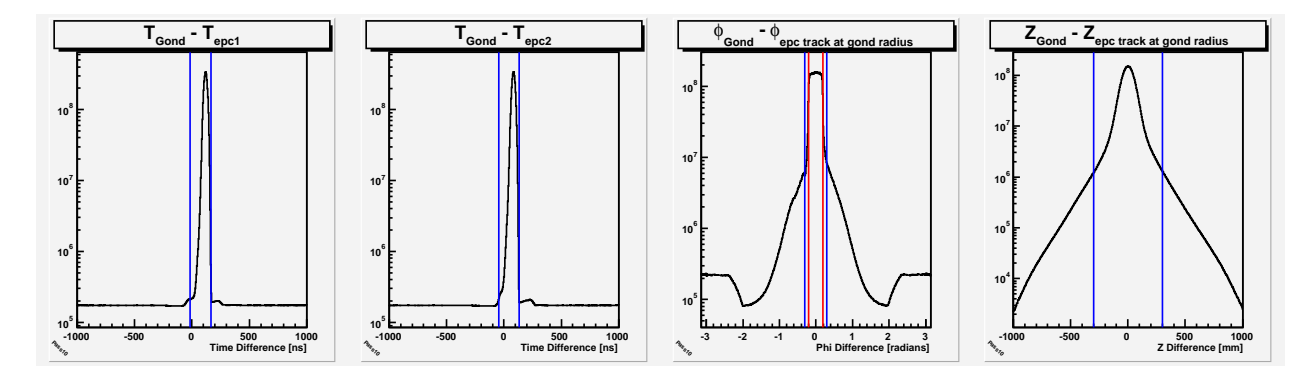


Figure 3.24: e-Detector Track Cuts: $eSC \times ePC1 \times ePC2$. The histograms displayed are based on the ePC hits subject to "Cathode OR" selection (see sec. 3.4).

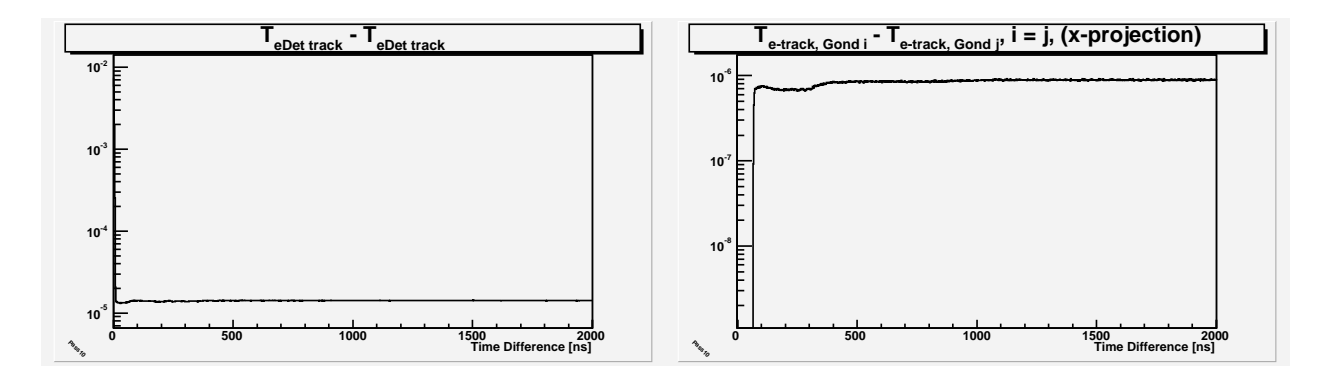


Figure 3.25: e-Detector Tracks (eSC×ePC1×ePC2) Autocorrelation. Left: autocorrelation of all tracks; Right: autocorrelation of tracks hitting the same eSC segment. The histograms displayed are based on the ePC hits subject to "Cathode OR" selection (see sec. 3.4).

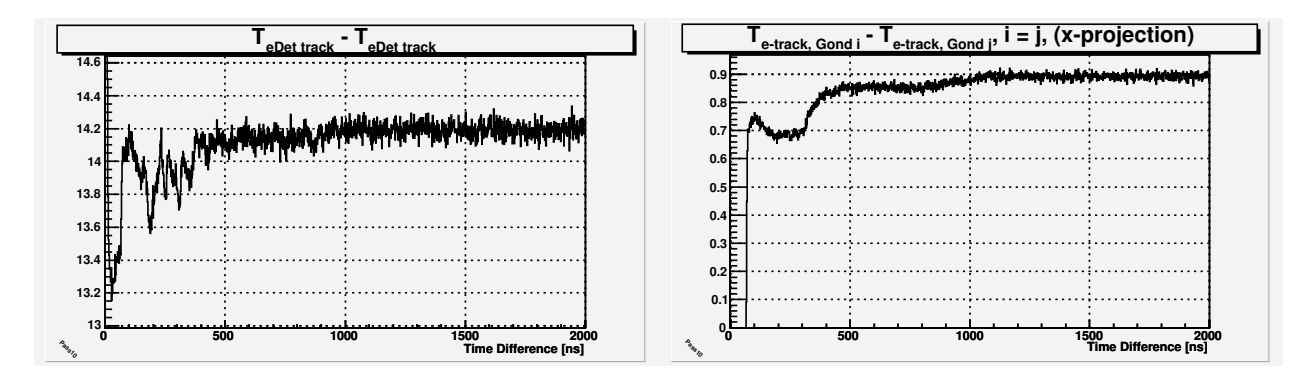


Figure 3.26: e-Detector Tracks (eSC \times ePC1 \times ePC2) Autocorrelation, zoomed linear scale. These are the same histograms as in figure 3.25.

3.6 Electron Detector Self-Consistent Alignment

electron detector self-consistent alignment procedure.

3.7 Electron Detector Efficiencies

Efficiency plots for ePC1, ePC2, and eSC are shown in figures 3.27, 3.28, and 3.29.

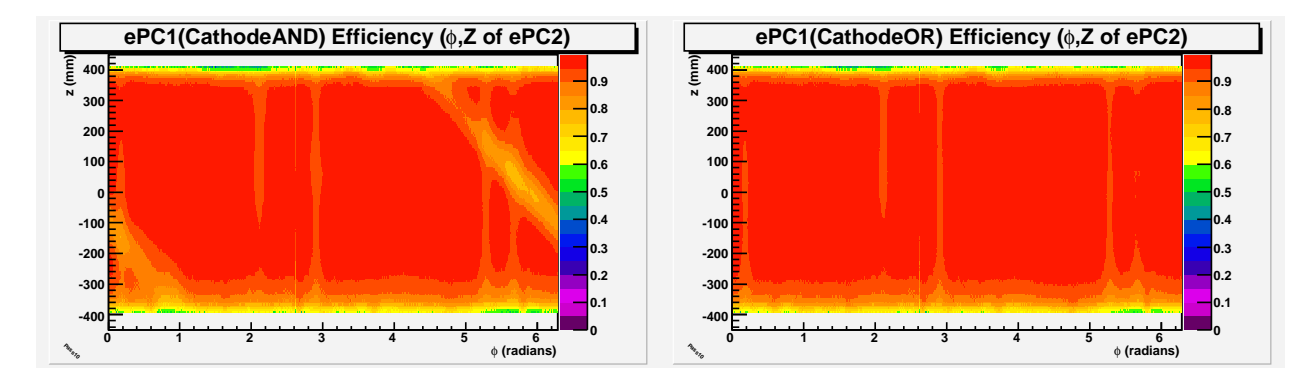


Figure 3.27: ePC1 Efficiency vs. (ϕ, z) . For each unambiguous ePC2×eSC coincidence, the fraction of times there is also a full ePC1×ePC2×eSC track is displayed. Left: tracks requiring hits in both ePC1 cathode planes; Right: tracks requiring hits in either ePC1 cathode plane.

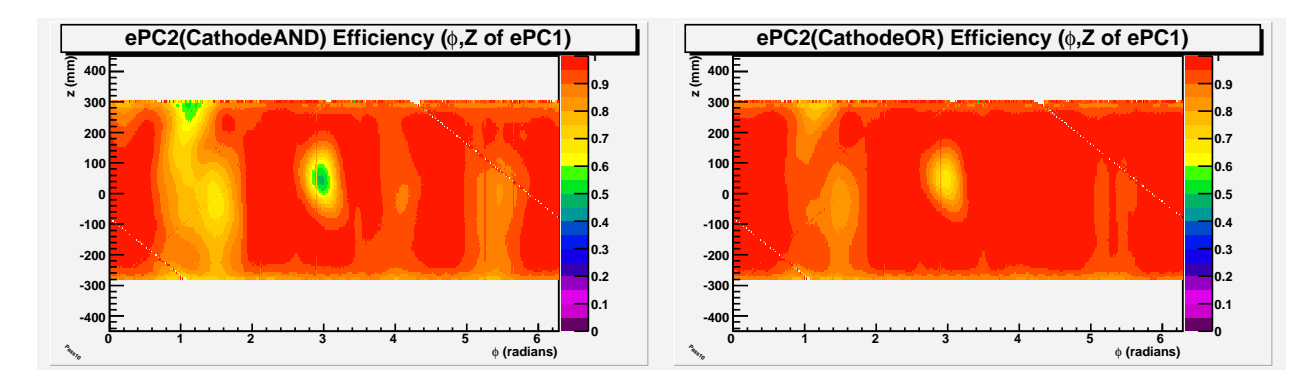


Figure 3.28: ePC2 Efficiency vs. (ϕ, z) . For each unambiguous ePC1×eSC coincidence, the fraction of times there is also a full ePC1×ePC2×eSC track is displayed. Left: tracks requiring hits in both ePC2 cathode planes; Right: tracks requiring hits in either ePC2 cathode plane.

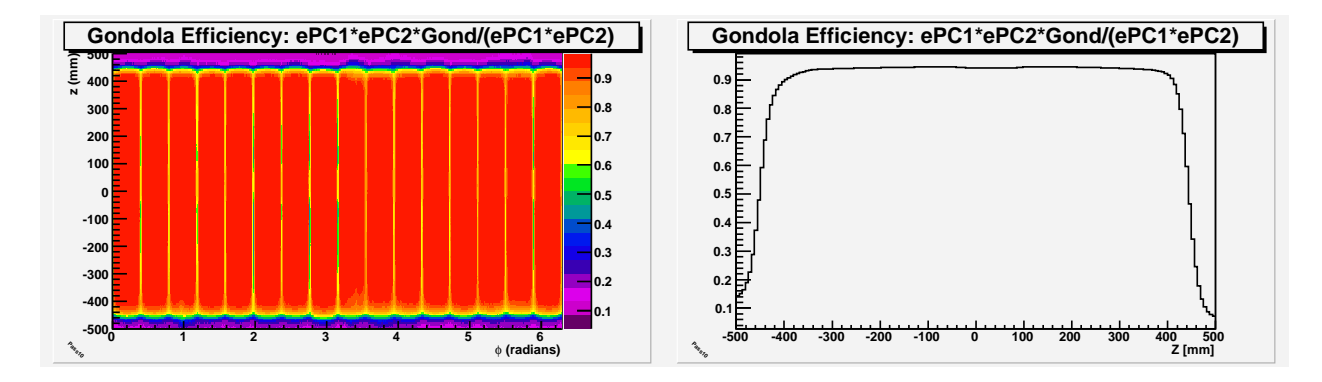


Figure 3.29: eSC Efficiency. For each unambiguous ePC1×ePC2 coincidence, the fraction of times there is also a full ePC1×ePC2×eSC track is displayed. Left: efficiency at (phi,z) of the ePC1×ePC2 track extended to the eSC radius; Right: efficiency vs. z (z-projection of plot in the left panel divided by the number of ϕ -bins).

Muon Detector Analysis

4.1 Muon Detector Configuration

Configuration: diagram geometry; list some specs.

4.2 Muon Entrance Scintillators (MuSC and MuSCA)

Describe algorithm; show autocorrs.; MUSC, MUFP (includes MuSCA); deadtimes.

4.3 Muon Entrance Wire Chamber (MuPC)

Clustering of MuPC1 singles hits uses the same routines as for the ePCs.

- Figure 4.1: Singles Autocorrelations.
- Figure 4.2: Singles Hit Distributions.
- Figure 4.3: Wire Gap Distributions.
- Figure 4.4: Cluster Size Distributions.
- Figure 4.5: Cluster Autocorrelations.
- Figure 4.6: T_{Xclu} T_{Yclu} Histogram, (x, y) distribution of interplane coincident clusters.
- Figure 4.7: $T_{MuPC} T_{MuSC}$ Histogram.

4.4 Software Definition of Muon Entrance

Describe algorithm. Document MuEntrance_t structure.

```
Double_t fT; // MuSC time of muon
UShort_t fMupcXWire_x100; // MuPC1 x-plane wire number (1-24) multiplied by 100
UShort_t fMupcYWire_x100; // MuPC1 y-plane wire number (1-24) multiplied by 100
Float_t fEntranceX; //! (don't stream) X coordinate of MuPC1 hit (if present)
Float_t fEntranceY; //! (don't stream) Y coordinate of MuPC1 hit (if present)
```

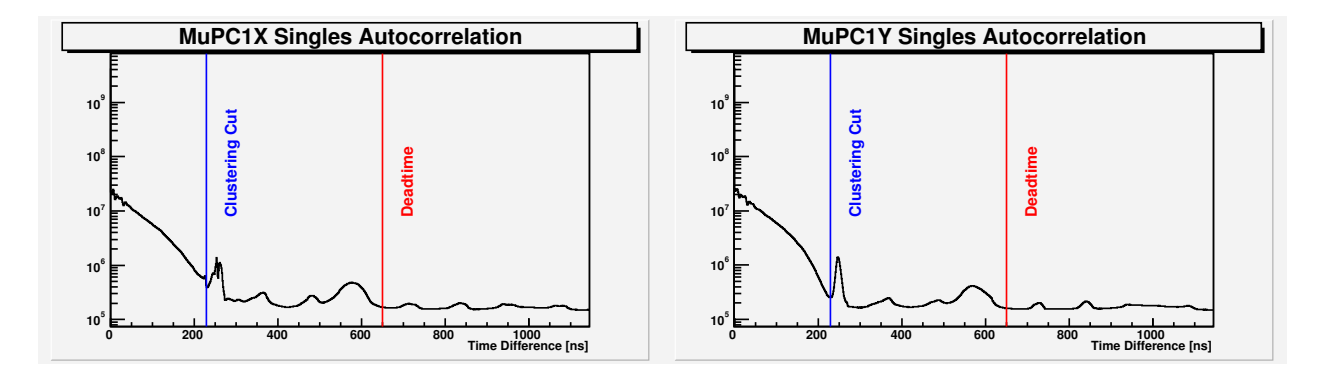


Figure 4.1: MuPC1 Singles Autocorrelations. Left: X-plane; Right: Y-plane. The clustering times and artificial deadtimes are indicated. (The similar spectrum of time difference between successive singles hits would be more appropriate here, but unfortunately these histograms were not created.)

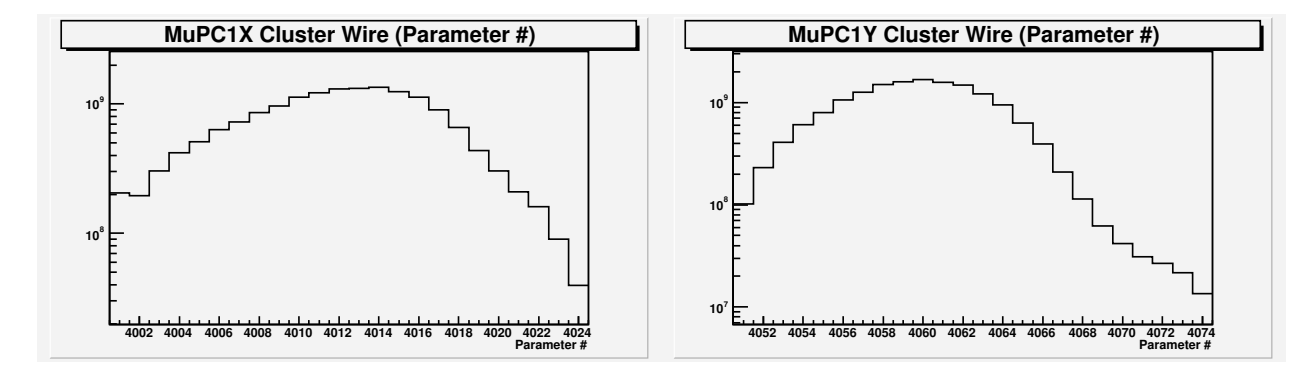


Figure 4.2: MuPC1 Singles Hit Distributions. Left: X-plane; Right: Y-plane.

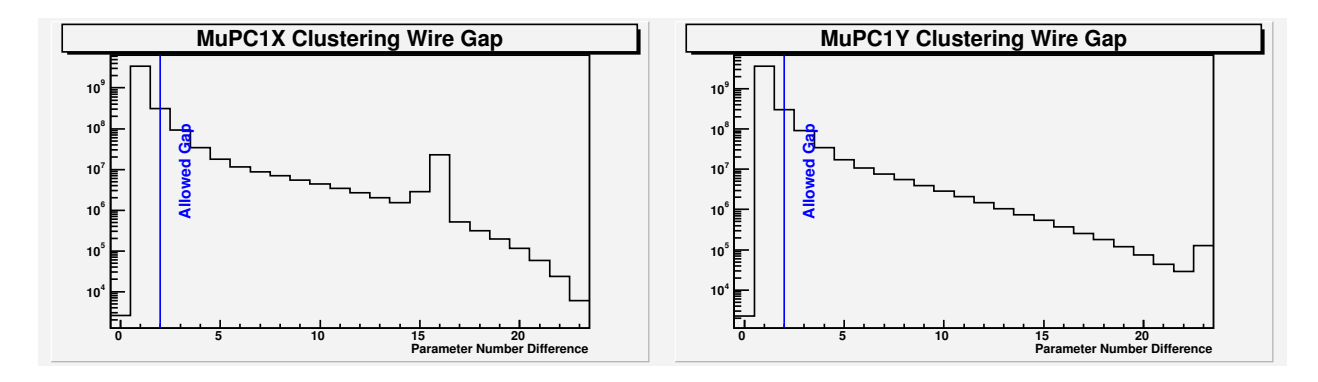


Figure 4.3: MuPC1 Wire Gap Distributions. For time-coincident singles hits, the hits are sorted into wire number order, and the wire number differences between neighbors in the sorted list are histogrammed. Left: X-plane; Right: Y-plane.

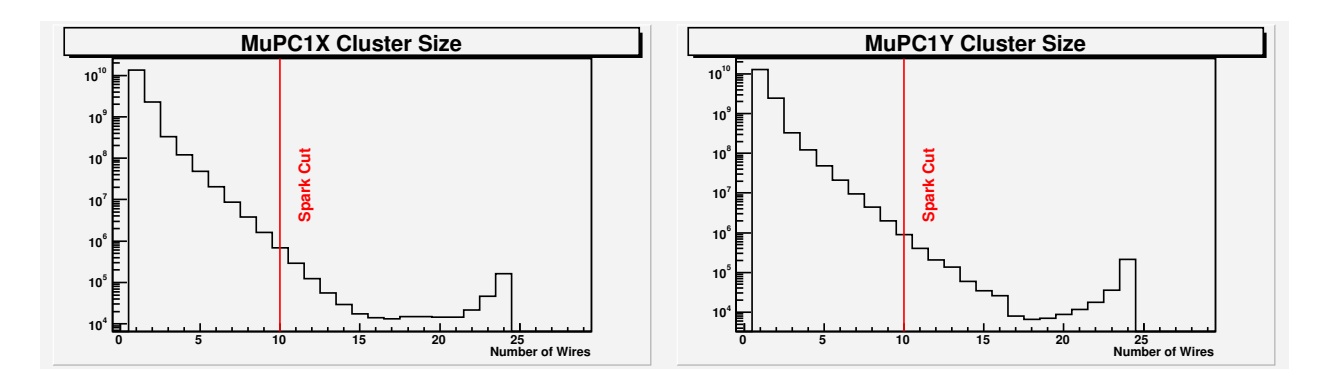


Figure 4.4: MuPC1 Cluster Size Distribution (number of wires). Left: X-plane; Right: Y-plane.

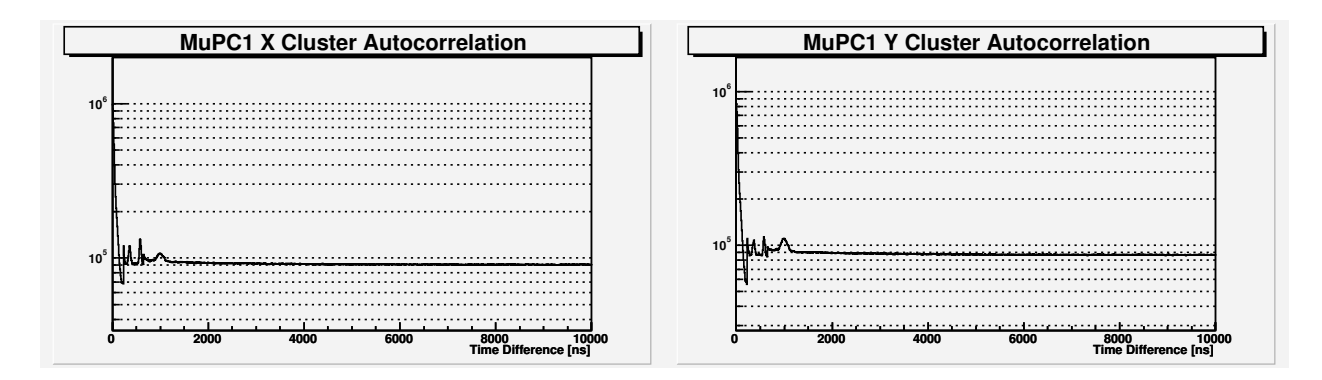


Figure 4.5: MuPC1 Cluster Autocorrelations. Left: X-plane; Right: Y-plane.

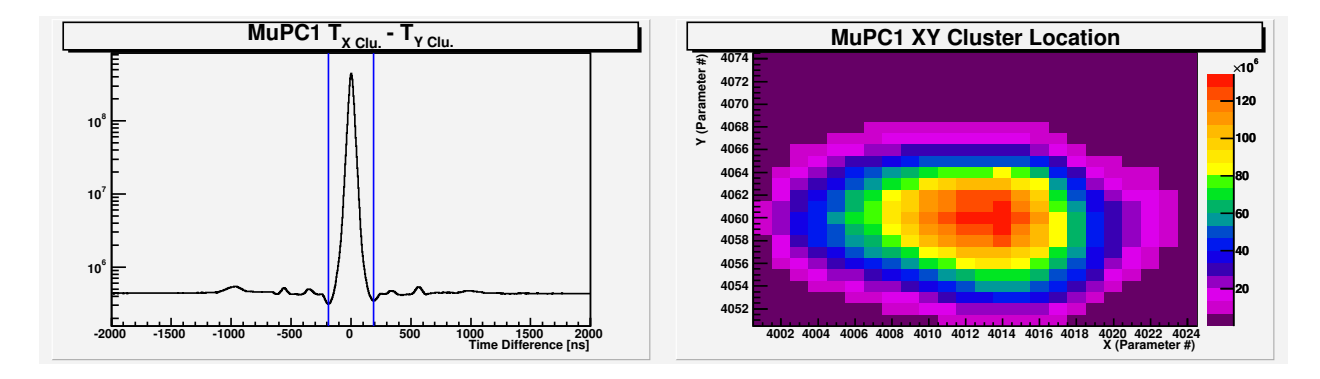


Figure 4.6: MuPC1 Cluster Coincidences. Left: X- and Y-plane Time Difference. Coincidence cuts are indicated by the vertical blue lines. Right: Time-Coincident Cluster Location.

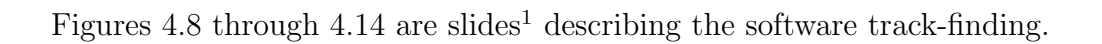
```
UShort_t fEntranceFlags; // bit 1 = MuPC X coinc.
                         // bit 2 = MuPC Y coinc.
                         // bit 3 = MuPC XY coinc.
                         // bit 4 = MuPC X pileup
                         // bit 5 = MuPC Y pileup
                         // bit 6 = MuPC XY pileup
                         // bit 7 = MuSCPP-triggered entrance
                         // bit 8 = MuPCXYPP-triggered entrance
                         // bit 9 = MUFP coinc.
                         // bit 10 = MUFP pileup
                         // bit 11 = TPC "Spark" veto
                         // bit 12 = other "Spark" veto (muPC, ePC, etc.)
                         // bit 13 = MuPC X long pileup (-25 \text{ to } +35 \text{ us})
                         // bit 14 = MuPC Y long pileup (-25 to +35 us)
                         // bit 15 = MuPC XY long pileup (-25 to +35 us)
                         // bit 16 = MuSC long pileup (-25 to +35 us)
UShort_t fMuscDTFlags; // from TMuscWithDTs. bit 1 means standard deadtime
UShort_t fMupcDTFlags;
                         // bit 1 = MuPC_shortDT X coinc.
                         // bit 2 = MuPC_shortDT Y coinc.
                         // bit 3 = MuPC_shortDT XY coinc.
                         // bit 4 = MuPC_shortDT X pileup
                         // bit 5 = MuPC_shortDT Y pileup
                         // bit 6 = MuPC_shortDT XY pileup
                         // bit 9 = MuPC_longDT X coinc.
                         // bit 10 = MuPC_longDT Y coinc.
                         // bit 11 = MuPC_longDT XY coinc.
                         // bit 12 = MuPC_longDT X pileup
                         // bit 13 = MuPC_longDT Y pileup
                         // bit 14 = MuPC_longDT XY pileup
```

4.5 Muon Time Projection Chamber (TPC)

• Drift time/speed, geometry determination from TPC/MuSC correlations, etc.

4.6 Software Definition of Muon Stop

- Basic trigger. EH pixel in region of interest (ROI) with respect to a MuEntrance_t time (t_{zero}) . The ROI is $[t_{zero}, t_{zero} + 25 \mu s]$, or $[t_{zero}, t_{zero} + 35 \mu s]$ if there are no other entrance detector hits in $[-25 \mu s, 35 \mu s]$. The longer ROI will be used for impurity capture searches.
- Track-finding algorithm. The class TtpcNew loops over all muon entrance objects, passes TDC400 data to a TTpcROI object for pattern recognition, and stores any TPC events found into a TMuStop object. Each TPC event with an EH pixel (track, spot, or other) is stored in a TMuStop object.



¹The slides are taken from my presentation at the 2006 MuCap Berkeley collaboration meeting.

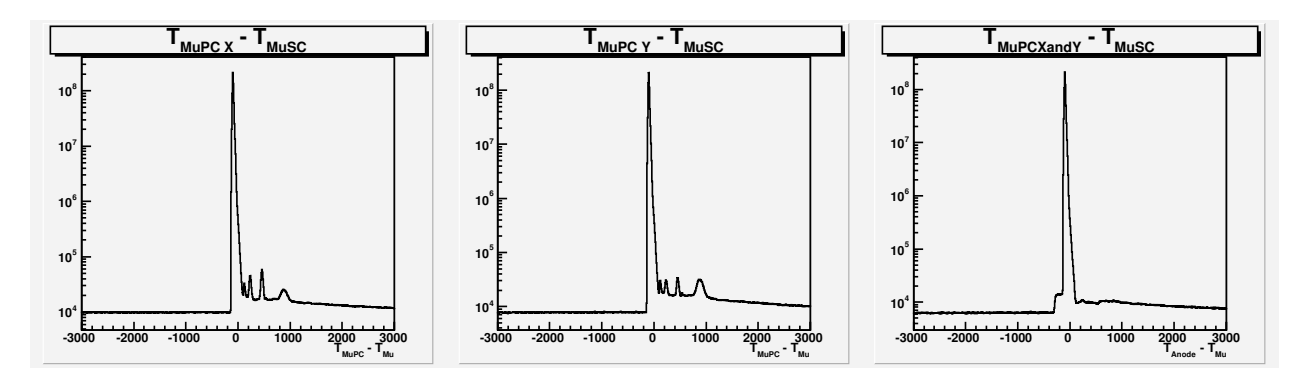
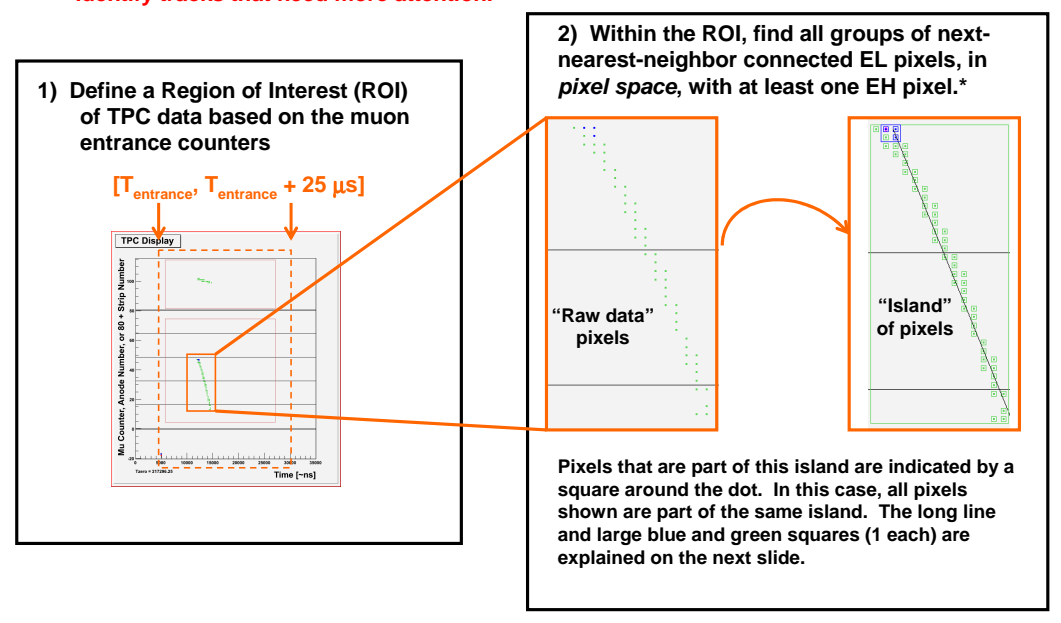


Figure 4.7: Time Difference Between MuPC1 Cluster and MuSC. Left: MupcX, MuSC Time Difference. Middle: MupcY, MuSC Time Difference. Right: MupcXandY, MuSC Time Difference.

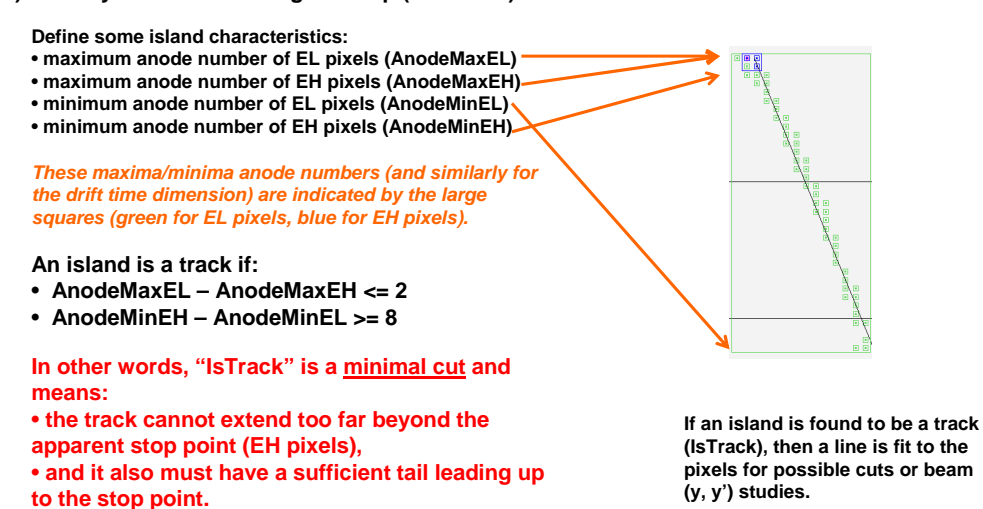
Goal of new stop definition: to be more robust against noise and distorted tracks, and to identify tracks that need more attention.



^{* &}quot;Pixel Space" is the 2-dimensional space of: (drift time divided by TDC400 clock period, anode number); it corresponds to spatial (y, z) coordinates.

Figure 4.8: MuStop Slide 1.

3) Identify if the island is a good stop ("IsTrack").



The (y, z) stop location is defined as that of the most downstream EH pixel, the one with the minimum drift time.

Figure 4.9: MuStop Slide 2.

4) If the island is not a track ("!IsTrack"), check if it is a spot ("IsSpot")

An island is a spot if:

AnodeMaxEL – AnodeMaxEH <= 2

AnodeMinEH – AnodeMinEL <= 2

DriftTimeMinEH – DriftTimeMinEL <= 3 (?)

DriftTimeMaxEL – DriftTimeMaxEH <= 3 (?)

The (y, z) location of the spot is defined as the average of the EVH pixels if present, otherwise of the EH pixels. (This may be changed to be the average of the earliest EVH or EH pixels.)

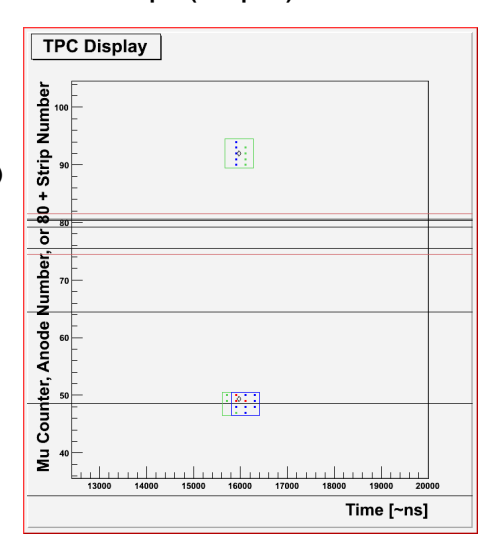
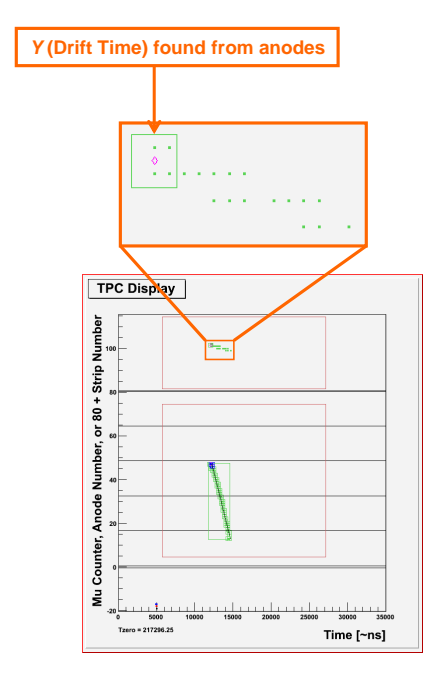


Figure 4.10: MuStop Slide 3.

Location in x (strips dimension)

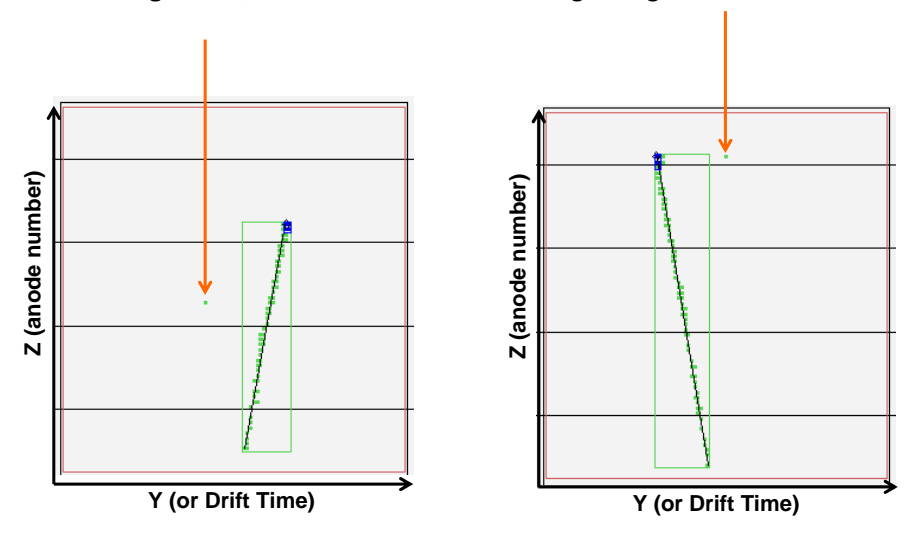


- Stop x is taken to be the average of the strips that have a hit at the stop time ($T_{\rm stop}$) determined from the anodes.
- The maximum and minimum x of the muon stop are based on strips hit at T_{stop} , T_{stop} +1 and T_{stop} -1.

Figure 4.11: MuStop Slide 4.

TPC Event Categories 2 Extra EL pixel in Region of Interest (ROI)

Occasionally (~2% of good stops), there are one or more EL pixels, unassociated with any EH-containing island, and downstream of the beginning of the muon track.*



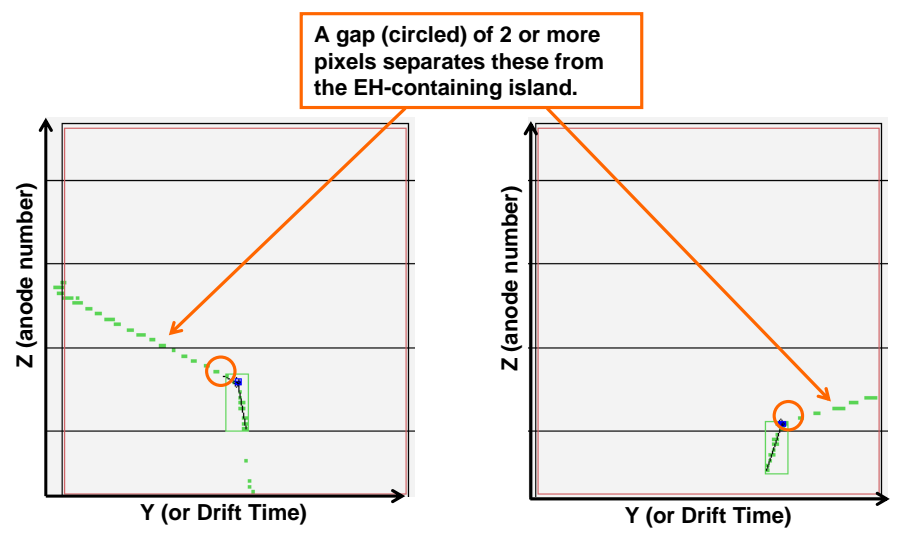
^{*} Most of the "extra EL pixels" upstream of the beginning of the track are merely from when the muon had not yet sufficiently slowed to leave a connected track.

Figure 4.12: MuStop Slide 5.

TPC Event Categories 3

Many Extra EL pixels in Region of Interest (ROI)

Very rarely ($<10^{-4}$ per muon stop), there are 8 or more extra EL pixels. Most ($\sim90\%$) point to the stop position.



These are likely muon-proton scattering events, in which the recoiling proton has enough energy to make an EH pixel, and which can be mistaken for a good muon stop.

Figure 4.13: MuStop Slide 6.

TPC Event Categories 4 Many Extra EL pixels in Region of Interest (ROI)

Very rarely (<10⁻⁴ per muon stop), there are 8 or more extra EL pixels. A few (10%) do not point to the stop position.

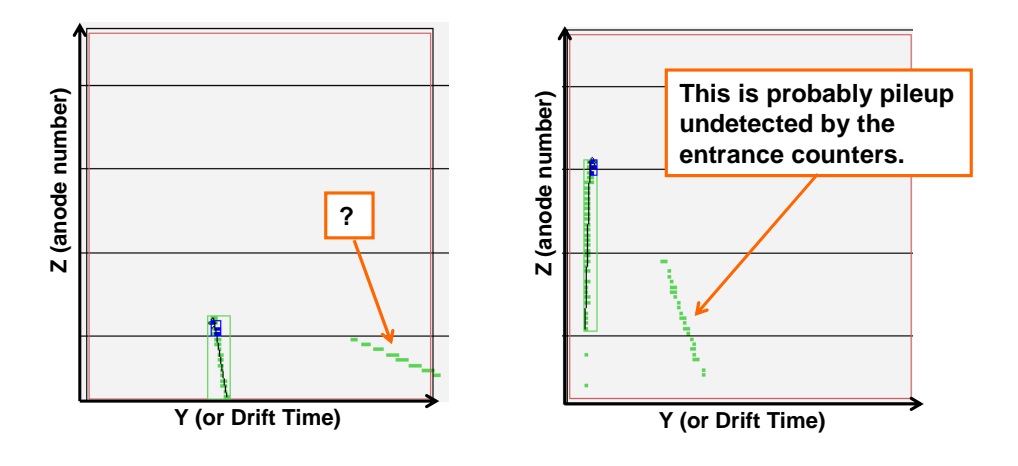


Figure 4.14: MuStop Slide 7.

Class TMuStop public inherits from TMuEntrance. In addition to all the data of the muon entrance class, the muon stop class contains the following data:

```
Float_t fX; //! (don't stream) X coordinate of stop position
Float_t fY; //! (don't stream) Y coordinate of stop position
Float_t fZ; //! (don't stream) Z coordinate of stop position
UShort_t fStopAnode_x100; // stop anode position multiplied by 100
UShort_t fStopStrip_x100; // stop strip position multiplied by 100
UShort_t fStopYPixel_x100; // stop Tdiff position [200 ns clk ticks]*100 wrt fTDiffYC
UShort_t fStopFlags; // see TMuStop.h for flag assignments
UShort_t fNPixelsEL; // number of EL pixels in this track (connected pixels)
UShort_t fNPixelsEH; // number of EH pixels in this track
UShort_t fNExtraPixelsEL; // number of unassigned EL pixels downstream of start of tr
UShort_t fNPixelsEVH; // number of EVH pixels in this track
Float_t fXminEL; //! (don't stream) Xmin [mm] of track EL points
Float_t fXmaxEL; //! (don't stream) Xmax [mm] of track EL points
Float_t fYminEL; //! (don't stream) Ymin [mm] of track EL points
Float_t fYmaxEL; //! (don't stream) Ymax [mm] of track EL points
Float_t fZminEL; //! (don't stream) Zmin [mm] of track EL points
Float_t fZmaxEL; //! (don't stream) Zmax [mm] of track EL points
Float_t fYminEH; //! (don't stream) Ymin [mm] of track EH points
Float_t fYmaxEH; //! (don't stream) Ymax [mm] of track EH points
Float_t fZminEH; //! (don't stream) Zmin [mm] of track EH points
Float_t fZmaxEH; //! (don't stream) Zmax [mm] of track EH points
Float_t fYminEVH; //! (don't stream) Ymin [mm] of track EVH points
Float_t fYmaxEVH; //! (don't stream) Ymax [mm] of track EVH points
Float_t fZminEVH; //! (don't stream) Zmin [mm] of track EVH points
Float_t fZmaxEVH; //! (don't stream) Zmax [mm] of track EVH points
UChar_t fAnodeMinEL; // minimum EL anode number in this island
UChar_t fAnodeMaxEL; // maximum EL anode number in this island
UChar_t fAnodeMinEH; // minimum EH anode number in this island
UChar_t fAnodeMaxEH; // maximum EH anode number in this island
UChar_t fAnodeMinEVH; // minimum EVH anode number in this island
UChar_t fAnodeMaxEVH; // maximum EVH anode number in this island
UChar_t fStripMinEL; // minimum EL strip number in this island
UChar_t fStripMaxEL; // maximum EL strip number in this island
UChar_t fYPixelMinEL; // minimum TDiffY of EL points (pixel space)
UChar_t fYPixelMaxEL; // maximum TDiffY of EL points (pixel space)
UChar_t fYPixelMinEH; // minimum TDiffY of EH points (pixel space)
UChar_t fYPixelMaxEH; // maximum TDiffY of EH points (pixel space)
UChar_t fYPixelMinEVH; // minimum TDiffY of EVH points (pixel space)
UChar_t fYPixelMaxEVH; // maximum TDiffY of EVH points (pixel space)
Float_t fTDiffYO; // time offset [ns] wrt fMuscTime of 1st nonzero ROI pixels.
               // This is necessary to convert from "pixel space" to drift-time.
```

```
TOneLine *fOneLine; //-> (always ptr to valid object) single line, in pixel space TTwoLine *fTwoLine; // 2 connected line segments, in pixel space TTpcPixelList *fTpcPixelList; // pointer to TPC singles data, if saved
```

4.7 Entrance Detector Efficiencies

One method to find the inefficiency of the MuSC detector is to look at all TPC×MuPCXandY coincidences, and count the number of times the MuSC is not also in coincidence. This is implemented in the MIAS tree analysis by (1) selecting each muon stop (TMuStop object) within the fiducial volume that is a good track, with MuPCXandY-coincident entrance, and pileup protected by MuPCXorY and the MuSC; (2) filling the MuPC (x, y)-coordinates into a 2D histogram for normalization; and (3) If the entrance is not coincident with any MuSC channel (the "MUFP" bank of the raw analysis), filling the MuPC (x, y)-coordinates into a 2D histogram for "missing MuSC" entrances. Dividing the "missing MuSC" histogram by the normalization histogram gives the inefficiency of the MuSC vs. MuPC (x, y)-coordinate. Figures 4.16 to 4.17 show the histograms and the resulting inefficiency plot for each of four chronological run groups (subgroups of Prod50 data). The total MuSC inefficiency, the ratio of the integral of the "missing MuSC" histogram to that of the normalization histogram, is shown vs. run number in figure 4.20.

Also plotted in figure 4.20 are estimates of the MuPC inefficiencies vs. run number. These are found by selecting MuSC-triggered, good muon stops that are pileup-protected with all entrance detector planes, and counting the fraction of events without the plane of interest.

 $^{^2}$ To have the possibility of a muon entrance without a pileup-protected MuSC hit requires starting from unskimmed raw data.

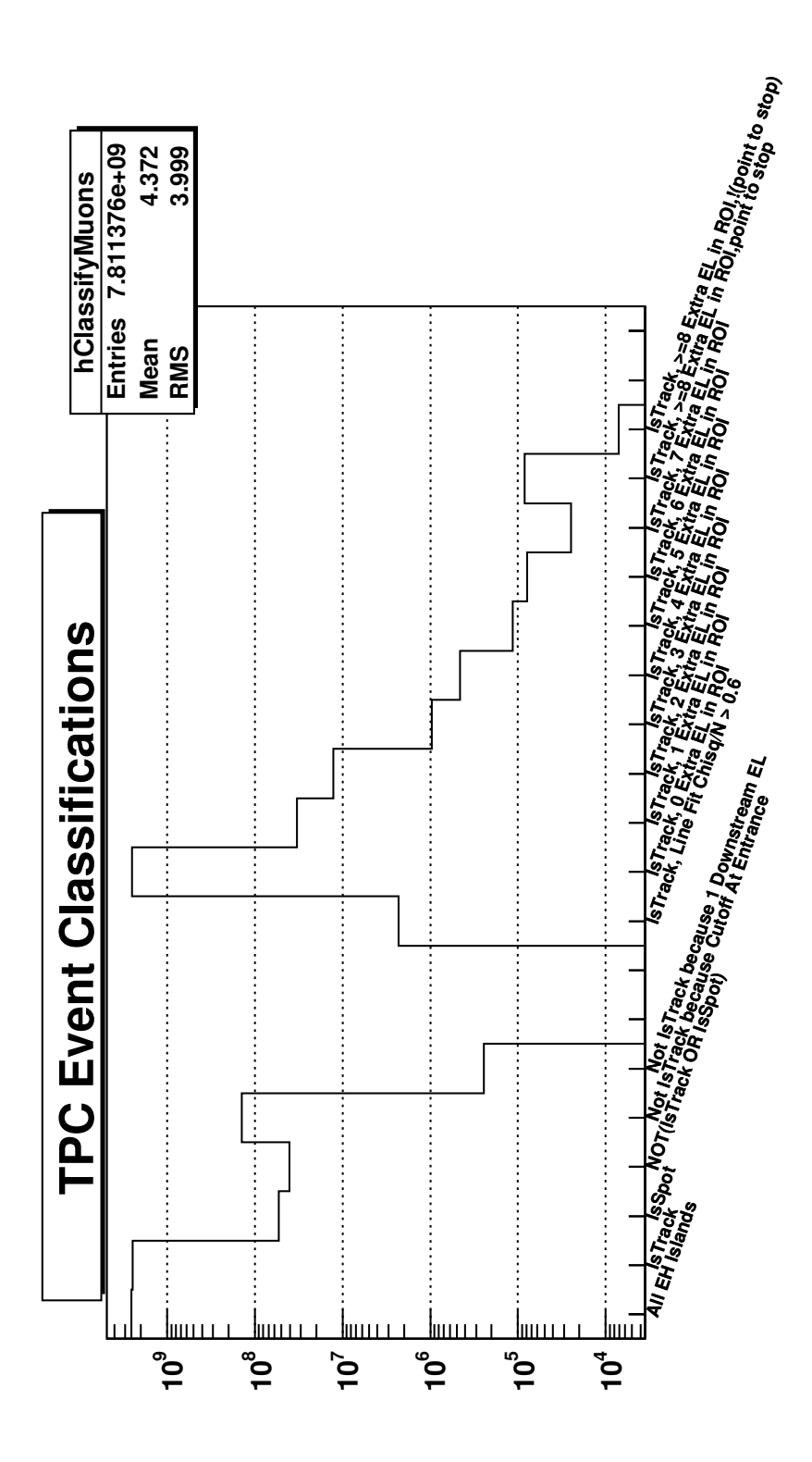


Figure 4.15: MuStop event classification statistics.

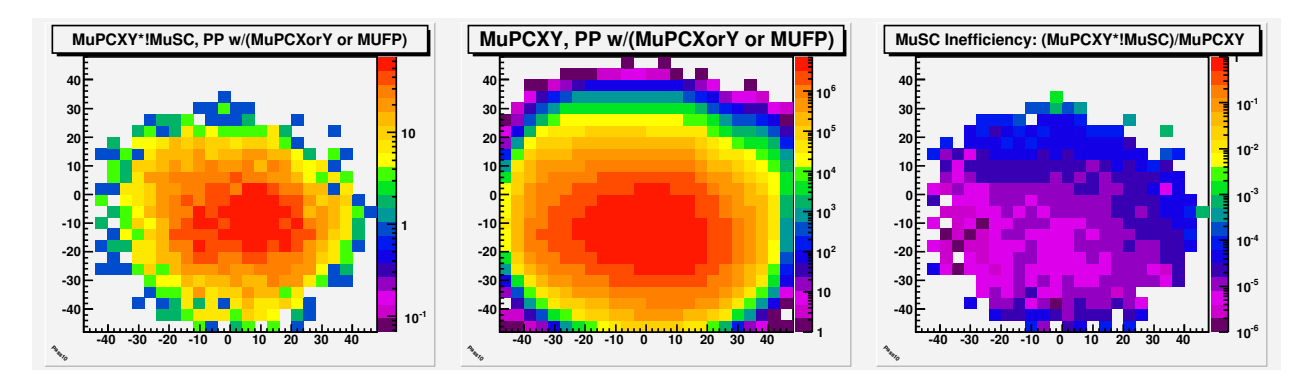


Figure 4.16: MuSC Inefficiency Plots, Prod50 Group1. Left: all MuPCXY-triggered entrances with MuStop, pileup-protected with both MuPCXorY and MUFP. Middle: same as left plot, but requiring no MuSC coincidence. Right: MuSC inefficiency (left plot divided by middle plot).

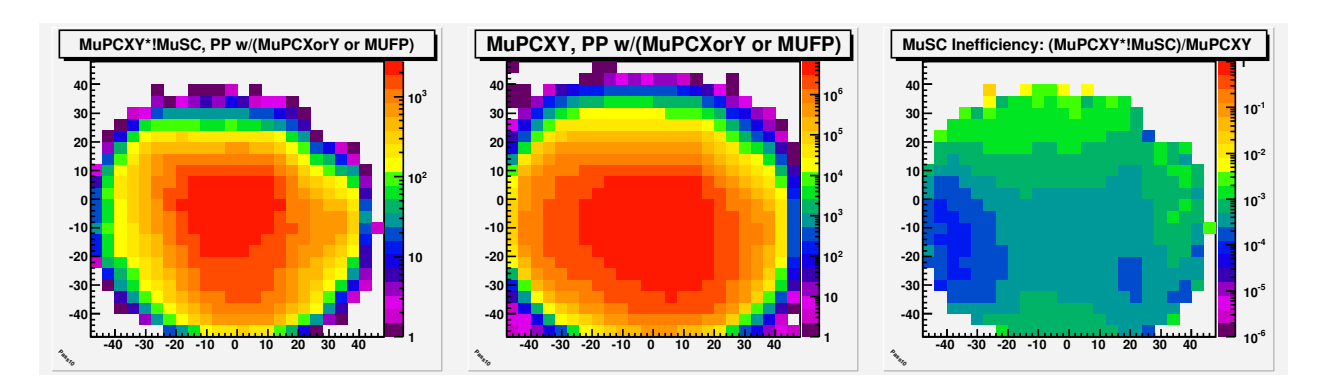


Figure 4.17: MuSC Inefficiency Plots, Prod50 Group2. Left: all MuPCXY-triggered entrances with MuStop, pileup-protected with both MuPCXorY and MUFP. Middle: same as left plot, but requiring no MuSC coincidence. Right: MuSC inefficiency (left plot divided by middle plot).

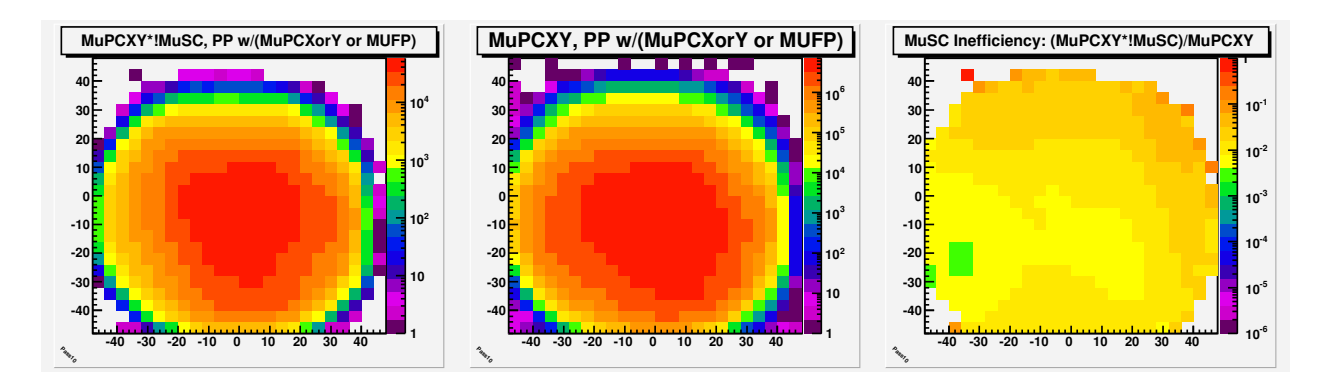


Figure 4.18: MuSC Inefficiency Plots, Prod50 Group3. Left: all MuPCXY-triggered entrances with MuStop, pileup-protected with both MuPCXorY and MUFP. Middle: same as left plot, but requiring no MuSC coincidence. Right: MuSC inefficiency (left plot divided by middle plot).

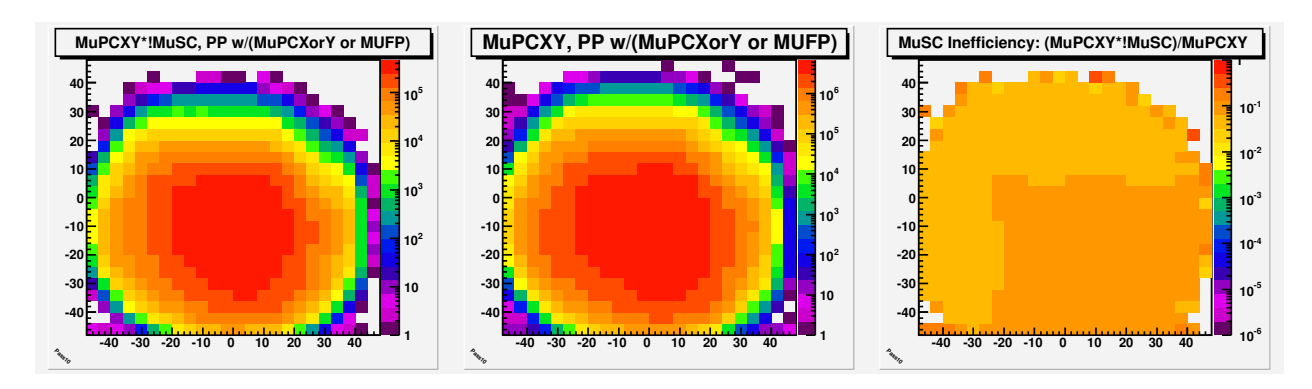


Figure 4.19: MuSC Inefficiency Plots, Prod50 Group4. Left: all MuPCXY-triggered entrances with MuStop, pileup-protected with both MuPCXorY and MUFP. Middle: same as left plot, but requiring no MuSC coincidence. Right: MuSC inefficiency (left plot divided by middle plot).

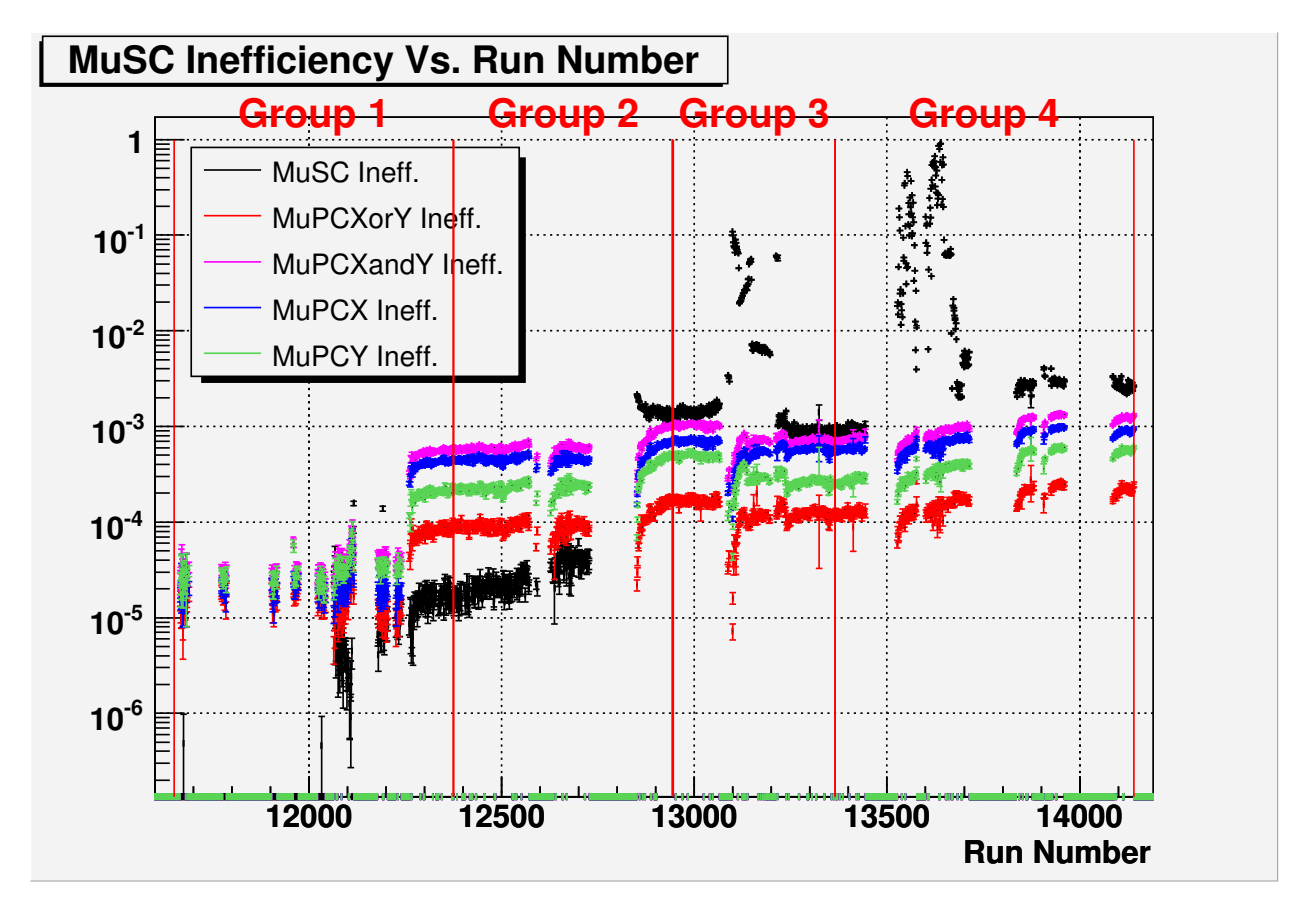


Figure 4.20: Entrance Detector Inefficiencies vs. Run Number, Prod50.

Other Raw Analysis Modules

5.1 Spark Cuts

Sparks or high-multiplicity events in MWPCs are identified at different stages of the raw analysis.

- 1. Before the clustering procedures, sparks in MWPC planes are roughly identified by an unusually high number of singles hits within a specified time interval in a given plane. Figures 5.1 through 5.3 show histograms of the number of singles hits found per 45 μ s time interval. The red vertical lines in the figures show the cuts. Most likely the sparks identified here would also be caught in subsequent cluster size cuts.
- 2. After the clustering step (see section 3.2.1), the analysis loops over clusters and considers those with size greater than CLU_PARAM::SizeCut to be sparks. If the spark is found in an electron detector plane, a "muon spark" is also registered that contains the electron spark interval plus an additional 25 μs on either end. This explicit cluster size cut is the reason for the drammatic difference in the cluster size distributions, comparing with to without spark cuts, in figures 3.4 and 3.12; the few post-spark-cut histogram entries at greater than the cluster size cut are from rare cases in which the number of registered sparks in an event block exceeds a software limit.¹
- 3. Sparks in the TPC are identified by signals on the nonamplifying anodes 1–4. The muon entrance routine searches for these and sets a flag if found, and the TPC track-finding routine skips these entrances.

The most aggressive spark cut by far is that on the ePC cluster size.

The class TSparkTimes keeps track of time intervals identified elsewhere to contain sparks.

- TSparkTimes::AddInterval(tmin, tmax) adds an interval.
- TSparkTimes::Veto(time) returns 1 if time lies within a registered spark interval, and 0 otherwise.
- TSparkTimes::CombineIntervals() should be called after spark intervals are added.

Two global instances of TSparkTimes are created: one for muon detector sparks, and one for electron detector sparks. If a muon entrance object (TMuEntrance) falls within a muon spark interval, a flag is set in the entrance object.

¹The limit, which can be increased, is the size of an array in TSparkTimes.

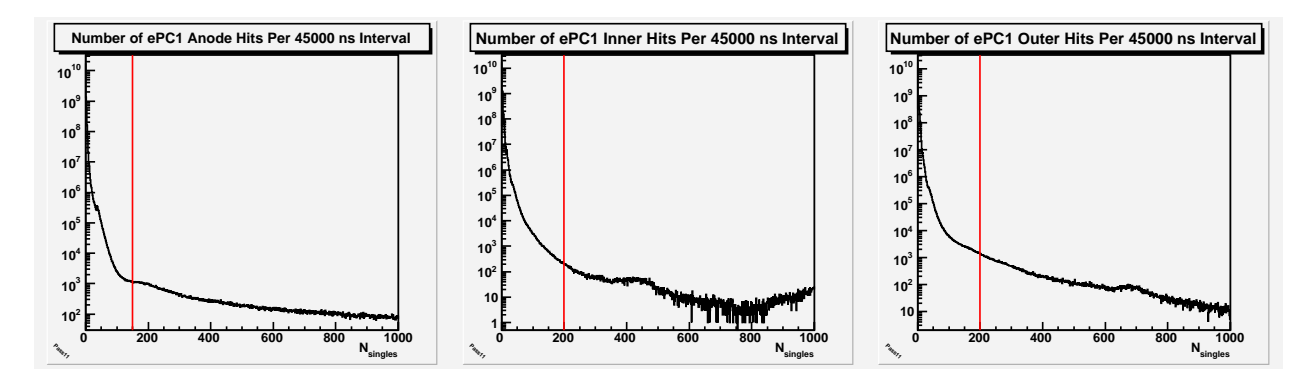


Figure 5.1: Histograms of the Number of Singles Hits per 45 μ s Time Interval in ePC1 Planes. Intervals with greater than the number indicated by the red vertical line are considered sparks.

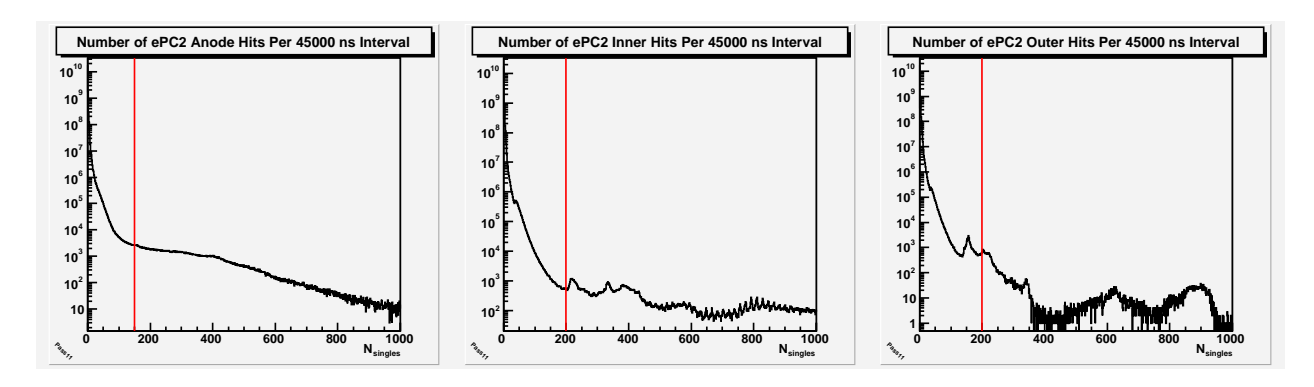


Figure 5.2: Histograms of the Number of Singles Hits per 45 μ s Time Interval in ePC2 Planes. Intervals with greater than the number indicated by the red vertical line are considered sparks.

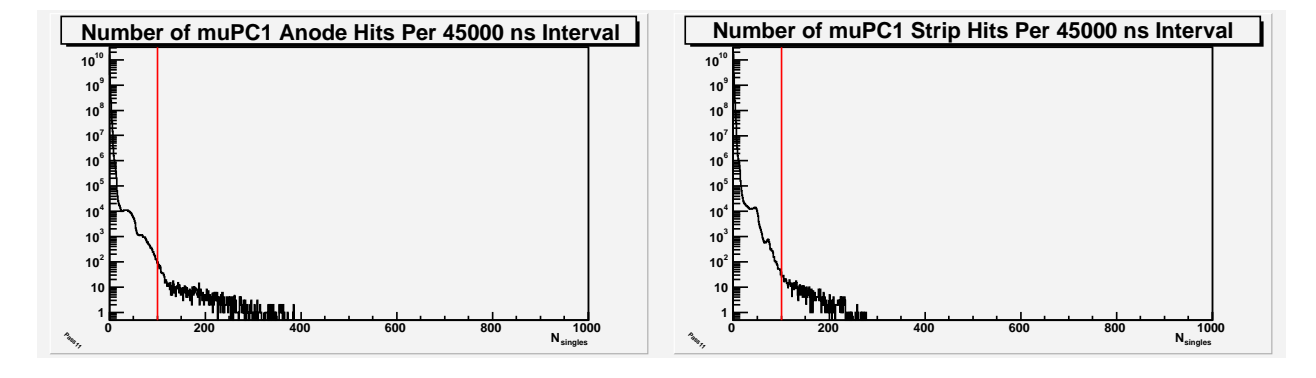


Figure 5.3: Histograms of the Number of Singles Hits per 45 μ s Time Interval in MuPC Planes. Intervals with greater than the number indicated by the red vertical line are considered sparks.

5.2 Noisy Wires Suppression

The class ThotWiresAnalysis checks the number of singles hits on each ePC wire over a given DAQ livetime and accordingly masks those wires with excessive count rate. This is done on a per-run basis; that is, at the beginning of each run all wires are unmasked, and once a mask is set it persists for the duration of the run. Here are the relavent parameters:

```
HOTWIRES_PARAM hotwires_parameters = {
          // event_interval
                             event interval to check for hot wires
 1.0e9,
         // min_livetime
                             [ns] minimum livetime interval required
                             to check count freq.
                             max allowed singles frequency [Hz]
 500., // freq_epc1Anodes
 2500., // freq_epc1Inner
                             max allowed singles frequency [Hz]
 2500., // freq_epc10uter
                             max allowed singles frequency [Hz]
 250., // freq_epc2Anodes
                             max allowed singles frequency [Hz]
 1300., // freq_epc2Inner
                             max allowed singles frequency [Hz]
  1300., // freq_epc20uter
                             max allowed singles frequency [Hz]
};
```

The frequency thresholds are much higher than the average hit rate seen by an individual wire, certainly much higher than the rate due to real particles.

Software Tree Structure

Describe the data that is written to the tree (MucapEvent object). Here are the data members of the TMucapEvent class:

```
fNmuon;
                                  //Number of tracks
Int_t
TClonesArray
              *fMuons; //->array with all muons (TMuStop)
                                      //Number of tracks
Int_t
               fNelectron;
TClonesArray *fElectrons; //->array with all electrons (TElectron)
               fNelectron_cathAND;
Int_t
                                              //Number of tracks
TClonesArray *fElectrons_cathAND; //->array with all electrons (TElectron)
               fNelectron_anodesOnly;
                                                 //Number of tracks
Int_t
TClonesArray *fElectrons_anodesOnly; //->array with all electrons (TElectron)
               fNgondCaen;
                                      //Number of tracks
Int_t
TClonesArray *fGondCaens;
                            //->array with all gond-only 4-fold hits, caens
               fNgondComp;
Int_t
                                      //Number of tracks
TClonesArray *fGondComps; //->array with all gond-only 4-fold hits, comps
Int_t
               fNgondNonClu;
                                        //Number of tracks
TClonesArray *fGondNonClus;
                             //->array with all non-clustered gond-only
                              // singles, caens
TFadcRun8
              *fFadcRun8;
                            // pointer FADC data, if saved
Bool_t
               fIsValid;
                                   //
Int_t
               fSerialNumber;
```

Part II Tree Analysis Studies

"Extra EL Pixels" in the TPC

Pattern recognition of muon stops in the TPC must be decay-time independent to avoid distortion of the lifetime measurement. Potential sources of decay-time dependent track acceptance, it turns out, are extra EL pixels around the track. The definition of "extra EL pixels" was given previously in figure 4.12, and the number distribution of these extra EL pixels in a mu stop are included in the histogram of figure 4.15. The effect on the lifetime of selecting on these extra EL pixels is shown in figure 7.1, which compares the lifetime vs. eSC Segment (or ϕ) for muon stops with zero or one extra EL pixels. Requiring one extra EL pixel gives an enormous effect — a large signal for the so-called "gondola effect;" requiring no extra EL pixels also gives an effect, and apparently in the opposite direction. Not selecting on the extra EL pixels eliminates the gondola effect completely. The extra EL pixels are thus clearly connected to muon decay time.

As the lifetime ϕ -variation was a problem for quite some time in the MuCap analysis due to implicit cuts on the extra EL pixels, it is worth understanding the source of these strays. Figure 7.3 shows the absolute position of the extra EL pixels, the relative positions, and the impact parameter between the absolute position and electron tracks. We learn that the extra pixels are distributed throughout the TPC volume (at least in the yz-plane); they occur in all directions around the muon stop position; and the electron track at least roughly points at the extra pixels.

A more illuminating study is shown in figure 7.4, in which the center of the extra EL pixel distribution, with respect to the muon stop position, appears to move toward +y (opposite TPC drift direction) with increasing muon decay time. In fact, the distribution moves toward +y at exactly the TPC drift velocity specified in the analysis software. This is consistent with extra EL pixels actually occurring at the time of the electron track, not at the muSC time as is assumed when calculating y from the TPC drift time.

Finally, figure 7.5 shows the extra EL pixel positions relative to the muon stop, selecting events with electron tracks involving a given gondola in a given decay time interval. These distributions are consistent with the hypothesis that extra EL pixels are occasionally deposited along the path of the decay electron. Likely sources are delta electrons kicked off by the minimum-ionizing decay electrons. As to whether or not the number and distribution of extra EL pixels are completely consistent with delta electrons emitted transverse to the track but quickly randomized¹ would require detailed study. In the context of the Run8 analysis it is sufficient to know that these extra EL pixels occur along the electron paths,

¹see F. Sauli, "Principles of Operation of Multiwire Proportional and Drift Chambers," sections 2.4 and 2.5

and we must be careful not to accept or reject muon tracks based on them.

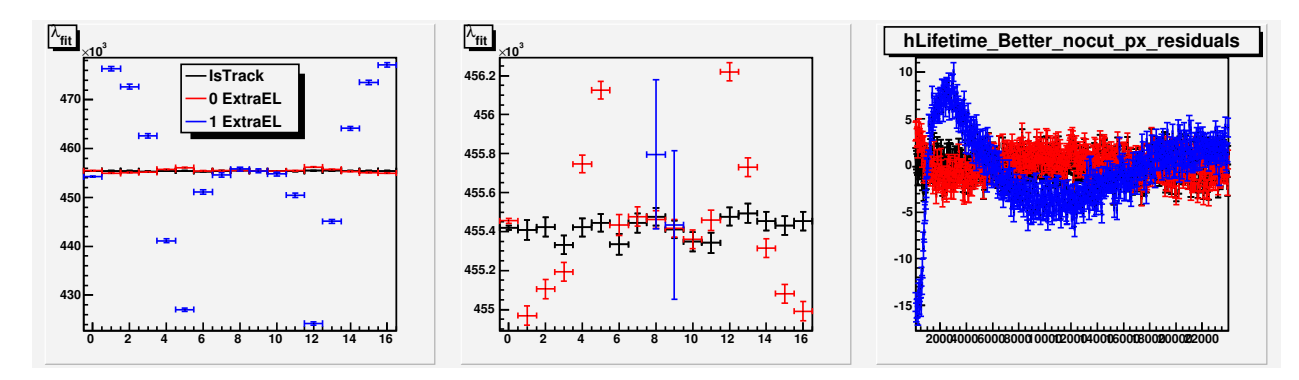


Figure 7.1: Lifetime Fits vs. eSC Segment, with no requirement on the number of extra EL pixels (black), requiring exactly 0 extra EL pixels (red), and requiring exactly 1 extra EL pixel (blue). Left panel: λ_{fit} ; The leftmost bin is the fit to the sum over all eSC segments. Middle panel: zoomed-in version of the plot in the left panel. Right panel: fit residuals (normalized) to the fits of the sum of all eSC segments.

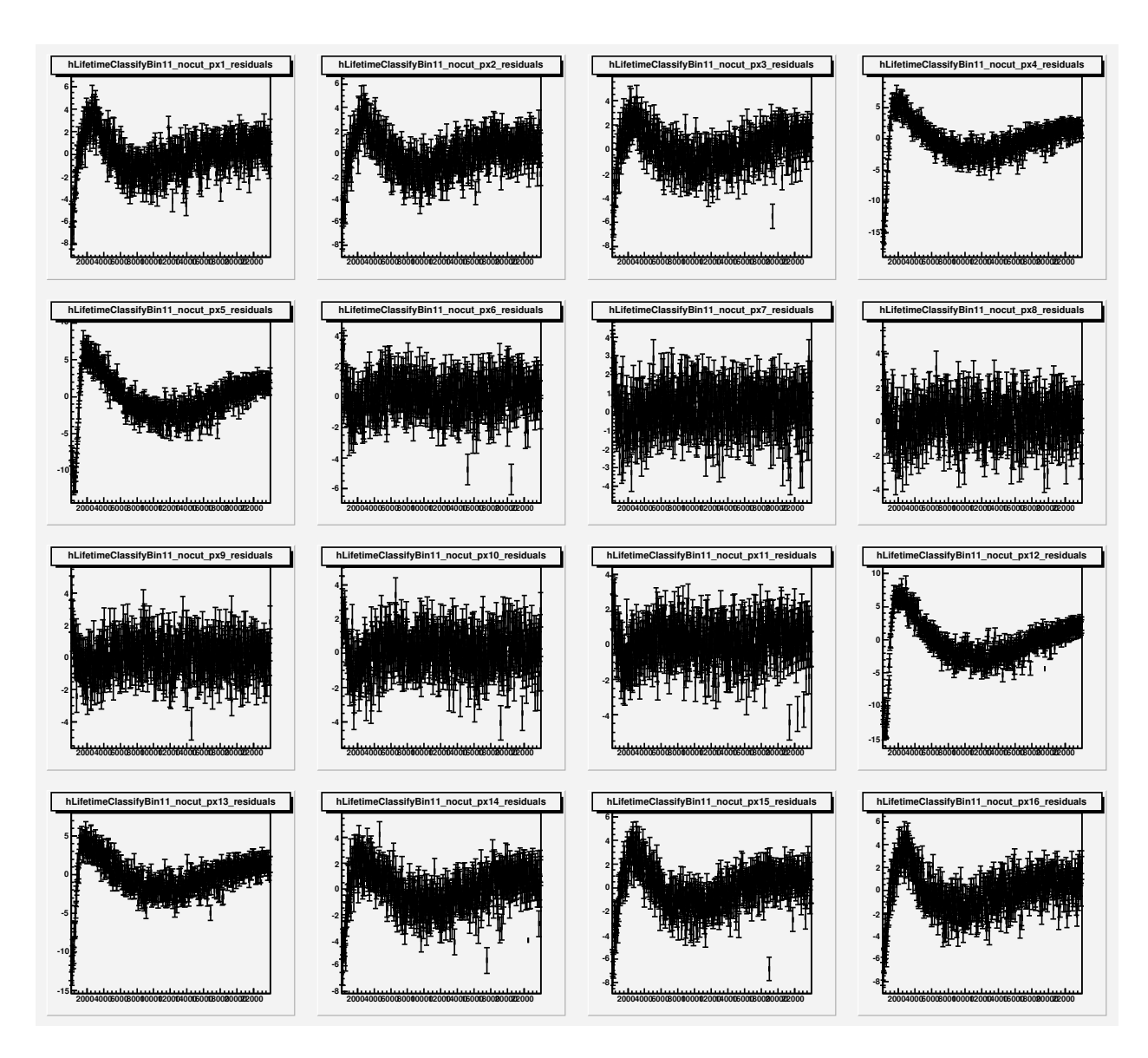


Figure 7.2: Residuals of Lifetime Fits vs. eSC Segment, of lifetime spectra requiring exactly 1 extra EL pixel. eSC segments 1-16 are shown in order left to right, top to bottom.

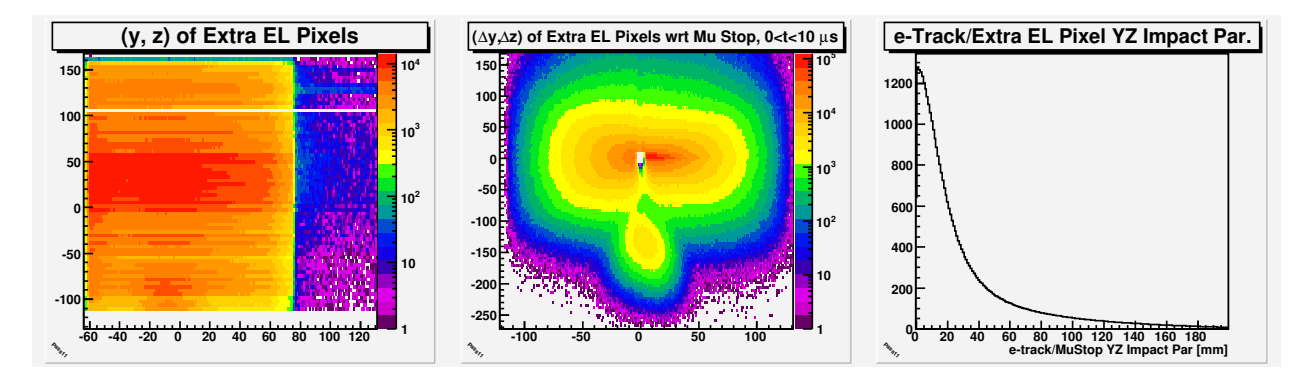


Figure 7.3: Spatial distributions of TPC EL pixels unconnected to the muon track, selecting events that have fewer than 8 of these in the region of interest of a muon stop. Left: absolute position of the pixels in the (y, z)-plane. Middle: position of the pixels with respect to the muon stop position. Right: distance of closest approach ("impact parameter") of electron track vectors to the extra EL pixels.

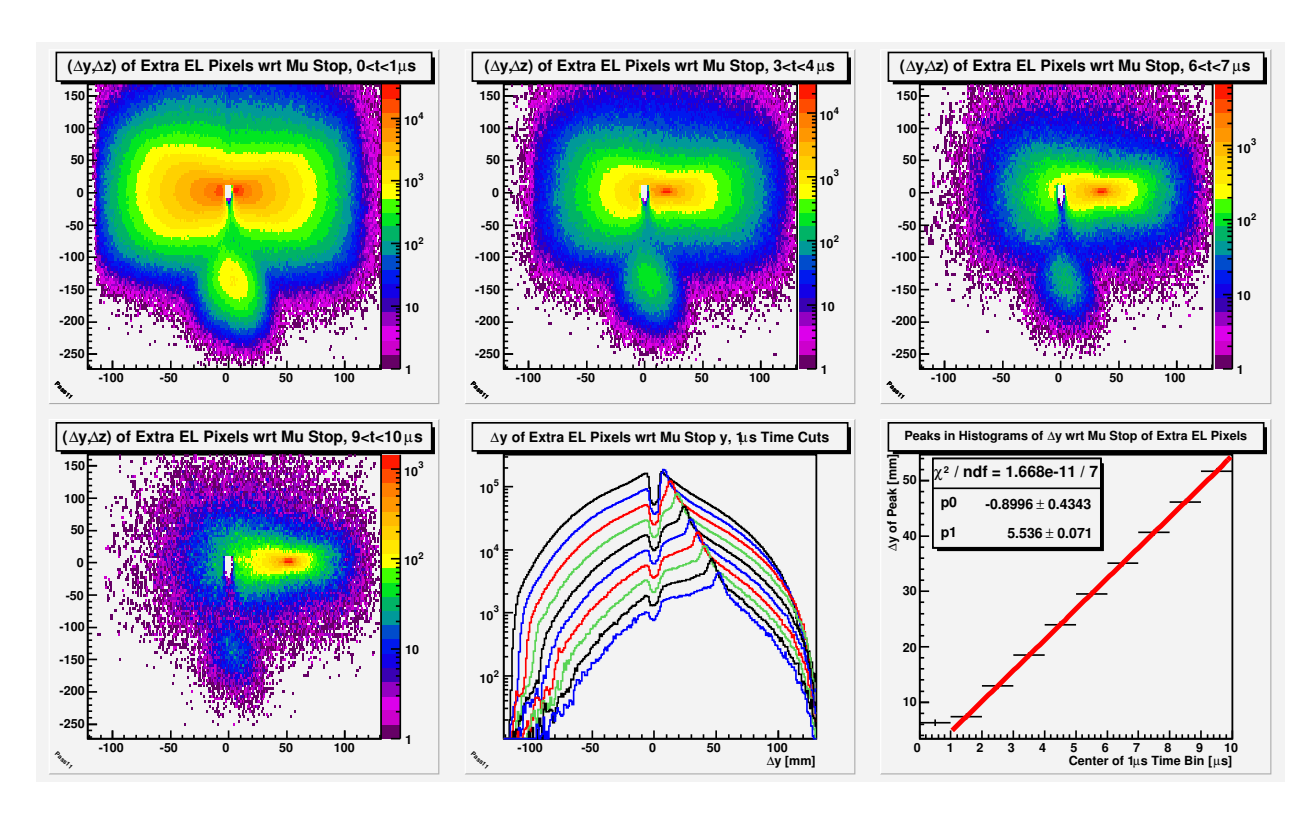


Figure 7.4: Spatial distributions with respect to the mu stop position of TPC EL pixels unconnected to the muon track vs. muon decay time, selecting events that have fewer than 8 of these in the region of interest of a muon stop. The histograms are (moving left to right, top to bottom): Panels 1 to 4: position of the pixels with respect to the muon stop position for events with e-decays in the time interval specified in the histogram titles. Panel 5: projections onto the Δy -axis of the $(\Delta y, \Delta z)$ distibutions of panels 1 to 4, also including distributions of other time intervals not shown. Panel 6: positions (Δy) of the peaks of panel 5 vs. corresponding decay time intervals; a linear fit is also shown, excluding the $0 < t_{decay} < 1\mu s$ peak, which is distorted by the muon track.

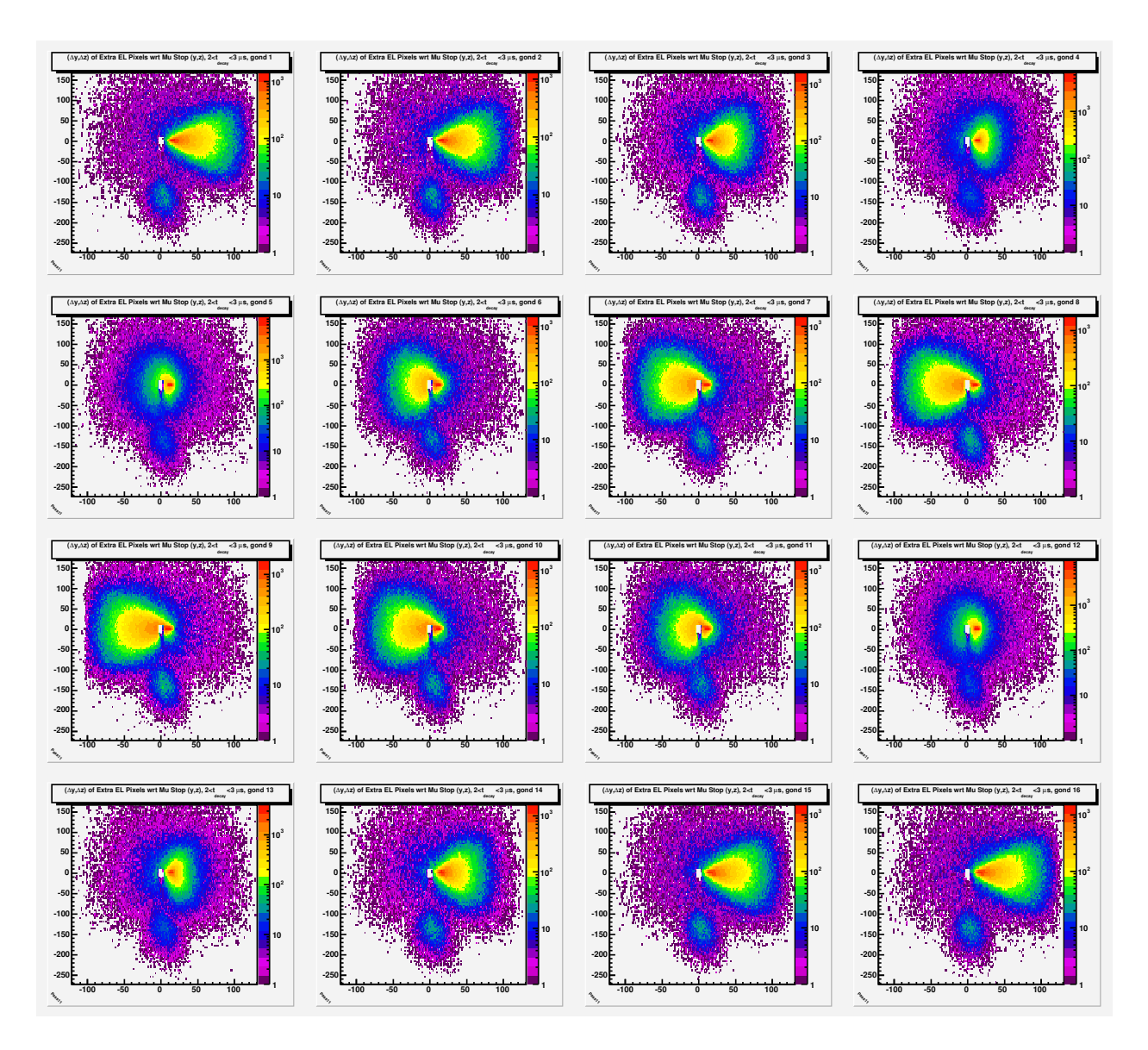


Figure 7.5: Spatial distributions $(\Delta y, \Delta z)$ with respect to the mu stop position of TPC EL pixels unconnected to the muon track vs. eSC Segment, selecting events that have fewer than 8 of these in the region of interest of a muon stop, and with e-track times between 2 and 3 μ s. The histograms are for electron tracks hitting gondolas 1 to 16 (left to right, top to bottom). The distributions are consistent with the hypothesis that extra EL pixels are occasionally deposited along the path of the decay electron.

$\mu + p$ Scatters

Occasionally a muon can scatter off a proton at a large angle, imparting enough energy to the proton that it creates an EH pixel. This can mimic a good muon stop if 1) the muon had already slowed enough to leave a track of EL pixels and 2) the muon scatters to a trajectory for which the TPC is less efficient, leaving large gaps in the track (see fig 4.13). In general we want to eliminate these scatter events, as they are not fully tracked to the stop position and could end up in wall material. There is nothing we can do if the scattered muon leaves very few EL pixels: these cannot be distiguished from extra EL pixels left by delta electrons, and therefore cannot be cut without distorting the lifetime spectrum (see chapter 7).

Scattered muons that leave enough extra EL pixels in the TPC do have a characteristic pattern, and they can be found in the analysis. The first step is to fit a line to the extra EL pixels. If the χ^2 of the linear fit is reasonable, and the line points toward the muon stop position, then the extra EL pixels are likely left by a scattered muon, and the event can be eliminated. Figure 8.1 shows the " χ^2/N ", in this case a figure-of-merit of the linear fit with errors set to 1, and the "impact parameter" of the line to the apparent muon stop position; impact parameter values of < 3 wires seem to indicate scatter events.

Figure 8.2 shows lifetime fits to all muon tracks and recognized scatter events. Although the scatter events result in a significantly higher λ , there are so few of them that the effect is small, $\sim 1 \text{ s}^{-1}$ when mixed with the main data, much smaller than the Run8 statistical error. That is, for the events that are recognized as scatters in the analysis, the effect on the lifetime is small. These recognized scatters were not removed from most lifetime spectra, and a correction will be made to the final result to account for this.

To make this more quantitative, a lifetime spectrum was prepared with a 120 mm impact parameter cut and recognized scatters removed. The (analysis Pass11) lifetime is $455434.0 \pm 12.1 \text{ s}^{-1}$ with scatters included and $455432.9 \pm 12.1 \text{ s}^{-1}$ with recognized scatters excluded, a difference of -1.1 s^{-1} . Tom Banks has done SRIM studies to help constrain the number of unseen scatter events, and we should consider these when deciding on the final correction for $\mu + p$ scatters.

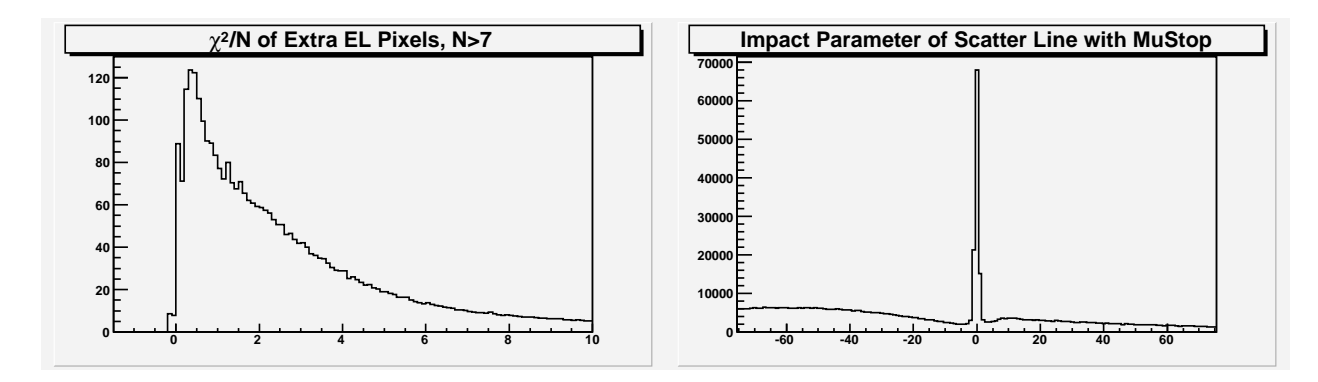


Figure 8.1: Scatter-finding Histograms. Left: χ^2/N of linear fit to extra EL pixels, where N is the number of extra EL pixels, and $N \geq 8$. Right: distance (impact parameter b) in the yz-plane between the linear fit to the extra EL pixels ($N \geq 8$) and the muon stop position. Scatter events are identified by at least 8 extra EL pixels, and a linear fit to these pixels with $\chi^2/N < 1$ and |b| < 3 pixels.

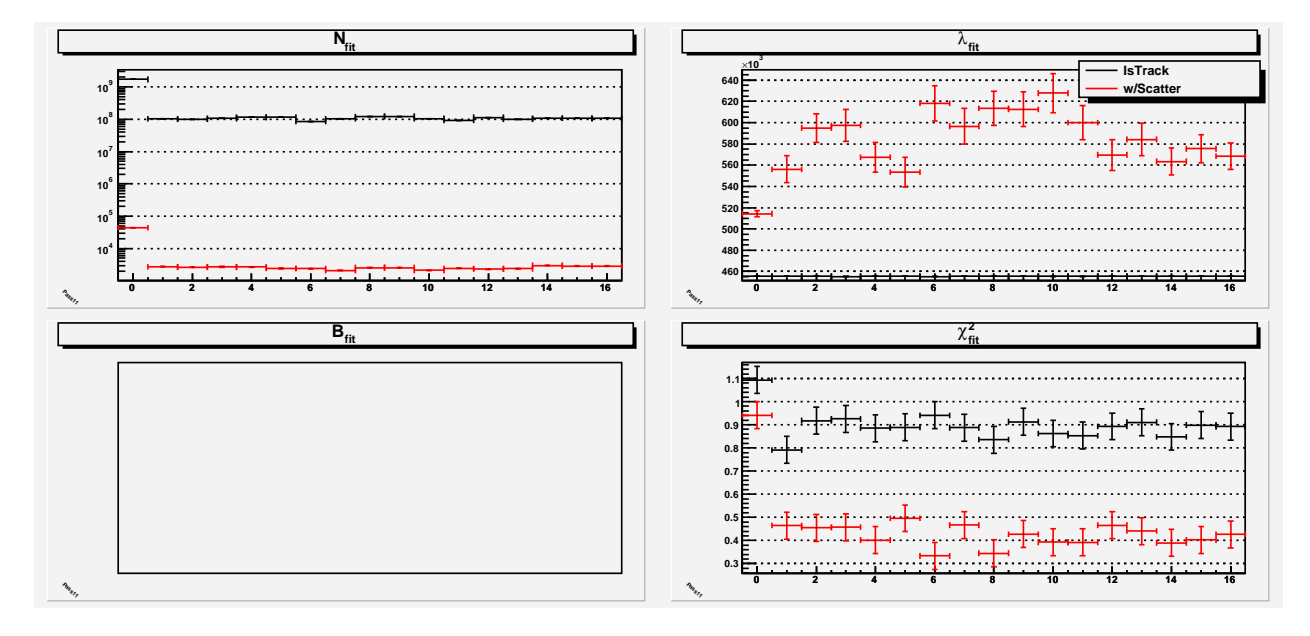


Figure 8.2: Fit results for all muon tracks within the fiducial volume (black) and all identified scatter events (red). No impact parameter cut is imposed.

"Cosmics" Contribution to Background

Particles that traverse the electron detector, starting from external sources, can lead to double counting in the backgrounds of lifetime spectra. Figure 9.1 illustrates a throughgoing track, and figure 9.2 shows evidence of these in the data. As will be demonstrated in this chapter, the effect of double counting on the lifetime result appears to be minimal, $\sim 0.1 \, \rm s^{-1}$, but the χ^2 of the lifetime fit improves significantly. It will also be shown that we can attribute approximately half of the flat background to doubly counted throughgoing tracks, regardless of whether or not a 120 mm impact parameter cut is imposed.

The calculation of how to correct the bin errors for double counting in the flat background begins by defining a given bin as comprised of signal S and background B. B is further comprised of the doubly-counted particles B_{double} and singly-counted B_{single} ; if each particle were counted only once, instead of $B = B_{single} + B_{double}$, it would be $B_{correct} = B_{single} + B_{double}/2$. If uncorrected, the error of B is taken to be the usual $\sigma_B = \sqrt{B}$. However, the single and double components should be considered separately and their errors added in quadrature.

$$\begin{split} &\sigma_{B,single} = \sqrt{B_{single}} \\ &\sigma_{B,double} = 2\sqrt{B_{double}/2} = \sqrt{2B_{double}} \\ &\sigma_{B} = \sqrt{\sigma_{B,single}^2 + \sigma_{B,double}^2} = \sqrt{B_{single} + 2B_{double}} \end{split}$$

. The last equation, for the corrected error of B, can be rewritten in terms of the fraction of the flat background due to doubly-counted particles, $m = B_{double}/B$:

$$\sigma_B = \sqrt{B + mB} = \sqrt{(1+m)B}. (9.1)$$

The total error for a given histogram bin with contents C is $\sigma_C = \sqrt{\sigma_B^2 + \sigma_S^2}$. Rewriting S = C - B and some substitutions gives:

$$\sigma_C = \sqrt{(1+m)B + C - B} = \sqrt{C + mB}.$$
(9.2)

The procedure for correcting the bin errors of a given lifetime spectrum, for example the black spectrum of figure 9.3, could go something like this:

- 1. Under the same conditions as the lifetime spectrum, fill a similar histogram selecting only electron tracks that are time coincident with another track, and have $|\phi_1 \phi_2| > 2.6$. This is the blue spectrum in figure 9.3.
- 2. Fit both spectra (the original and the "cosmics"), and take the ratio of the *B*-terms to find m, $m = B_{cosmics}/B_{all}$. Table 9.1, rows 1 and 3 show these fits, and we see that $m \approx 0.5$.
- 3. For each bin of the lifetime spectrum, recalculate the errors according to equation 9.2.
- 4. Fit the spectrum again using the corrected bin errors. Results for the example are shown in last row of table 9.1 and should be compared to the first row, which is the fit with uncorrected bin errors.

Fits to spectra as described by the above procedure are shown in table 9.1, for the lifetime spectra with 120 mm impact parameter cut, and table 9.2, for the lifetime spectra with no impact parameter cut. In both cases, and in spite of quite different total background levels, the fraction of the background due to throughgoing tracks is $m \approx 0.5$. It may be also interesting to note, that by comparing the spectrum of all time-coincident electrons with the spectrum of time-coincident, ϕ -opposite electrons, we see that the flat backgound of the former is almost entirely accounted for by the latter.

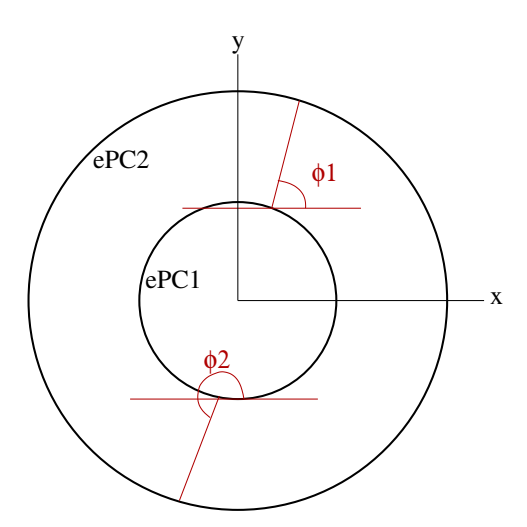


Figure 9.1: Beam-view Diagram of ϕ of Electron Track. Time-coincident electron tracks with $|\phi_1 - \phi_2| > 2.6$ are considered throughgoing tracks.

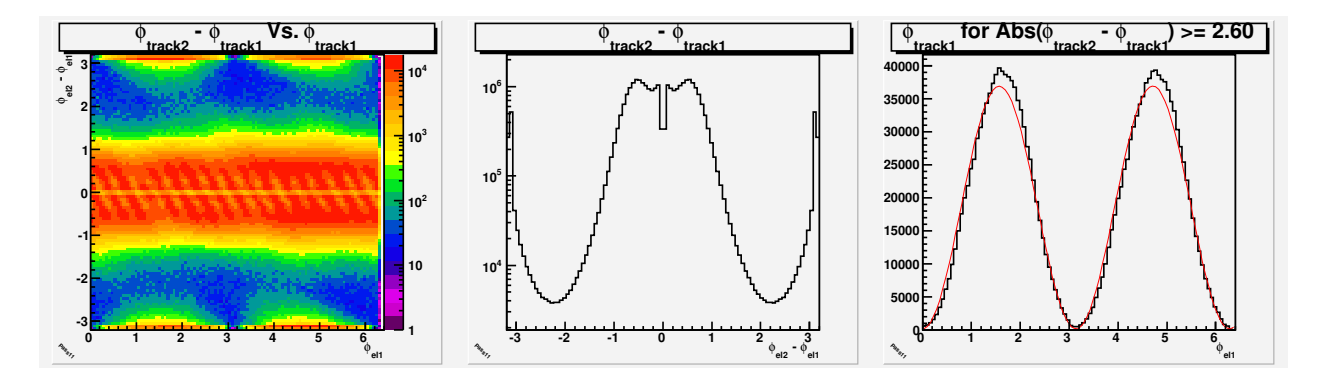


Figure 9.2: Relative Angle in the (x, y)-plane of Time-Coincident e-Detector Tracks, 120 mm Impact Parameter Cut with a MuStop. Left: $\Delta \phi$ vs. ϕ of one of the tracks; Middle: projection of the leftmost histogram onto the $\Delta \phi$ axis; Right: projection of the leftmost histogram onto the ϕ axis for $|\Delta \phi| \geq 2.6$. Time-coincident electron tracks with $|\Delta \phi| > 2.6$ are considered throughgoing tracks.

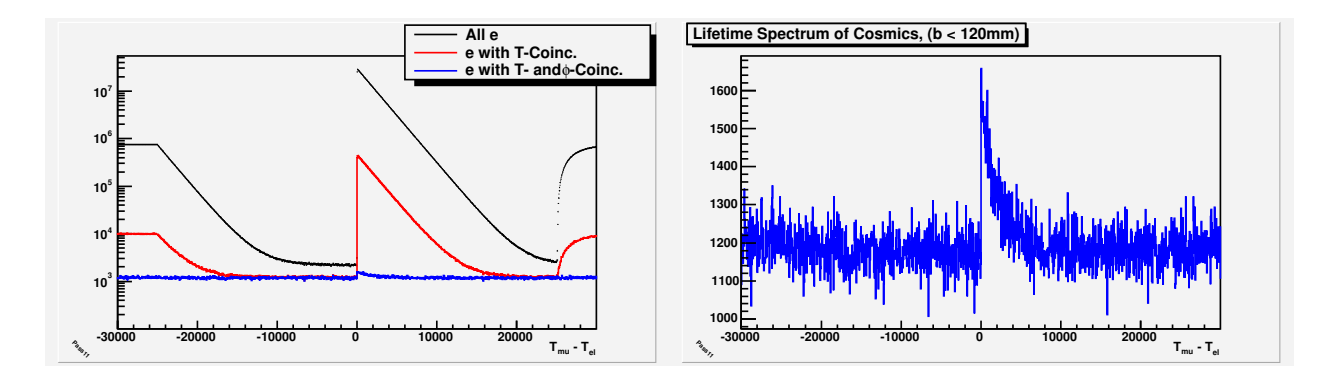


Figure 9.3: Spectra of Throughgoing Tracks Study, 120 mm Impact Parameter Cut. Muons are stopped within the TPC fiducial volume; electrons are fully tracked (eSC×ePC1×ePC2); and a 120 mm impact parameter cut is imposed.

	N	$\lambda [\mathrm{s}^{-1}]$	В	B/N	χ^2/DOF
all e	1.632×10^{9}		2191.8 ± 5.1	1.343×10^{-6}	1.05 ± 0.06
T-coinc. e	2.520×10^{7}	455372.6 ± 108.0	1215.5 ± 2.3	4.824×10^{-5}	1.82 ± 0.06
T-coinc. and ϕ -opp. e	2.067×10^4	501877.2 ± 20909.4	1178.1 ± 1.7	5.701×10^{-2}	1.81 ± 0.06
T-coinc. and NOT ϕ -opp. e	2.518×10^{7}	455311.8 ± 97.1	34.5 ± 0.6		1.96 ± 0.06
all e, errs. adjusted, $m = 0.54$	1.632×10^{9}	455434.0 ± 12.1	2191.3 ± 5.7	1.343×10^{-6}	0.97 ± 0.06
Pass11					

Table 9.1: Fits to Spectra of Throughgoing Tracks Study, 120 mm Impact Parameter Cut. The fit function is $y = Nw\lambda e^{-\lambda t} + B$, where w is the (fixed) bin width of 40 ns; the fit range is 0.1 μ s to 24 μ s. Muons are stopped within the TPC fiducial volume; electrons are fully tracked (eSC×ePC1×ePC2); and a 120 mm impact parameter vertex cut is imposed. "T-coinc. e" means time-coincident electron tracks. " ϕ -opp.," or " ϕ -opposite," means time-coincident electron tracks with $|\phi_1 - \phi_2| > 2.6$. The fit of the last row is of the lifetime spectrum after correcting bin errors by the procedure suggested in this chapter.

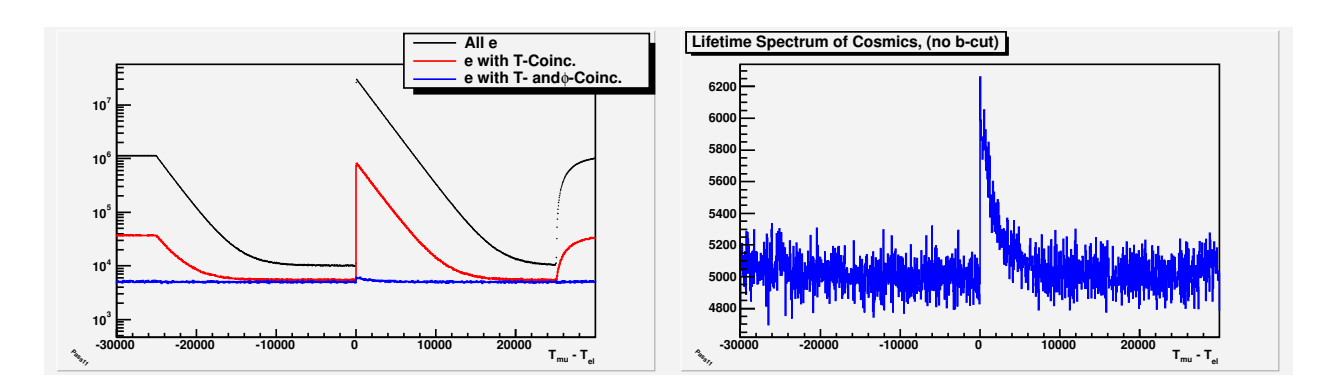


Figure 9.4: Spectra of Throughgoing Tracks Study, No Impact Parameter Cut. Muons are stopped within the TPC fiducial volume; electrons are fully tracked (eSC×ePC1×ePC2); and no impact parameter cut is imposed.

	N	$\lambda [\mathrm{s}^{-1}]$	В	B/N	χ^2/DOF
all e	1.710×10^9	455419.7 ± 12.1	10105.0 ± 8.3		
T-coinc. e	4.633×10^{7}	455387.1 ± 85.0		1.182×10^{-4}	
T-coinc. and ϕ -opp. e	5.176×10^4	490795.6 ± 16771.2	5012.3 ± 3.6	9.684×10^{-2}	1.90 ± 0.06
T-coinc. and NOT ϕ -opp. e	4.628×10^{7}	455301.9 ± 74.4		9.903×10^{-6}	
all e, errs. adjusted, $m = 0.50$	1.710×10^{9}	455419.8 ± 12.2	10105.3 ± 9.5	5.911×10^{-6}	1.09 ± 0.06

Pass11

Table 9.2: Fits to Spectra of Throughgoing Tracks Study, No Impact Parameter Cut. The fit function is $y = Nw\lambda e^{-\lambda t} + B$, where w is the (fixed) bin width of 40 ns; the fit range is 0.1 μ s to 24 μ s. Muons are stopped within the TPC fiducial volume; electrons are fully tracked (eSC×ePC1×ePC2); and no impact parameter vertex cut is imposed. "T-coinc. e" means time-coincident electron tracks. " ϕ -opp.," or " ϕ -opposite," means time-coincident electron tracks with $|\phi_1 - \phi_2| > 2.6$. The fit of the last row is of the lifetime spectrum after correcting bin errors by the procedure suggested in this chapter.

Muon Lifetime Studies

Lifetime spectra are fit with the usual exponential plus flat background,

$$f(t) = N\lambda w e^{-\lambda t} + B, (10.1)$$

where w is fixed to the lifetime histogram bin width of 40 ns, and N, λ , and B are fit parameters. Unless otherwise noted, the lifetime spectra with complete electron detector tracking, requiring an OR of the cathodes in each ePC, is used. The standard fit range is 100 ns to 24000 ns; considering the binning phase of the lifetime spectra, the effective fit range is 120 ns to 24000 ns after the muon stop. Bin errors are corrected for double counting in the flat background with m = 0.50 (see chapter 9), except in the case of "1 electron gated" spectra, which exclude double counting events by construction.

10.1 Lifetime vs. eDetector Treatment

Here we compare the lifetime dependence on how we choose to define an electron event. Fit results are shown in Figure 10.1 and table 10.1. No impact parameter cut is imposed on any of these spectra to facilitate comparison with the eSC-only case; however, there are implicit geometrical cuts when taking the ePC1 and ePC2 in coincidence as in the complete e-detector tracks. The different cases considered, with longer descriptions than appear in the table, are listed:

- eSC. The simplest case considered, this ignores all ePC information and defines an electron event as any 4-fold (all four PMTs on a given gondola) coincidence.
- eTrack, AnodesOnly. These are complete e-detector tracks (ePC1×ePC2×eSC) in which ePC cathode data are ignored.
- eTrack, CathOR. These are complete e-detector tracks (ePC1×ePC2×eSC) in which individual ePC hits are required to have anode and one or the other or both cathode planes.
- eTrack, CathAND. These are complete e-detector tracks (ePC1×ePC2×eSC) in which individual ePC hits are required to have anode and both cathode planes.

The next four rows in table 10.1 are of the same detector conditions as above, but only one electron is allowed in the range -10 μ s to 24.5 μ s around the muon stop. For the electron

tracks in these "1e" spectra, any ambiguities that were flagged in the raw data analysis stage also veto the muon.

The lifetimes in most cases appear to be more or less statistically consistent. Numerical studies were done to show that the lifetime difference between the "eSC" and "eTrack, CathOR" is statistically allowed at 1σ . The other differences still need to be similarly studied in detail, but at the moment I see no reason not to continue to favor the "eTrack, CathOR" lifetime.

	N	$\lambda [\mathrm{s}^{-1}]$	В	B/N	χ^2/DOF
eSC	1.819×10^9	455425.1 ± 12.6	48552.3 ± 17.8	2.670×10^{-5}	1.00 ± 0.06
eTrack, AnodesOnly	1.749×10^9	455417.2 ± 12.1	10384.8 ± 9.7	5.937×10^{-6}	1.10 ± 0.06
eTrack, CathOR	1.710×10^{9}	455419.8 ± 12.2	10105.3 ± 9.5	5.911×10^{-6}	1.09 ± 0.06
eTrack, CathAND	1.610×10^9	455415.6 ± 12.6	9410.6 ± 9.2	5.845×10^{-6}	1.08 ± 0.06
eSC, 1e	1.734×10^9	455424.2 ± 11.9	8557.7 ± 7.8	4.935×10^{-6}	1.00 ± 0.06
eTrack, AnodesOnly, 1e	1.564×10^9	455421.4 ± 12.2	1242.0 ± 4.4	7.943×10^{-7}	1.00 ± 0.06
eTrack, CathOR, 1e	1.526×10^{9}	455423.4 ± 12.4	1292.1 ± 4.4	8.466×10^{-7}	1.01 ± 0.06
eTrack, CathAND, 1e	1.457×10^9	455419.5 ± 12.7	1475.6 ± 4.5	1.013×10^{-6}	1.02 ± 0.06

Pass11

Table 10.1: Lifetime vs. eDetector Treatment. Muons are stopped within the TPC fiducial volume, and no impact parameter cut is imposed on any of the spectra.

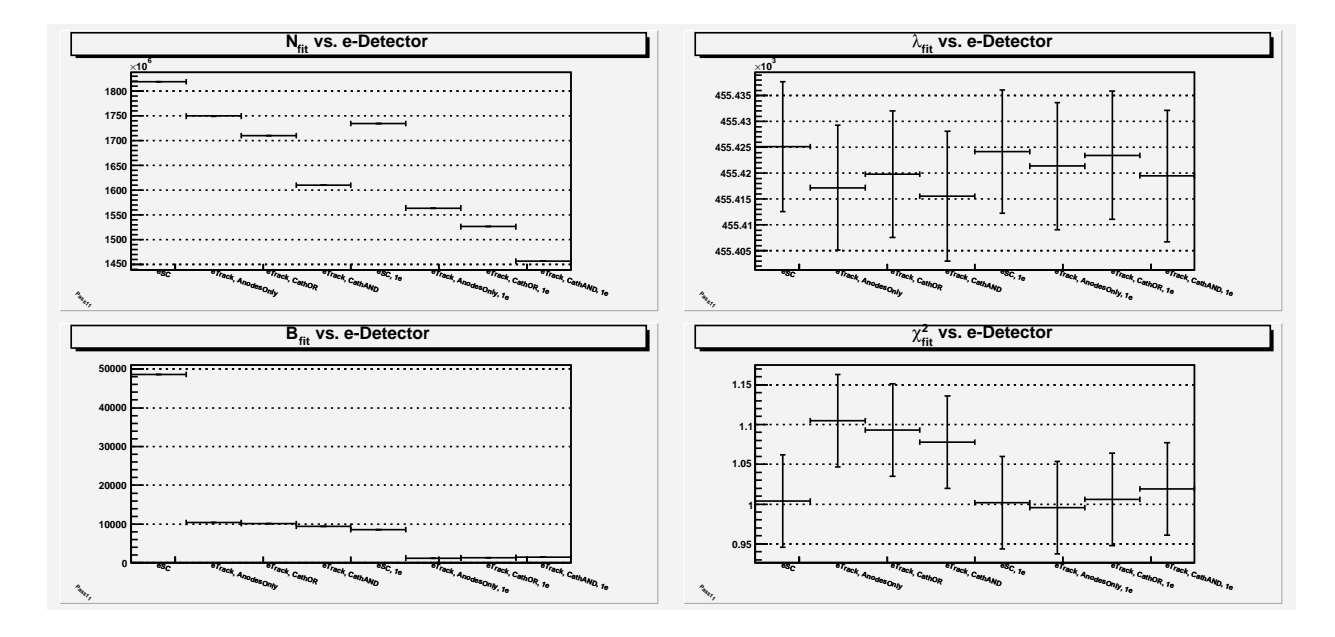


Figure 10.1: Lifetime vs. eDetector Treatment. Muons are stopped within the TPC fiducial volume, and no impact parameter cut is imposed on any of the spectra.

10.2 Lifetime vs. Muon-Electron Vertex Cut

In this study, lifetime histograms are filled based on the distance of closest approach of electrons tracked back to the muon stop position, the "impact parameter" b. Table 10.2

shows fit results to spectra with $b < b_{cut}$, where b_{cut} is the value in the first column; the fit parameters in the table are plotted in figure 10.2. The strong deviation of lifetime with impact parameter cut is caused by μp and μd diffusion, as will be explained in chapter 12.

Impact Parameter [mm]	N	$\lambda [\mathrm{s}^{-1}]$	В	B/N	χ^2/DOF
10	2.243×10^{8}	456543.7 ± 32.1	15.5 ± 1.3	6.905×10^{-8}	1.00 ± 0.06
20	6.622×10^{8}	456158.0 ± 18.7	60.9 ± 2.2	9.198×10^{-8}	1.00 ± 0.06
30	1.008×10^9	455800.2 ± 15.2	133.4 ± 2.8	1.324×10^{-7}	0.99 ± 0.06
40	1.222×10^9	455618.6 ± 13.8	241.8 ± 3.3	1.979×10^{-7}	0.99 ± 0.06
50	1.353×10^{9}	455542.1 ± 13.1	382.0 ± 3.6	2.822×10^{-7}	0.99 ± 0.06
60	1.438×10^9	455496.5 ± 12.7	550.3 ± 4.0	3.826×10^{-7}	1.00 ± 0.06
70	1.497×10^{9}	455467.6 ± 12.5	749.5 ± 4.3	5.007×10^{-7}	1.01 ± 0.06
80	1.539×10^{9}	455453.4 ± 12.4	980.1 ± 4.6	6.367×10^{-7}	1.02 ± 0.06
90	1.571×10^9	455444.6 ± 12.3	1240.0 ± 4.9	7.891×10^{-7}	1.02 ± 0.06
100	1.596×10^{9}	455439.5 ± 12.2	1528.4 ± 5.1	9.575×10^{-7}	1.01 ± 0.06
110	1.616×10^9	455436.5 ± 12.1	1844.8 ± 5.4	1.141×10^{-6}	0.99 ± 0.06
120	1.632×10^9	455434.0 ± 12.1	2191.4 ± 5.7	1.343×10^{-6}	0.97 ± 0.06
130	1.645×10^{9}	455432.1 ± 12.1	2566.7 ± 6.0	1.560×10^{-6}	0.98 ± 0.06
140	1.656×10^{9}	455429.8 ± 12.1	2964.7 ± 6.3	1.790×10^{-6}	0.98 ± 0.06
150	1.665×10^{9}	455428.6 ± 12.1	3383.9 ± 6.5	2.033×10^{-6}	1.00 ± 0.06

Pass11

Table 10.2: Lifetime vs. Impact Parameter Cut. Muons are stopped within the TPC fiducial volume; electrons are fully tracked (eSC×ePC1×ePC2); and the impact parameter cut indicated on the x-axis is imposed. As argued in chapter 12, the deviation of lifetime with impact parameter cut is explained by μp and μd diffusion.

10.3 Lifetime vs. TPC Fiducial Volume

The purpose of this study is to confirm that the standard fiducial volume is sufficiently far from TPC boundaries. The TPC volume is logically divided into a series of nested boxes, starting with the largest fiducial volume possible and becoming successively smaller. The space between each box and the next smaller one is a fiducial volume shell. Since there is no overlap between different volume shells, the lifetime spectra vs. volume shell are statistically independent. Fit results are shown in figure 10.3 (no impact parameter cut) and figure 10.4 (120 mm impact parameter cut). The standard fiducial volume, indicated by the vertical green line in the figures, seems fine.

10.4 Lifetime vs. eSC Segment ("Gondola")

Lifetime histograms are filled based on which eSC segment (1-16) is included in the electron track. Fit results are shown in Figure 10.5 and table 10.3. The lifetime vs. eSC segment are statistically consistent.

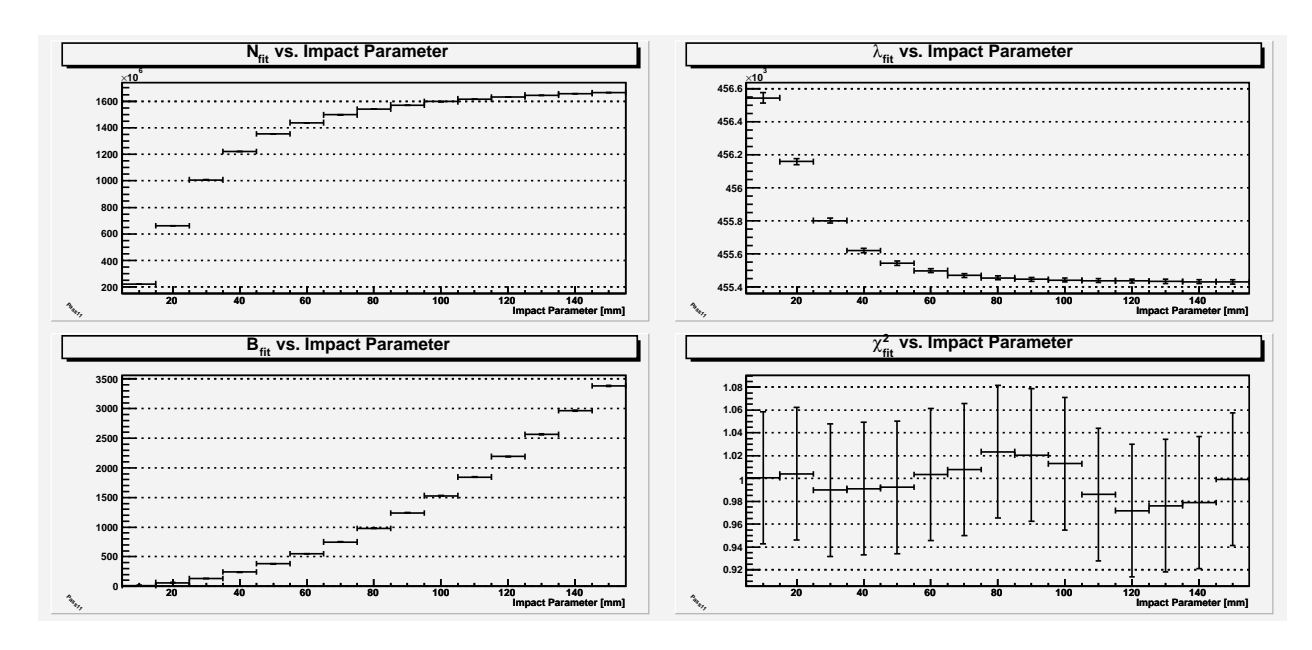


Figure 10.2: Lifetime vs. Impact Parameter Cut. Muons are stopped within the TPC fiducial volume; electrons are fully tracked (eSC×ePC1×ePC2); and the impact parameter cut indicated on the x-axis is imposed. As argued in chapter 12, the deviation of lifetime with impact parameter cut is explained by μp and μd diffusion.

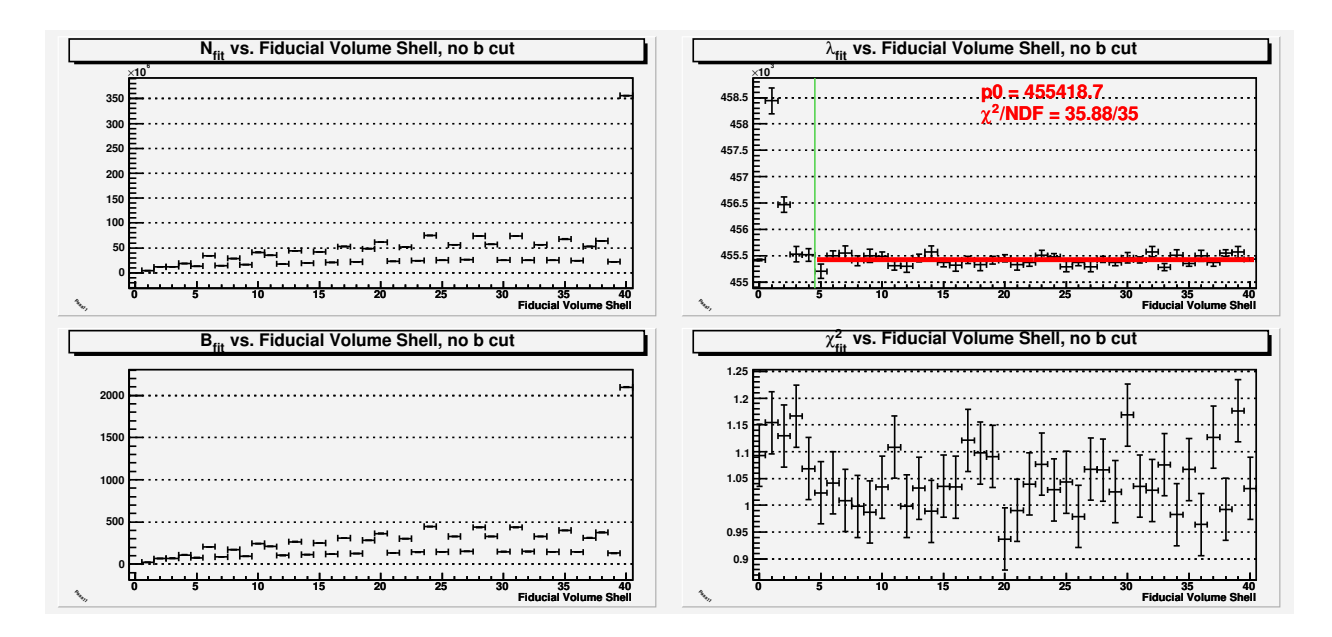


Figure 10.3: Lifetime vs. TPC Fiducial Volume Shell, No Impact Parameter Cut. The fit parameters in the leftmost bin are for reference: they are from stops in the standard fiducial volume in the UIUC analysis ("BetterBox"), which are well away from the walls. The rest of the fits represent statistically independent data of muon stops in successively smaller, nested volume shells. The shells are of uniform thickness ≈ 1.1 mm, except the volume corresponding to the rightmost bin, which does not have an inner bounding surface. The sum of all events included in the fits to the right of the vertical green line are those of the standard UIUC fiducial volume ("BetterBox"). The spectra are of fully tracked electrons (eSC×ePC1×ePC2), and no impact parameter vertex cut is imposed.

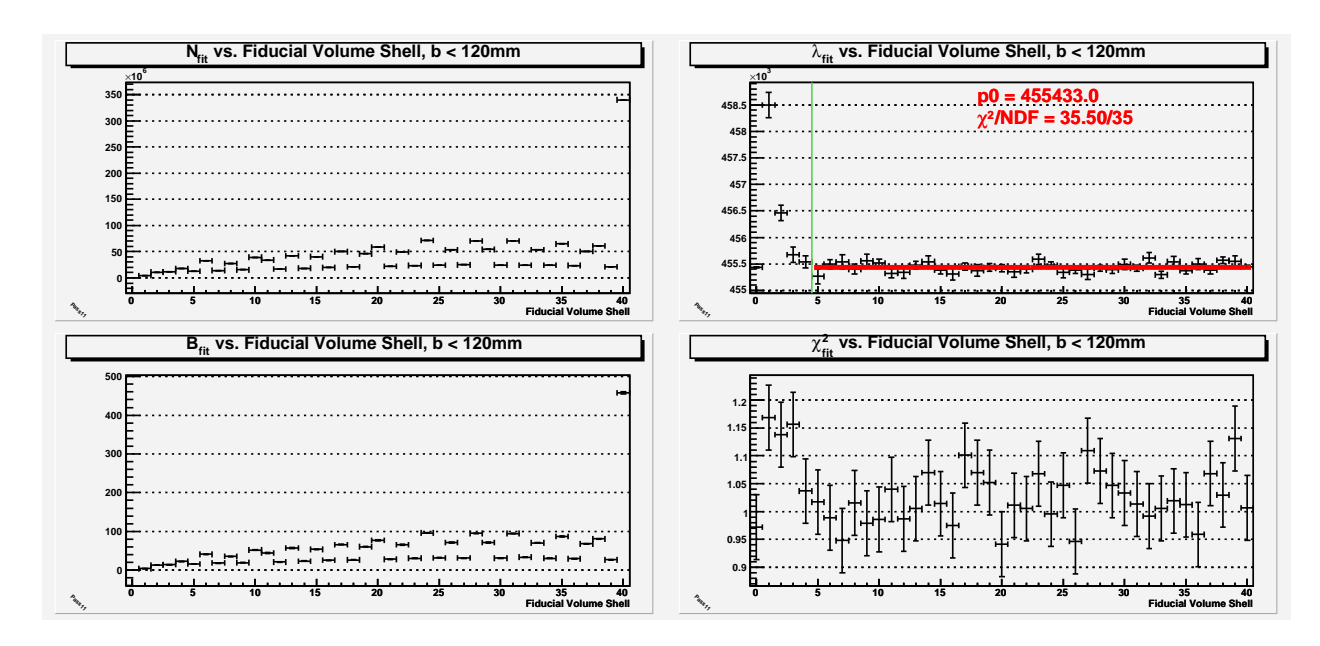


Figure 10.4: Lifetime vs. TPC Fiducial Volume Shell, 120 mm Impact Parameter Cut. This is the same study as in figure 10.3 except for the impact parameter condition.

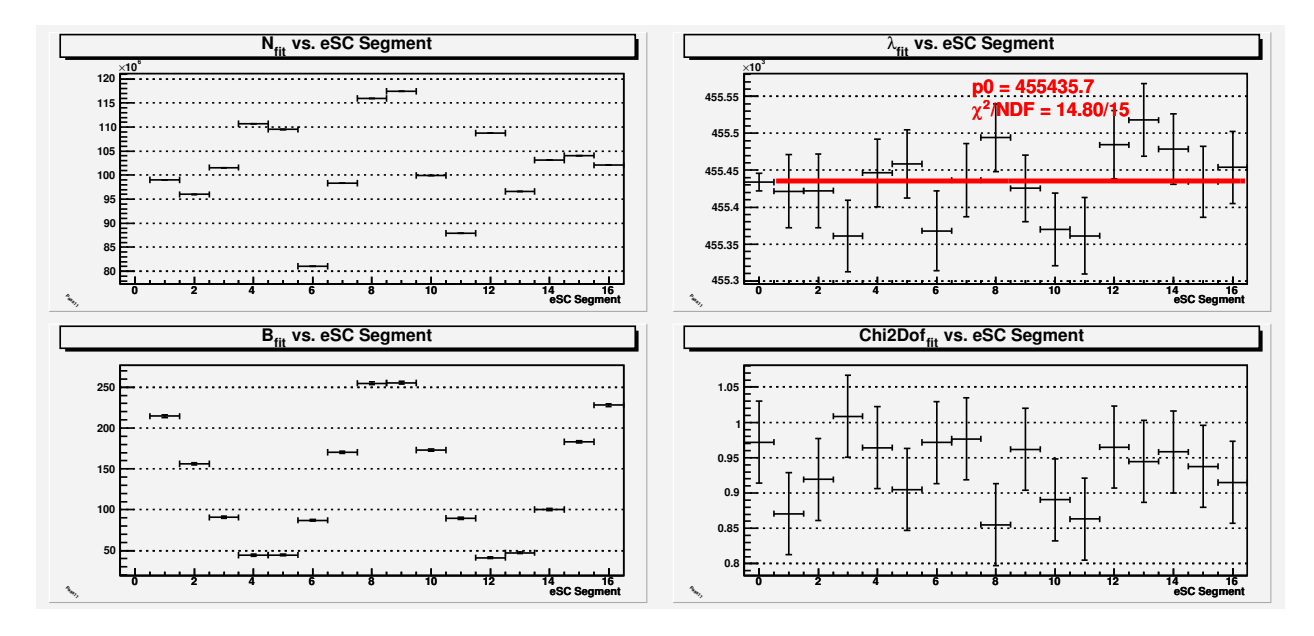


Figure 10.5: Lifetime vs. eSC Segment, 120 mm Impact Parameter Cut. Muons are stopped within the TPC fiducial volume; electrons are fully tracked (eSC \times ePC1 \times ePC2); and a 120 mm impact parameter cut is imposed. Bin 0 is the fit to the sum over all eSC segments.

eSC Segment	N	$\lambda [\mathrm{s}^{-1}]$	В	B/N	χ^2/DOF
0	1.632×10^{9}	455434.0 ± 12.1	2191.4 ± 5.7	1.343×10^{-6}	0.97 ± 0.06
1	9.901×10^{7}	455421.6 ± 49.5	214.5 ± 1.6	2.166×10^{-6}	0.87 ± 0.06
2	9.598×10^{7}	455422.2 ± 50.1	156.2 ± 1.5	1.628×10^{-6}	0.92 ± 0.06
3	1.016×10^{8}	455360.9 ± 48.3	90.7 ± 1.3	8.928×10^{-7}	1.01 ± 0.06
4	1.107×10^{8}	455446.3 ± 45.9	44.5 ± 1.1	4.015×10^{-7}	0.96 ± 0.06
5	1.095×10^{8}	455458.5 ± 46.2	44.7 ± 1.1	4.079×10^{-7}	0.90 ± 0.06
6	8.106×10^{7}	455367.9 ± 54.2	87.0 ± 1.2	1.074×10^{-6}	0.97 ± 0.06
7	9.834×10^{7}	455436.4 ± 49.5	170.3 ± 1.5	1.732×10^{-6}	0.98 ± 0.06
8	1.160×10^{8}	455494.3 ± 45.8	254.7 ± 1.8	2.196×10^{-6}	0.86 ± 0.06
9	1.175×10^{8}	455425.4 ± 45.5	255.3 ± 1.8	2.174×10^{-6}	0.96 ± 0.06
10	9.993×10^{7}	455369.9 ± 49.1	172.9 ± 1.5	1.730×10^{-6}	0.89 ± 0.06
11	8.792×10^7	455361.1 ± 52.0	89.4 ± 1.2	1.017×10^{-6}	0.86 ± 0.06
12	1.088×10^{8}	455484.4 ± 46.3	41.2 ± 1.1	3.786×10^{-7}	0.96 ± 0.06
13	9.663×10^{7}	455518.0 ± 49.3	47.2 ± 1.1	4.888×10^{-7}	0.94 ± 0.06
14	1.031×10^{8}	455478.6 ± 48.0	100.3 ± 1.3	9.724×10^{-7}	0.96 ± 0.06
15	1.041×10^{8}	455434.4 ± 48.1	183.2 ± 1.6	1.760×10^{-6}	0.94 ± 0.06
16	1.021×10^{8}	455454.0 ± 48.8	228.0 ± 1.7	2.233×10^{-6}	0.91 ± 0.06

Pass11

Table 10.3: Lifetime vs. eSC Segment, 120 mm Impact Parameter Cut. Muons are stopped within the TPC fiducial volume; electrons are fully tracked (eSC×ePC1×ePC2); and a 120 mm impact parameter vertex cut is imposed. Bin 0 is the fit to the sum over all eSC segments.

10.5 Lifetime vs. MuPC Pileup Protection

Pileup protection with the MuPC can use the x- and y-planes as separate detectors or require them to be in coincidence. Table 10.4 shows fit parameters to spectra with different pileup protection levels. All cases have pileup protection with the MuSC.

- muPCX and Y. Coincident x- and y-plane hits are used for pileup protection.
- muPCX. The x-plane is used alone for pileup protection, ignoring the y-plane.
- muPCY. The y-plane is used alone for pileup protection, ignoring the x-plane.
- muPCXorY. The x- and y-planes are used separately for pileup protection. This is the standard, most stringent pileup protection level used in lifetime spectra in the UIUC analysis.

Table 10.5 shows the same lifetimes as in table 10.4 along with estimates of the inefficiencies of the MuPC combinations. If we take these inefficiency estimates seriously and extrapolate to perfect efficiency using the muPCXandY and muPCXorY rows, the correction to the lifetime to account for muPCXorY inefficiency would be $\delta \lambda = +1.1 \text{ s}^{-1}$.

10.6 Lifetime vs. MuSC Artificial Deadtime

The purpose of this study is to check the effect of missing muon pileup events due to the muSC deadtime. Separate versions of the muSC analysis were run, each with a different

artificial deadtime,¹ and each producing an array of muSC hits pileup-protected with itself. The union of the arrays were formed, with flags indicating which of the muSC deadtime conditions led to which entries. The raw analysis then proceeds as normal, with the muSC deadtime flags carried through to the output trees.

Table 10.6 shows the fits to spectra requiring different muSC deadtime conditions. The first row corresponds to the the standard, shortest deadtime. The effect on the lifetime of extending the muSC deadtime appears to be small, +3 s⁻¹ for the very long deadtime of 150 ns. If we do a linear extrapolation to 0 ns deadtime using the 10 ns and 150 ns points, the correction to the lifetime with standard deadtime is $\delta \lambda = -0.2$ s⁻¹.

The last row of the table is a somewhat different muSC study, in which the time independent muSC inefficiency was artificially increased by randomly ignoring 1% of the hits. The effect on the lifetime seems to be minimal, $\approx 1 \text{ s}^{-1}$. We would have to consider the statistical overlap between the spectra of the first and last rows of the table, in order to calculate whether or not the observed lifetime difference is only statistics.

The spectra of table 10.6 were also created with a 120 mm impact parameter cut imposed. Fits to these are shown in table 10.7. The impact parameter cut reduces the effect of the muSC deadtime. Linear extrapolation results in a lifetime correction of $\delta\lambda = -0.06~\rm s^{-1}$, completely negligible.

The contents of tables 10.6 and 10.7 are plotted in figures 10.6 and 10.7, respectively.

10.7 Lifetime vs. ePC Artificial Deadtime

To check the effect of different ePC deadtimes on the lifetime, an analysis pass was done with much shorter ePC deadtime settings of 300 ns (compared to the standard ePC deadtime setting of ≈ 1000 ns), and another pass was done with longer ePC deadtime settings of 2000 ns. The results are summarized in table 10.8, and some details of the study are given in the table caption. Almost no change in the lifetime is observed.

10.8 Fit Start Time Scans

Fit results are shown in Figure 10.8 for the lifetime spectrum with 120 mm impact parameter cut, and figure 10.9 for the lifetime spectrum with no impact parameter cut.

10.9 Fit Stop Time Scans

Fit results are shown in Figure 10.10 for the lifetime spectrum with 120 mm impact parameter cut, and figure 10.11 for the lifetime spectrum with no impact parameter cut.

10.10 Lifetime vs. Run Group

Fit results are shown in Figure 10.12 and table 10.9.

¹Since the raw data skimming is based on the muSC pileup-protected with itself, it was necessary to use unskimmed raw data for this study.

Pileup Protection	N	$\lambda [\mathrm{s}^{-1}]$	В	B/N	χ^2/DOF
muPCXandY	1.714×10^{9}	455431.7 ± 11.8	2407.1 ± 5.9	1.404×10^{-6}	0.98 ± 0.06
muPCX	1.667×10^{9}	455433.8 ± 12.0	2318.4 ± 5.8	1.391×10^{-6}	0.97 ± 0.06
muPCY	1.691×10^{9}	455435.2 ± 11.9	2321.7 ± 5.8	1.373×10^{-6}	0.97 ± 0.06
muPCXorY	1.645×10^{9}	455437.6 ± 12.1	2236.3 ± 5.8	1.360×10^{-6}	0.97 ± 0.06

Pass11

Table 10.4: Lifetime vs. MuPC Pileup Protection. Muons are stopped within the TPC fiducial volume, and a 120 mm impact parameter cut is imposed.

Pileup Protection	Ineff. Estimate	$\lambda [\mathrm{s}^{-1}]$
muPCXandY	6.193×10^{-4}	455431.7 ± 11.8
muPCX	4.614×10^{-4}	455433.8 ± 12.0
muPCY	2.556×10^{-4}	455435.2 ± 11.9
muPCXorY	9.750×10^{-5}	455437.6 ± 12.1

Pass11

Table 10.5: Lifetime vs. MuPC Pileup Protection Inefficiency. These are the same lifetimes as in table 10.4. The efficiency of a given MuPC combination is estimated by taking the number of entrances with that combination in coincidence with the MuSC, and dividing by the total number of entrances with the MuSC; all entrances counted for this estimate are pileup protected with MuPCXorY.

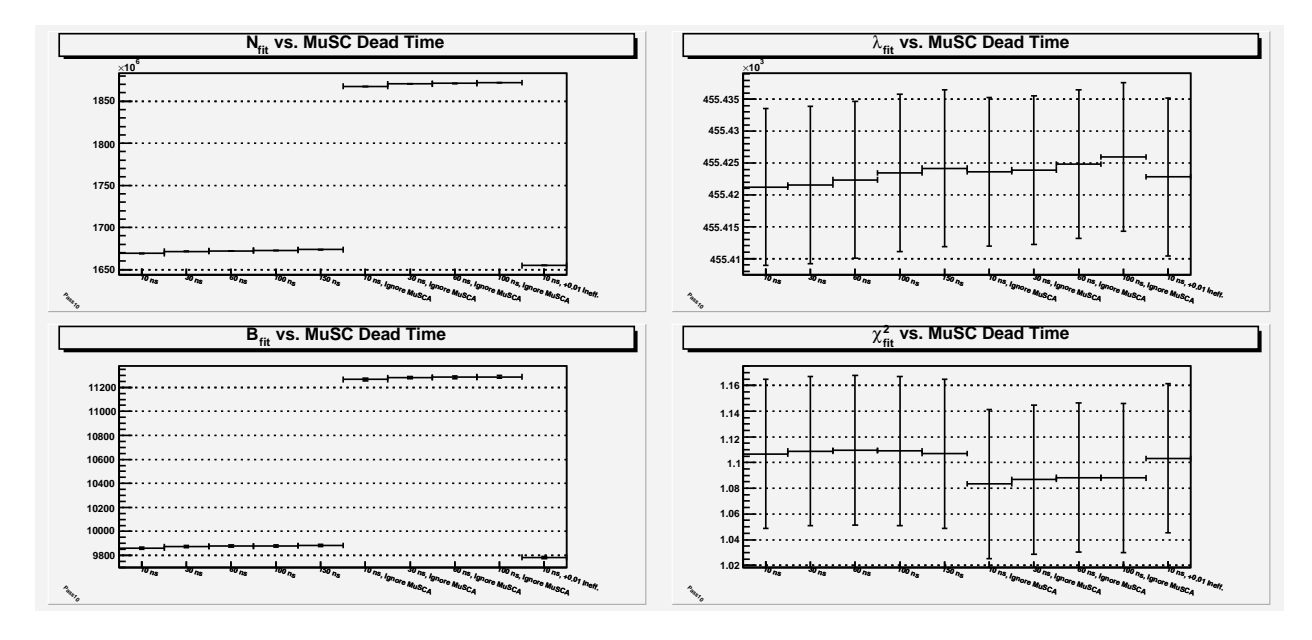


Figure 10.6: Lifetime vs. MuSC Artificial Dead Time, No Impact Parameter Cut. Muons are stopped within the TPC fiducial volume; electrons are fully tracked (eSC×ePC1×ePC2); and no impact parameter vertex cut is imposed. Bin 0 is the standard ("best") deadtime in the analysis. The rightmost bin shows the results of a somewhat different study, in which the time-independent inefficiency of the MuSC detector was artificially increased by randomly ignoring 1% of the hits.

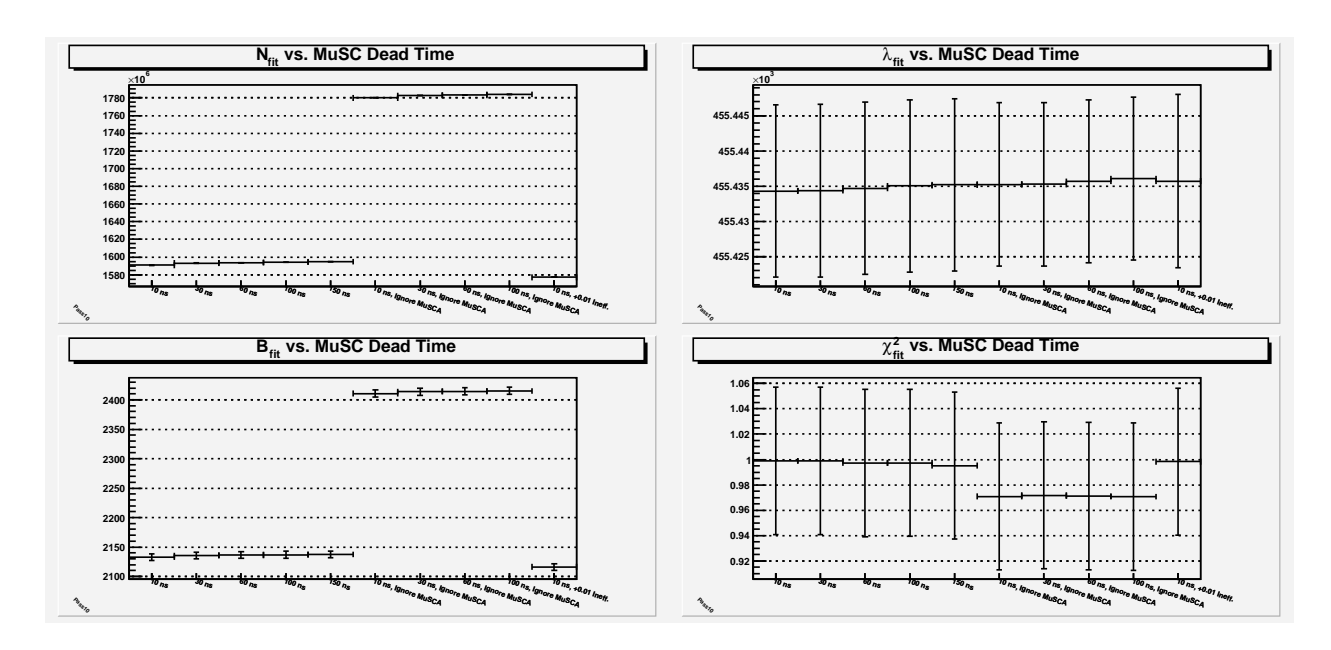


Figure 10.7: Lifetime vs. MuSC Artificial Dead Time, 120 mm Impact Parameter Cut. Muons are stopped within the TPC fiducial volume; electrons are fully tracked (eSC×ePC1×ePC2); and a 120 mm impact parameter vertex cut is imposed. Bin 0 is the standard ("best") deadtime in the analysis. The rightmost bin shows the results of a somewhat different study, in which the time-independent inefficiency of the MuSC detector was artificially increased by randomly ignoring 1% of the hits.

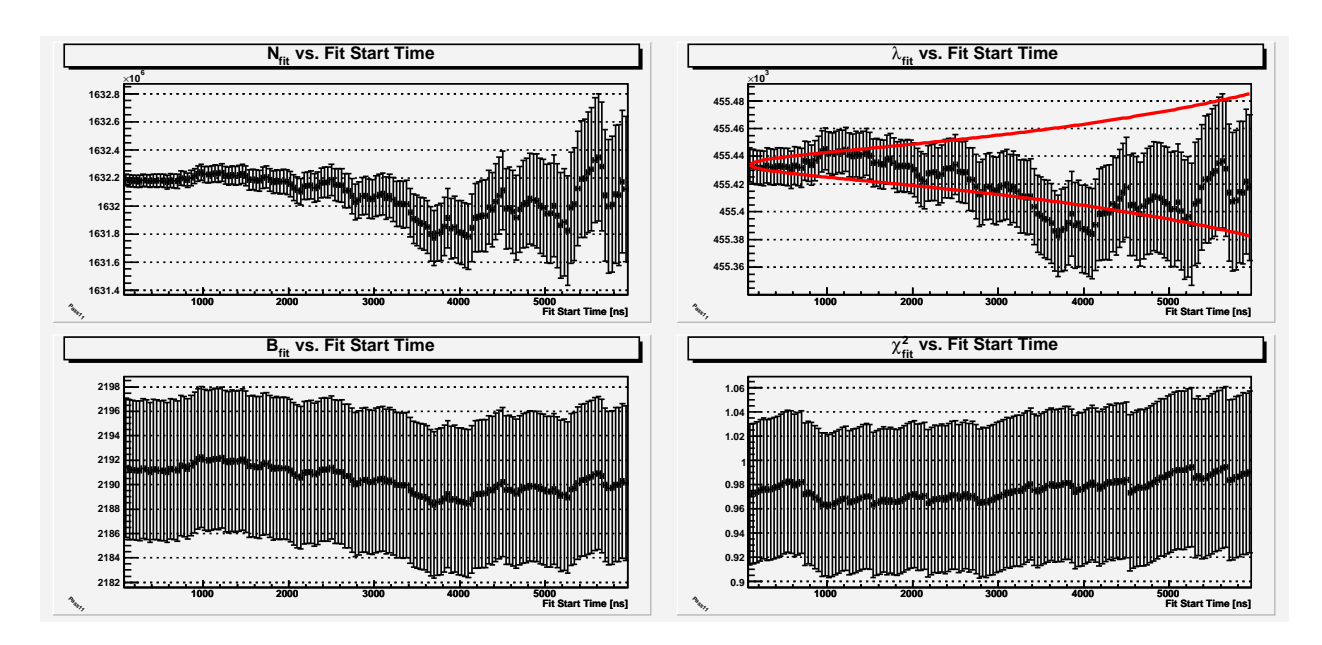


Figure 10.8: Fit Start Time Scan to Lifetime Spectrum with 120 mm Impact Parameter Cut. Electrons are fully tracked, and muons are stopped within the fiducial volume. The red curves in the λ_{fit} plot indicate the "Kawall" band with respect to the first fit range of 100 ns to 24 μ s.

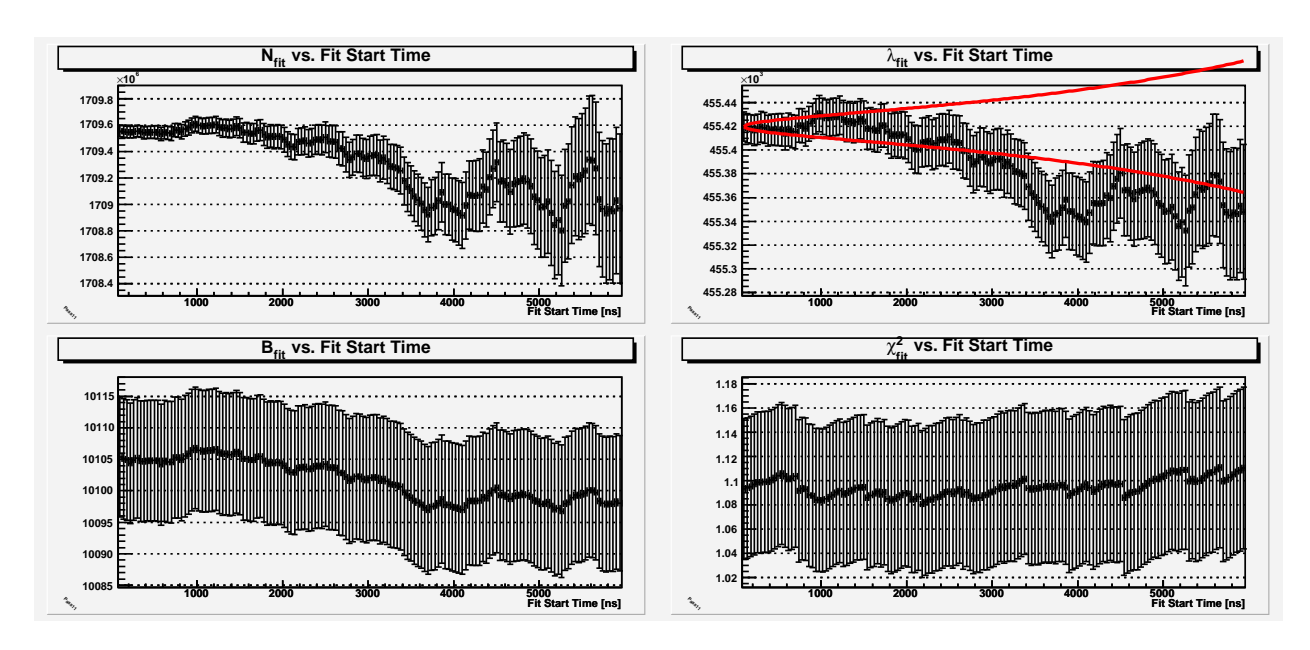


Figure 10.9: Fit Start Time Scan to Lifetime Spectrum with No Impact Parameter Cut. Electrons are fully tracked, and muons are stopped within the fiducial volume. The red curves in the λ_{fit} plot indicate the "Kawall" band with respect to the first fit range of 100 ns to 24 μ s.

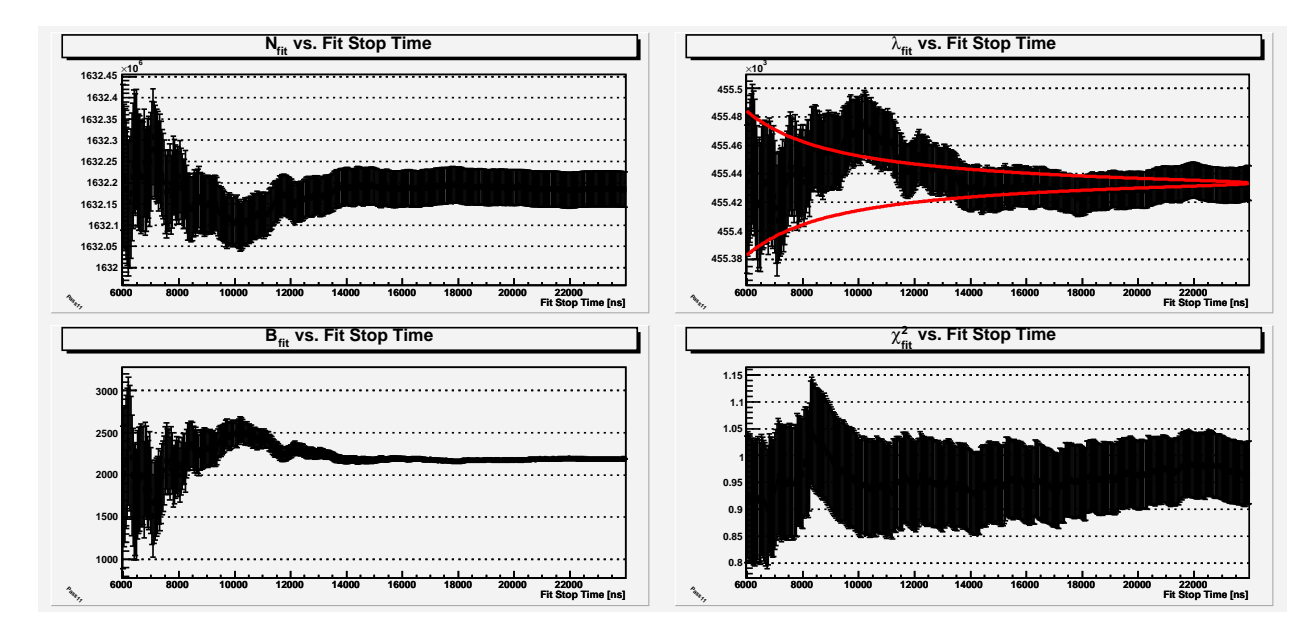


Figure 10.10: Fit Stop Time Scan to Lifetime Spectrum with 120 mm Impact Parameter Cut. Electrons are fully tracked; bin errors are corrected for overcounting (with m=0.5, see chapter 9); and muons are stopped within the fiducial volume. The red curves in the λ_{fit} plot indicate the "Kawall" band with respect to the longest fit range of 100 ns to 24 μ s.

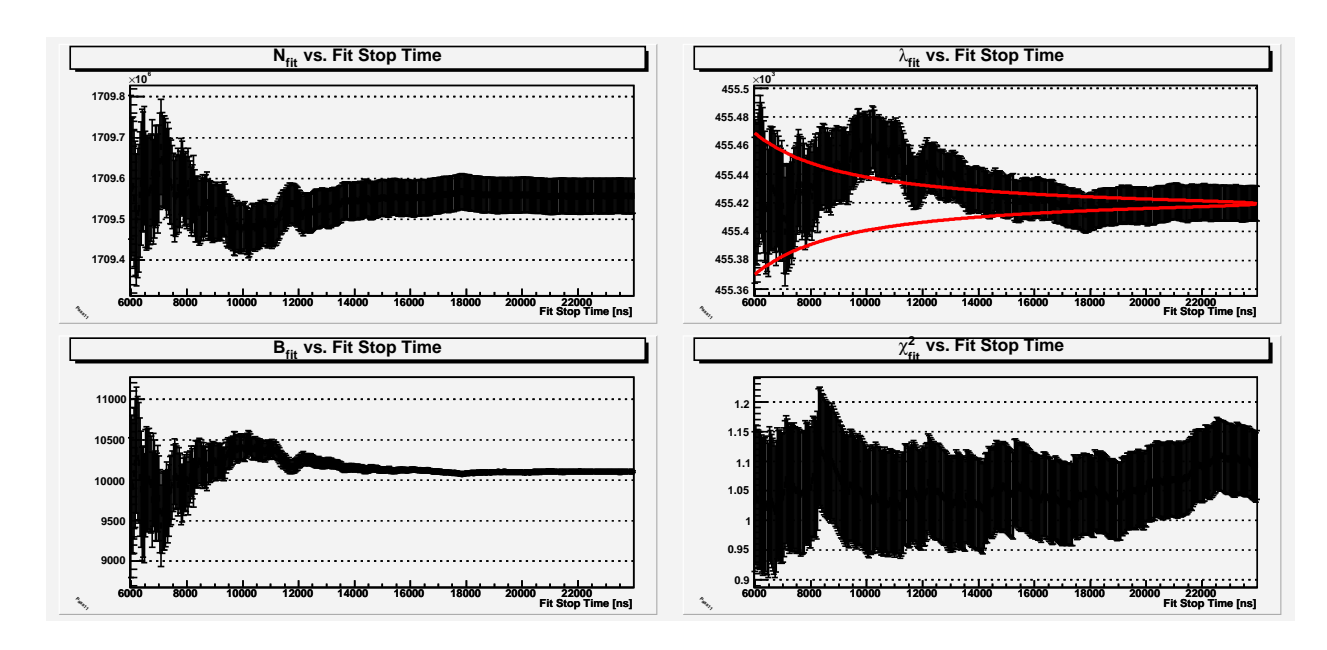


Figure 10.11: Fit Stop Time Scan to Lifetime Spectrum with No Impact Parameter Cut. Electrons are fully tracked; bin errors are corrected for overcounting (with m=0.5, see chapter 9); and muons are stopped within the fiducial volume. The red curves in the λ_{fit} plot indicate the "Kawall" band with respect to the longest fit range of 100 ns to 24 μ s.

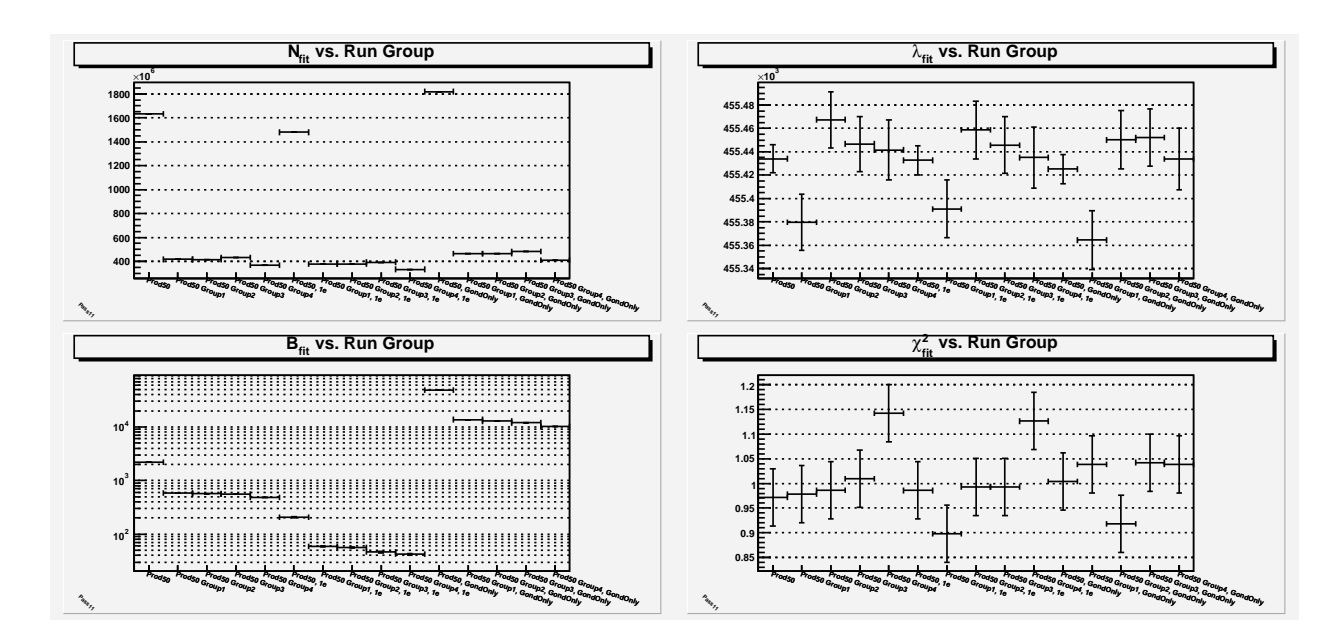


Figure 10.12: Lifetime vs. Run Group. Muons are stopped within the TPC fiducial volume. Three different electron definitions are treated: bins 1-5 are for fully tracked electrons with 120 mm impact parameter cut; bins 6-10 are for fully tracked, unique electrons with 120 mm impact parameter cut; and bins 11-15 are for the eSC only.

	N	$\lambda [\mathrm{s}^{-1}]$	В	B/N	χ^2/DOF
10 ns	1.669×10^{9}	455421.2 ± 12.3	9859.6 ± 9.4	5.907×10^{-6}	1.11 ± 0.06
30 ns	1.672×10^9	455421.5 ± 12.3	9874.6 ± 9.4	5.907×10^{-6}	1.11 ± 0.06
60 ns	1.672×10^9	455422.4 ± 12.3	9876.5 ± 9.4	5.906×10^{-6}	1.11 ± 0.06
100 ns	1.673×10^9	455423.4 ± 12.3	9879.2 ± 9.4	5.906×10^{-6}	1.11 ± 0.06
150 ns	1.674×10^9	455424.2 ± 12.3	9882.0 ± 9.4	5.905×10^{-6}	1.11 ± 0.06
10 ns, Ignore MuSCA	1.868×10^{9}	455423.6 ± 11.7	11265.8 ± 10.0	6.032×10^{-6}	1.08 ± 0.06
30 ns, Ignore MuSCA	1.870×10^{9}	455423.9 ± 11.7	11282.2 ± 10.1	6.032×10^{-6}	1.09 ± 0.06
60 ns, Ignore MuSCA	1.871×10^9	455424.8 ± 11.7	11284.4 ± 10.1	6.031×10^{-6}	1.09 ± 0.06
100 ns, Ignore MuSCA	1.872×10^{9}	455425.9 ± 11.7	11287.4 ± 10.1	6.030×10^{-6}	1.09 ± 0.06
10 ns, +0.01 Ineff.	1.655×10^{9}	455422.8 ± 12.4	9784.2 ± 9.4	5.913×10^{-6}	1.10 ± 0.06

Table 10.6: Lifetime vs. MuSC Artificial Dead Time, No Impact Parameter Cut. Muons are stopped within the TPC fiducial volume; electrons are fully tracked (eSC×ePC1×ePC2); and no impact parameter vertex cut is imposed. The first row is the standard ("best") deadtime in the analysis. The last row shows the results of a somewhat different study, in which the time-independent inefficiency of the MuSC detector was artificially increased by randomly ignoring 1% of the hits.

10.11 Lifetime vs. Rebinning Phase

The decay times entered into lifetime spectra are differences between the eSC and muSC, each with 1.25 ns resolution given by the CAEN interpolator. All spectra are rebinned by 32 to remove possible distortions due to differential nonlinearity of the interpolator. There is a choice of the phase of the rebinning, that is, which histogram bin to start with when adding 32 consecutive bins together. To study this, the rebinning phase of the same 1.25 ns-binned lifetime histogram was varied and fit; results are shown in figure 10.13. The observed variations in lifetime and χ^2 are expected based on statistics (see section 13.1). Note that although the fitting range is specified as 100 ns to 24 μ s, the effective fit range depends on how the bins line up.

10.12 Lifetime vs. Rebinning Factor

In this study the number of 1.25 ns histogram bins combined together, the "rebinning factor," is varied from 1 to 32 bins (standard rebinning is 32 bins). The rebinning phase and fit start time were chosen for each rebinning factor to have exactly the same actual start time of the fit.² Figure 10.14 shows the somewhat surprising results: in spite of the differential nonlinearity of the CAEN interpolator, the non-rebinned histogram gives almost exactly the same λ_{fit} as the rebinned-by-32 histogram, and the χ^2/NDF is excellent in both cases. The λ_{fit} for the other rebinning factors vary by at most 2.5 s⁻¹ from the standard case, though for some the χ^2/NDF is high.

²In TH1::Fit, the bins included in the fit, for specified range $[t_{min}, t_{max}]$, have $t_{min} \leq t_{BinCenter} \leq t_{max}$. The actual fit start time is the low edge of the first bin included.

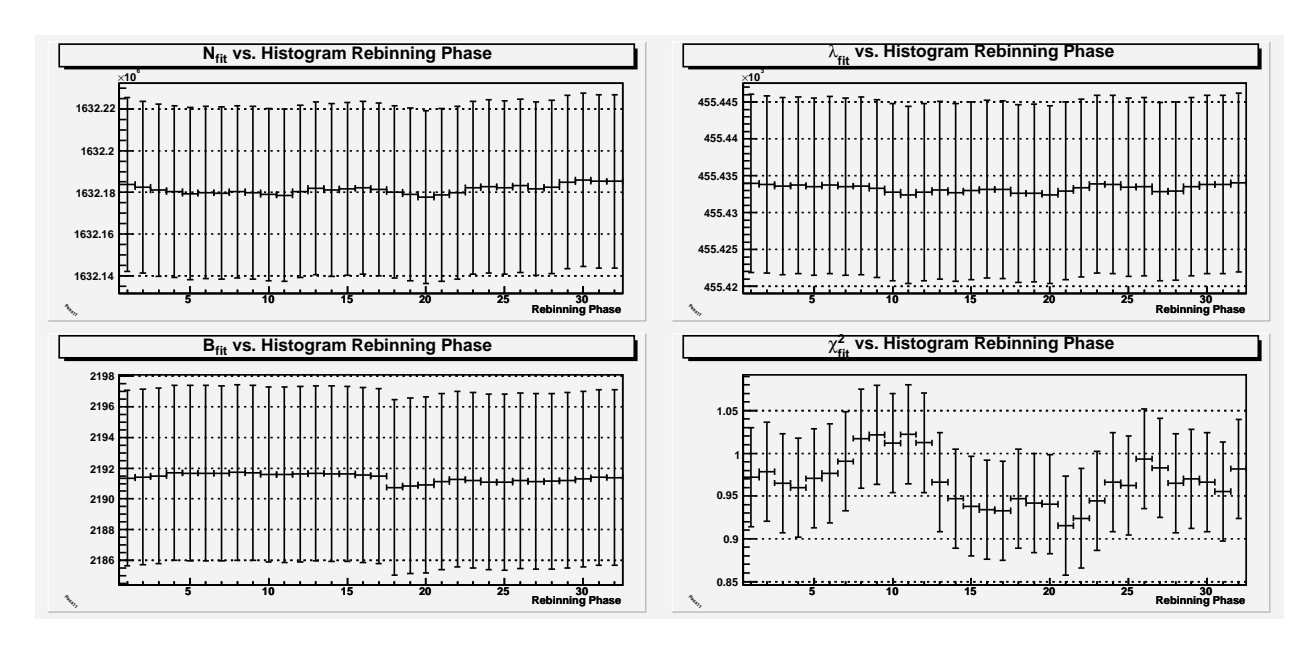


Figure 10.13: Lifetime vs. Histogram Rebinning Phase. The spectra are of fully tracked electrons (eSC \times ePC1 \times ePC2), ePC CathodeOR, and a 120 mm impact parameter cut is imposed. The standard rebinning starts with the first bin of the lifetime histogram ("Rebin Phase" = 1).

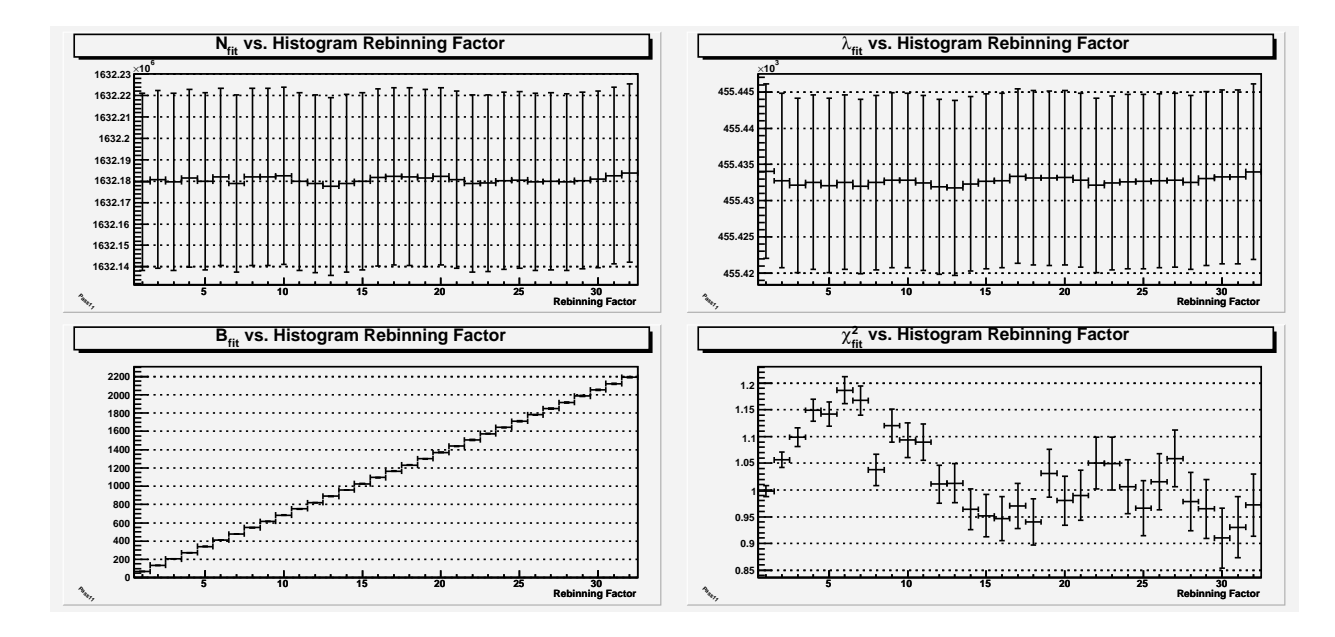


Figure 10.14: Lifetime vs. Histogram Rebinning Factor. The spectra are of fully tracked electrons (eSC×ePC1×ePC2), ePC CathodeOR, and a 120 mm impact parameter cut is imposed. The rightmost point in each panel corresponds to the standard lifetime function rebinning by 32. For a given rebinning factor, the rebinning phase is chosen such that the effective fit start time is exactly the same as the standard rebinning: 119.375 ns.

	N	$\lambda [\mathrm{s}^{-1}]$	В	B/N	χ^2/DOF
10 ns	1.591×10^{9}	455434.3 ± 12.3	2132.9 ± 5.6	1.341×10^{-6}	1.00 ± 0.06
30 ns	1.593×10^{9}	455434.4 ± 12.3	2135.8 ± 5.6	1.341×10^{-6}	1.00 ± 0.06
60 ns	1.594×10^{9}	455434.7 ± 12.3	2136.3 ± 5.6	1.341×10^{-6}	1.00 ± 0.06
100 ns	1.594×10^{9}	455435.0 ± 12.3	2137.0 ± 5.6	1.340×10^{-6}	1.00 ± 0.06
150 ns	1.595×10^{9}	455435.2 ± 12.2	2137.5 ± 5.6	1.340×10^{-6}	1.00 ± 0.06
10 ns, Ignore MuSCA	1.780×10^{9}	455435.3 ± 11.6	2410.7 ± 6.0	1.354×10^{-6}	0.97 ± 0.06
30 ns, Ignore MuSCA	1.783×10^{9}	455435.3 ± 11.6	2413.9 ± 6.0	1.354×10^{-6}	0.97 ± 0.06
60 ns, Ignore MuSCA	1.783×10^{9}	455435.7 ± 11.6	2414.4 ± 6.0	1.354×10^{-6}	0.97 ± 0.06
100 ns, Ignore MuSCA	1.784×10^{9}	455436.1 ± 11.6	2415.1 ± 6.0	1.354×10^{-6}	0.97 ± 0.06
10 ns, +0.01 Ineff.	1.577×10^{9}	455435.7 ± 12.3	2116.3 ± 5.6	1.342×10^{-6}	1.00 ± 0.06

Table 10.7: Lifetime vs. MuSC Artificial Dead Time, 120 mm Impact Parameter Cut. Muons are stopped within the TPC fiducial volume; electrons are fully tracked (eSC×ePC1×ePC2); and a 120 mm impact parameter vertex cut is imposed. The first row is the standard ("best") deadtime in the analysis. The last row shows the results of a somewhat different study, in which the time-independent inefficiency of the MuSC detector was artificially increased by randomly ignoring 1% of the hits.

10.13 Fit Function Modified to Include Wall Stops

The purpose of this study is to test whether the data is consistent with a fit function modified to include stops in aluminum and tungsten. Added to the usual exponential plus flat background are two additional exponential terms for wall stops:

$$f_{withZ}(t) = N\lambda w e^{-\lambda t} + B + N_Z w (\alpha \lambda_W e^{-\lambda_W t} + (1 - \alpha)\lambda_{Al} e^{-\lambda_{Al} t}), \tag{10.2}$$

where w is fixed to the lifetime histogram bin width of 40 ns, and N, λ , and B are the standard fit parameters. Of the new parameters, the rates will be fixed: $\lambda_W = 12.76 \times 10^6 \text{ s}^{-1}$ for the muon inverse lifetime on tungsten (gold has a similar total capture rate), and $\lambda_{Al} = 1.157 \times 10^6 \text{ s}^{-1}$ for the muon inverse lifetime on aluminum. The relative fraction of tungsten stops to total wall stops is represented by α , which will be fixed to values from 0 to 1 in this study. The parameter N_Z is allowed to float.

The modified fit function was applied to the spectrum of muon stops well within the TPC fiducial volume, with fully tracked electrons (ePC CathodeOR) and a 120 mm impact parameter cut: i.e., the standard best lifetime spectrum. Fit results are shown in figure 10.15. The fit for each fixed value of α was done in two steps:

- 1. The spectrum was fit to the standard three-parameter function to get starting values for N, λ and B. Bin errors were recalculated assuming background double-counting with m=0.5, as usual. Results of the standard fit are shown by the leftmost points in the plots of figure 10.15.
- 2. Using the N, λ and B from the simple fit and $N_Z = 0$ as starting values, the spectrum was fit to $f_{withZ}(t)$.

The resulting N_Z , plotted in the lower left panel of the figure, are consistent with zero. The ratio N_Z/N (lower right panel) suggest constraints on the influence of wall stops in the lifetime.

e Definition	Short DT ($\approx 300 \text{ ns}$)	Standard DT ($\approx 1000 \text{ ns}$)	Long DT ($\approx 2000 \text{ ns}$)
eSC	455438.8 ± 12.6	455438.7 ± 12.6	455438.7 ± 12.6
eTrack, AnodesOnly	455417.7 ± 12.3	455417.7 ± 12.3	455417.8 ± 12.3
eTrack, CathOR	455420.1 ± 12.4	455420.1 ± 12.4	455420.2 ± 12.4
eTrack, CathAND	455416.2 ± 12.8	455416.3 ± 12.8	455417.0 ± 12.8

Pass 7, 6, 8

Table 10.8: Lifetime vs. ePC Deadtime and eDetector Treatment. Muons are stopped within the TPC fiducial volume, and no impact parameter cut is imposed on any of the spectra. This study uses histograms from analysis Pass 6 (standard ePC deadtime), Pass 7 (short ePC deadtime), and Pass 8 (long ePC deadtime). In these analysis passes, the eSC deadtime was mistakenly set to ≈ 130 ns, longer than necessary, instead of the desired 65 ns. Still, the study may be valid in its purpose to show weak dependence of the lifetime on the ePC deadtime. The eSC lifetimes were expected to be exactly the same for the different passes; The reason a small difference is observed could be due to a combination of "spark cuts" on ePC cluster size and slightly different cluster sizes for the different deadtimes.

	N	$\lambda [\mathrm{s}^{-1}]$	В	B/N	χ^2/DOF
Prod50	1.632×10^{9}	455434.0 ± 12.1	2191.4 ± 5.7	1.343×10^{-6}	0.97 ± 0.06
Prod50 Group1	4.170×10^{8}	455379.7 ± 24.0	584.6 ± 2.9	1.402×10^{-6}	0.98 ± 0.06
Prod50 Group2	4.159×10^{8}	455467.4 ± 24.0	566.1 ± 2.9	1.361×10^{-6}	0.99 ± 0.06
Prod50 Group3	4.325×10^{8}	455446.7 ± 23.5	556.6 ± 2.9	1.287×10^{-6}	1.01 ± 0.06
Prod50 Group4	3.668×10^{8}	455441.5 ± 25.5	480.5 ± 2.7	1.310×10^{-6}	1.14 ± 0.06
Prod50, 1e	1.480×10^9	455432.7 ± 12.5	206.9 ± 3.3	1.398×10^{-7}	0.99 ± 0.06
Prod50 Group1, 1e	3.778×10^{8}	455391.0 ± 24.7	58.9 ± 1.7	1.559×10^{-7}	0.90 ± 0.06
Prod50 Group2, 1e	3.769×10^{8}	455458.7 ± 24.8	56.4 ± 1.7	1.497×10^{-7}	0.99 ± 0.06
Prod50 Group3, 1e	3.923×10^{8}	455445.7 ± 24.2	46.3 ± 1.7	1.180×10^{-7}	0.99 ± 0.06
Prod50 Group4, 1e	3.328×10^{8}	455435.0 ± 26.3	42.2 ± 1.6	1.269×10^{-7}	1.13 ± 0.06
Prod50, GondOnly	1.819×10^{9}	455425.1 ± 12.6	48552.3 ± 17.8	2.670×10^{-5}	1.00 ± 0.06
Prod50 Group1, GondOnly	4.635×10^{8}	455364.4 ± 25.0	13693.0 ± 9.4	2.954×10^{-5}	1.04 ± 0.06
Prod50 Group2, GondOnly	4.643×10^{8}	455450.1 ± 24.9	12840.5 ± 9.1	2.765×10^{-5}	0.92 ± 0.06
Prod50 Group3, GondOnly	4.822×10^{8}	455452.1 ± 24.3	11910.4 ± 8.9	2.470×10^{-5}	1.04 ± 0.06
Prod50 Group4, GondOnly	4.085×10^{8}	455433.8 ± 26.4	10105.5 ± 8.2	2.474×10^{-5}	1.04 ± 0.06

Pass11

Table 10.9: Lifetime vs. Run Group. Muons are stopped within the TPC fiducial volume. Three different electron definitions are treated: rows 1-5 are for fully tracked electrons with 120 mm impact parameter cut; rows 6-10 are for fully tracked, unique electrons with 120 mm impact parameter cut; and rows 11-15 are for the eSC only.

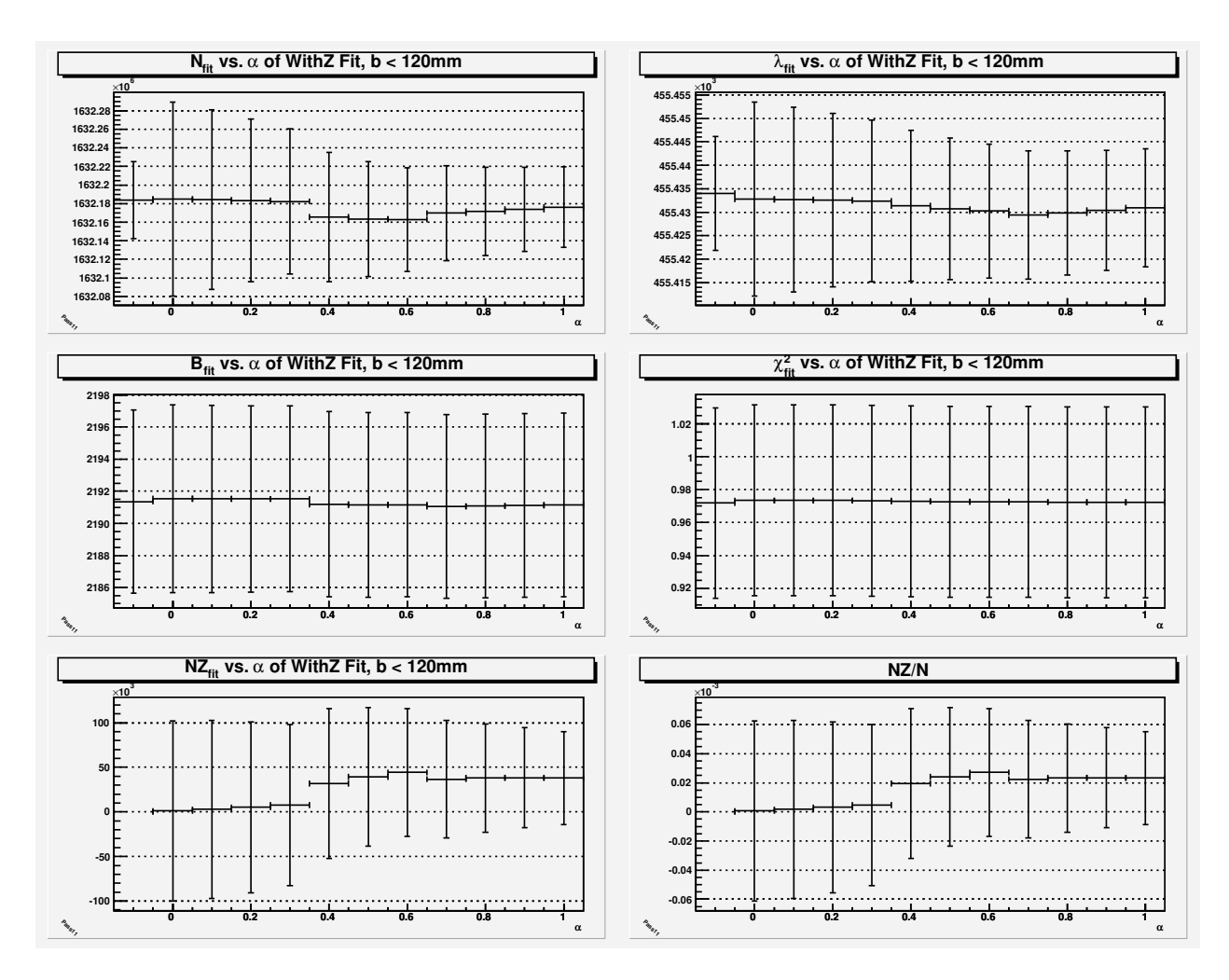


Figure 10.15: Lifetime vs. α of Fit Function Modified to Include Wall Stop Components (Section 10.13). α is the fraction of tungsten stops compared to all tungsten plus aluminum stops: $\alpha=0$ means N_Z is all aluminum, and $\alpha=1$ means all tungsten. The fit parameter in the leftmost bin, from the standard three-parameter fit function, is for reference. The spectra are of fully tracked electrons (eSC×ePC1×ePC2), ePC CathodeOR, and a 120 mm impact parameter cut is imposed.

Impurity Captures

Impurity capture events are identified in the TDC400 data by a fully pileup-protected, good muon stop well within the fiducial volume, followed by a very-high-threshold (EVH) "spot." An example of an impurity capture event is shown in figure 11.1. The position of the spot must be not more than one anode or strip away from the location of the muon stop; i.e., $\Delta x < 8$ mm and $\Delta z < 8$ mm — a difference of one anode or strip is okay, but two anodes or strips are too many. The remaining dimension, y, is converted into the capture time by dividing by drift velocity. The choice of Δx and Δz cuts are supported by figure 11.2.

Impurity corrections to the Prod50, NatH2, and CalibD2 lifetimes, assuming the only impurity is nitrogen, are given in table 11.2. There is ample evidence that the Prod50 impurity is not nitrogen and is likely water. The corrections listed in the table are there only to get an idea of the size.

Data Set	N	$\lambda [\mathrm{s}^{-1}]$	В	B/N	χ^2/DOF
Prod50	1.632×10^9	455434.0 ± 12.1	2191.4 ± 5.7	1.343×10^{-6}	0.97 ± 0.06
CalibN2	8.548×10^{7}	456370.4 ± 53.0	116.9 ± 1.3	1.367×10^{-6}	0.95 ± 0.06
NaturalH2	1.905×10^{8}	456471.7 ± 35.5	279.7 ± 2.0	1.468×10^{-6}	1.41 ± 0.06
CalibD2	2.155×10^{8}	455717.0 ± 33.4	309.2 ± 2.1	1.435×10^{-6}	1.03 ± 0.06

Table 11.1: Electron Lifetime Fit Results for Different Data Sets, 120 mm Impact Parameter Cut Spectra.

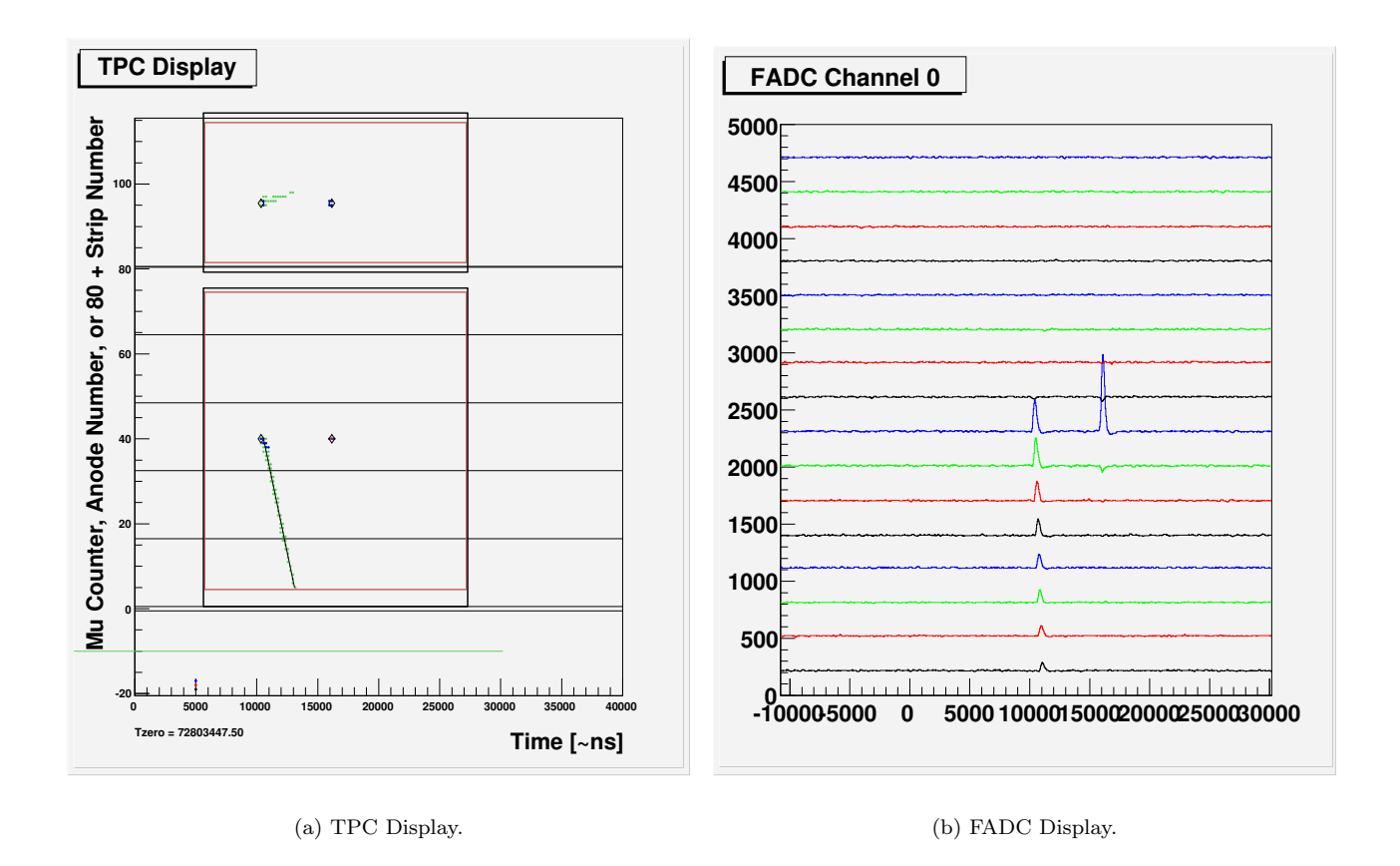


Figure 11.1: Event Display of an Impurity Capture, run13000 (Prod50). The UIUC capture search uses TDC400 data, as shown in the left panel, and vetoes based on electron detectors. In this case FADC data were also present (right panel).

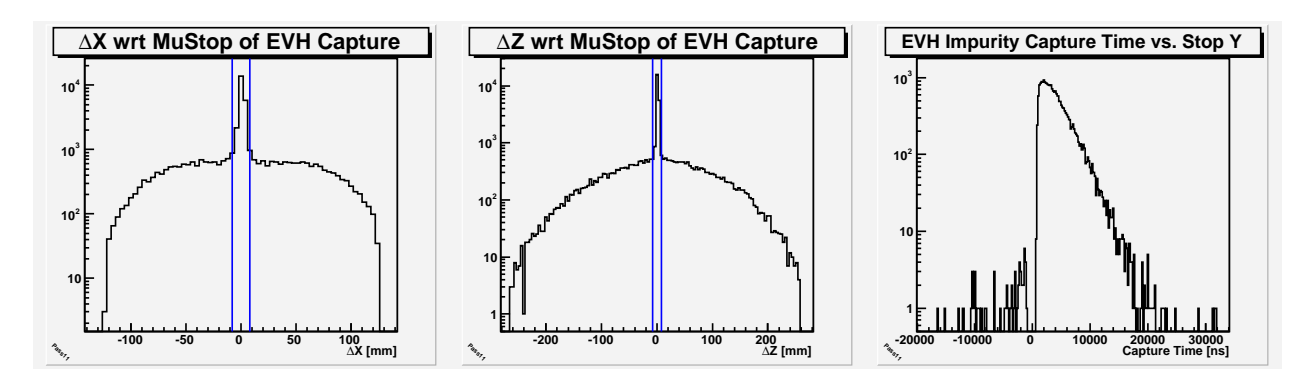


Figure 11.2: Relative Positions and Times of EVH Impurity Capture Events, Prod50 μ^- Data. In these histograms, the muon stops are required to be well within the fiducial region. Left: Δx of EVH Spot with respect to the Muon Stop Position. Middle: Δz of EVH Spot with respect to the Muon Stop Position. Right: Time of EVH Impurity Capture. The vertical blue lines in the left and middle panels show position cuts that are applied before filling the capture time histogram.

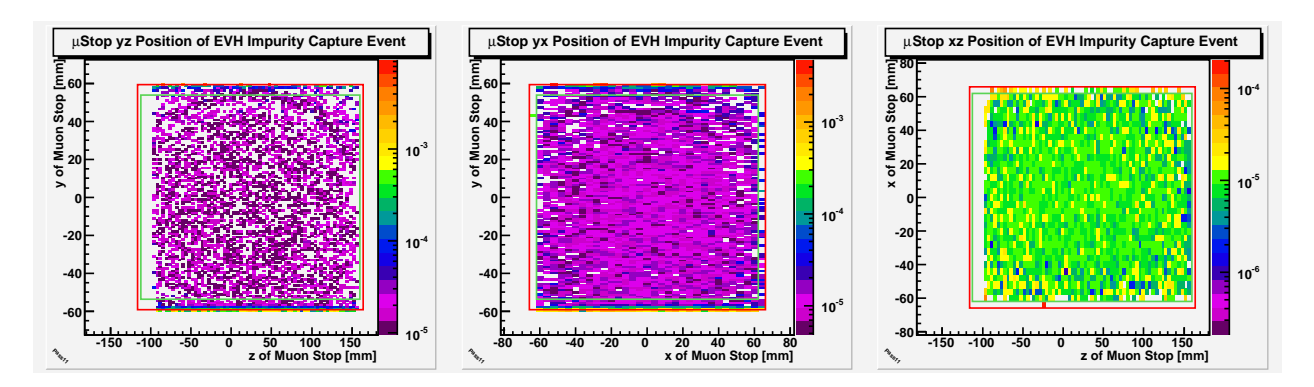


Figure 11.3: Impurity Capture Yield (Y_Z) Requiring EVH-Threshold vs. 2D Muon Stop Position, Prod50 μ^- Data. In each view, events near the walls in the dimension perpendicular to the plane are removed before projection of the 3D distribution onto the plane; thus, subsequent division by the normalization histogram of all μ -stops (projected onto the same plane) gives the capture yield untainted by stops near the edges in the projected-out dimension. The red boxes show the boundaries of the largest fiducial volume in the analysis to detect a muon stop ("MUTRACK_PARAM::GoodBox"), and the green boxes show the standard fiducial volume used for filling lifetime histograms ("MUTRACK_PARAM::BetterBox"). Left: Y_Z vs. (z,y). Middle: Y_Z vs. (x,y). Right: Y_Z vs. (z,x).

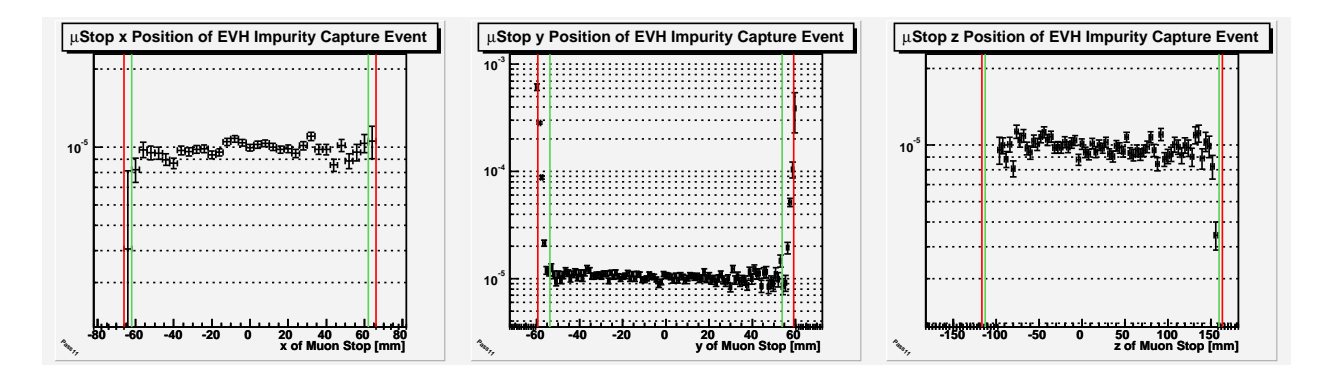


Figure 11.4: Impurity Capture Yield (Y_Z) Requiring EVH-Threshold vs. 1D Muon Stop Position, Prod50 μ^- Data. In each view, events near the walls in the dimensions perpendicular to the displayed axis are removed before projection of the 3D distribution; thus, subsequent division by the normalization histogram of all μ -stops (projected onto the same axis) gives the capture yield untainted by stops near the edges in the projected-out dimensions. The red lines show the boundaries of the largest fiducial volume in the analysis to detect a muon stop ("MUTRACK_PARAM::GoodBox"), and the green lines show the standard fiducial volume used for filling lifetime histograms ("MUTRACK_PARAM::BetterBox"). Left: Y_Z vs. x. Middle: Y_Z vs. y. Right: Y_Z vs. z.

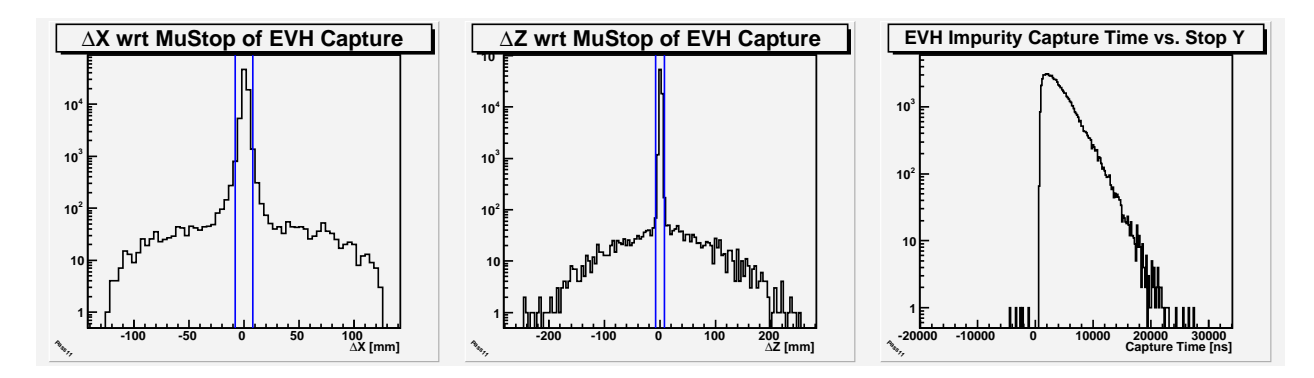


Figure 11.5: Relative Positions and Times of EVH Impurity Capture Events, CalibN2 μ^- Data. In these histograms, the muon stops are required to be well within the fiducial region. Left: Δx of EVH Spot with respect to the Muon Stop Position. Middle: Δz of EVH Spot with respect to the Muon Stop Position. Right: Time of EVH Impurity Capture. The vertical blue lines in the left and middle panels show position cuts that are applied before filling the capture time histogram.

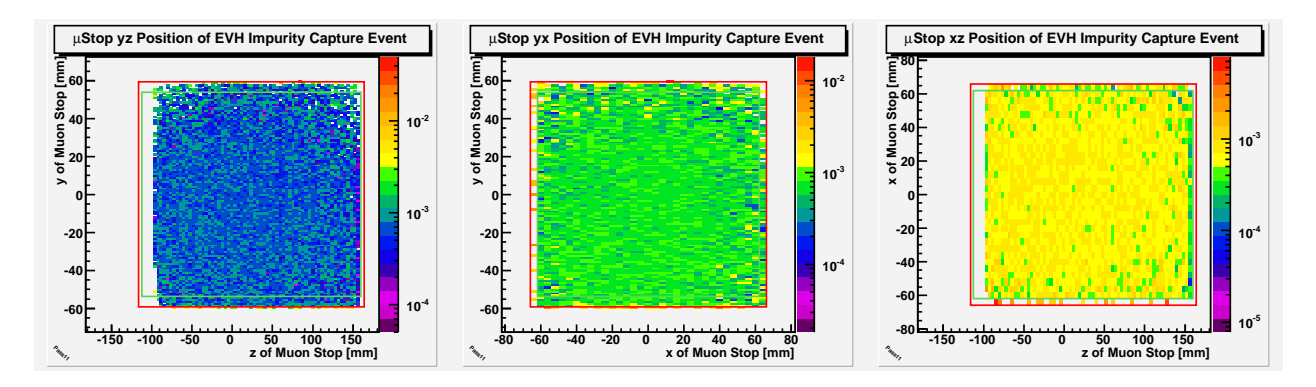


Figure 11.6: Impurity Capture Yield (Y_Z) Requiring EVH-Threshold vs. 2D Muon Stop Position, CalibN2 μ^- Data. In each view, events near the walls in the dimension perpendicular to the plane are removed before projection of the 3D distribution onto the plane; thus, subsequent division by the normalization histogram of all μ -stops (projected onto the same plane) gives the capture yield untainted by stops near the edges in the projected-out dimension. The red boxes show the boundaries of the largest fiducial volume in the analysis to detect a muon stop ("MUTRACK_PARAM::GoodBox"), and the green boxes show the standard fiducial volume used for filling lifetime histograms ("MUTRACK_PARAM::BetterBox"). Left: Y_Z vs. (z,y). Middle: Y_Z vs. (x,y). Right: Y_Z vs. (z,x).

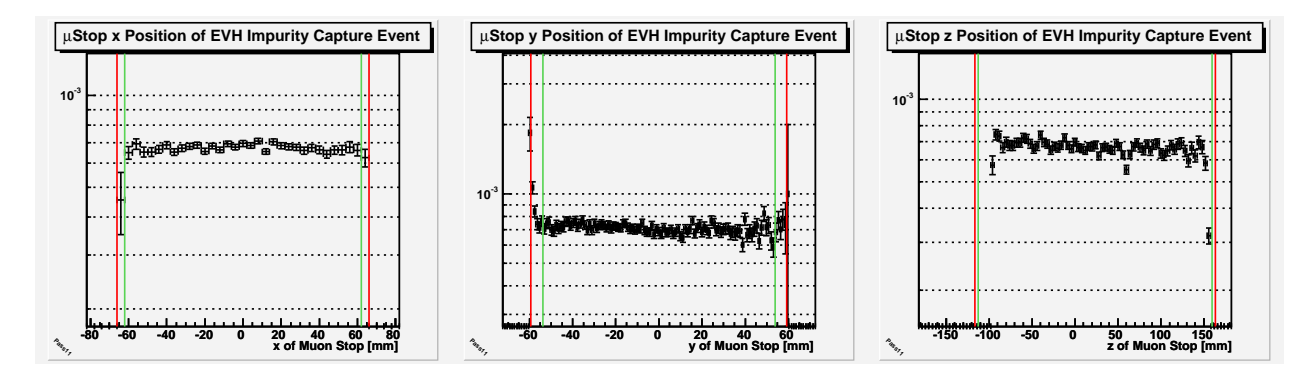


Figure 11.7: Impurity Capture Yield (Y_Z) Requiring EVH-Threshold vs. 1D Muon Stop Position, CalibN2 μ^- Data. In each view, events near the walls in the dimensions perpendicular to the displayed axis are removed before projection of the 3D distribution; thus, subsequent division by the normalization histogram of all μ -stops (projected onto the same axis) gives the capture yield untainted by stops near the edges in the projected-out dimensions. The red lines show the boundaries of the largest fiducial volume in the analysis to detect a muon stop ("MUTRACK_PARAM::GoodBox"), and the green lines show the standard fiducial volume used for filling lifetime histograms ("MUTRACK_PARAM::BetterBox"). Left: Y_Z vs. x. Middle: Y_Z vs. y. Right: Y_Z vs. z.

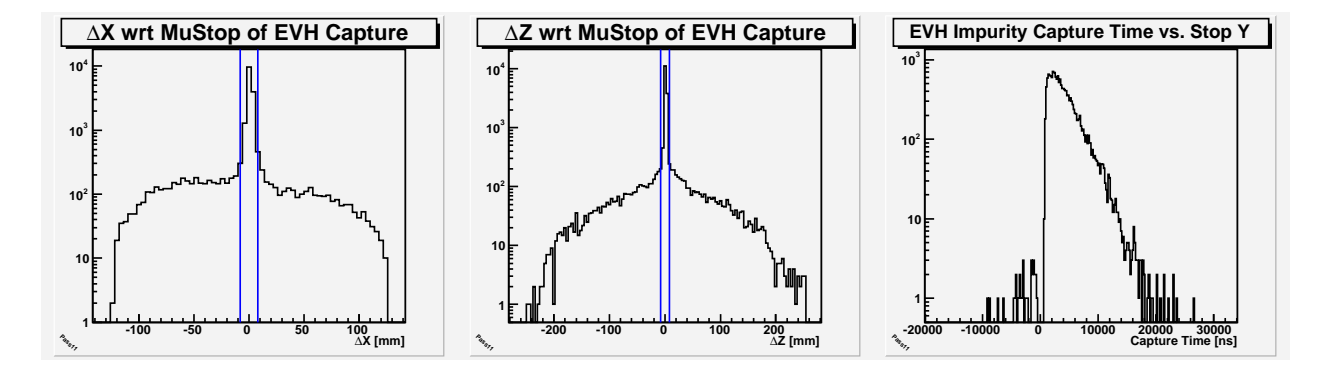


Figure 11.8: Relative Positions and Times of EVH Impurity Capture Events, NaturalH2 μ^- Data. In these histograms, the muon stops are required to be well within the fiducial region. Left: Δx of EVH Spot with respect to the Muon Stop Position. Middle: Δz of EVH Spot with respect to the Muon Stop Position. Right: Time of EVH Impurity Capture. The vertical blue lines in the left and middle panels show position cuts that are applied before filling the capture time histogram.

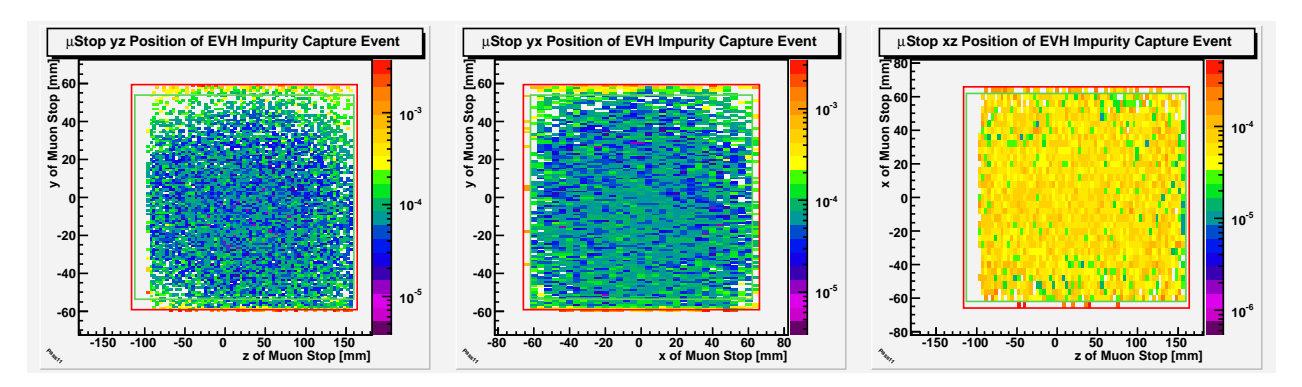


Figure 11.9: Impurity Capture Yield (Y_Z) Requiring EVH-Threshold vs. 2D Muon Stop Position, NaturalH2 μ^- Data. In each view, events near the walls in the dimension perpendicular to the plane are removed before projection of the 3D distribution onto the plane; thus, subsequent division by the normalization histogram of all μ -stops (projected onto the same plane) gives the capture yield untainted by stops near the edges in the projected-out dimension. The red boxes show the boundaries of the largest fiducial volume in the analysis to detect a muon stop ("MUTRACK_PARAM::GoodBox"), and the green boxes show the standard fiducial volume used for filling lifetime histograms ("MUTRACK_PARAM::BetterBox"). Left: Y_Z vs. (z,y). Middle: Y_Z vs. (x,y). Right: Y_Z vs. (z,x).

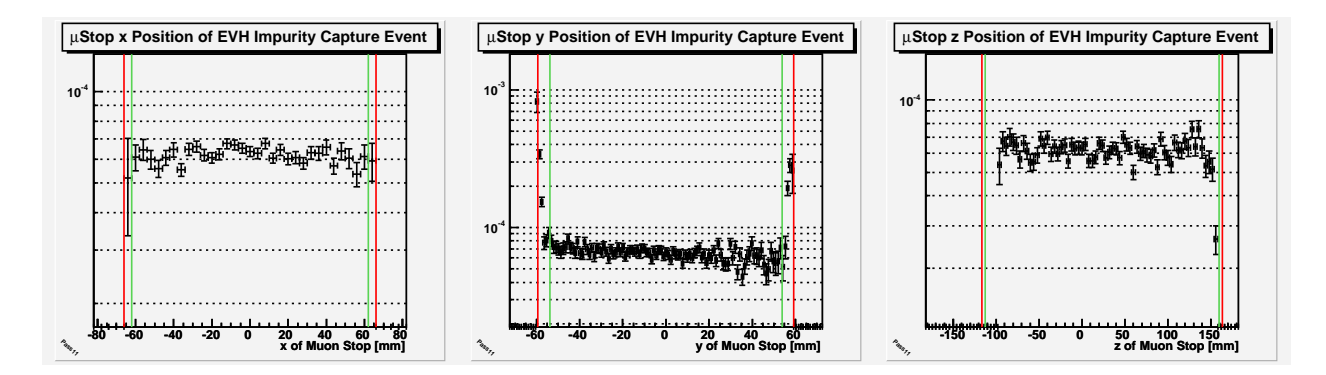


Figure 11.10: Impurity Capture Yield (Y_Z) Requiring EVH-Threshold vs. 1D Muon Stop Position, NaturalH2 μ^- Data. In each view, events near the walls in the dimensions perpendicular to the displayed axis are removed before projection of the 3D distribution; thus, subsequent division by the normalization histogram of all μ -stops (projected onto the same axis) gives the capture yield untainted by stops near the edges in the projected-out dimensions. The red lines show the boundaries of the largest fiducial volume in the analysis to detect a muon stop ("MUTRACK_PARAM::GoodBox"), and the green lines show the standard fiducial volume used for filling lifetime histograms ("MUTRACK_PARAM::BetterBox"). Left: Y_Z vs. x. Middle: Y_Z vs. y. Right: Y_Z vs. z.

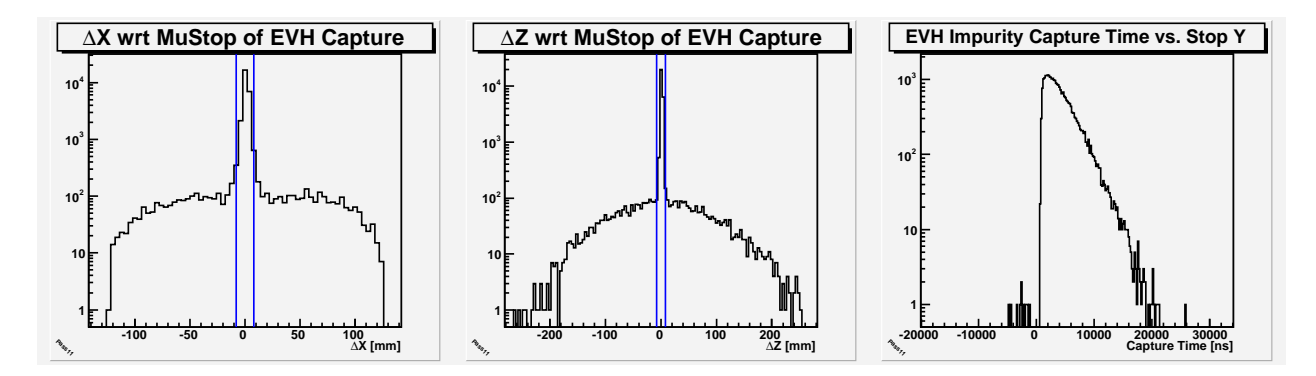


Figure 11.11: Relative Positions and Times of EVH Impurity Capture Events, CalibD2 μ^- Data. In these histograms, the muon stops are required to be well within the fiducial region. Left: Δx of EVH Spot with respect to the Muon Stop Position. Middle: Δz of EVH Spot with respect to the Muon Stop Position. Right: Time of EVH Impurity Capture. The vertical blue lines in the left and middle panels show position cuts that are applied before filling the capture time histogram.

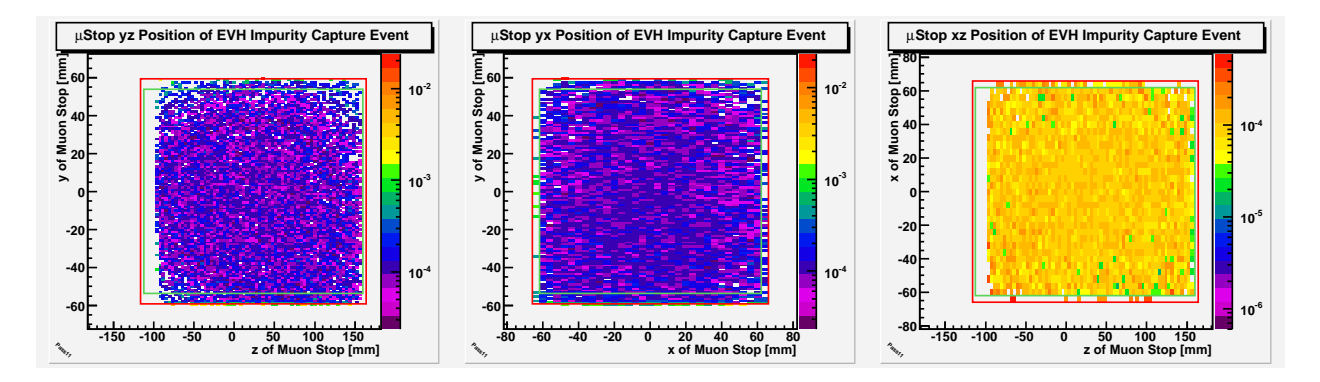


Figure 11.12: Impurity Capture Yield (Y_Z) Requiring EVH-Threshold vs. 2D Muon Stop Position, CalibD2 μ^- Data. In each view, events near the walls in the dimension perpendicular to the plane are removed before projection of the 3D distribution onto the plane; thus, subsequent division by the normalization histogram of all μ -stops (projected onto the same plane) gives the capture yield untainted by stops near the edges in the projected-out dimension. The red boxes show the boundaries of the largest fiducial volume in the analysis to detect a muon stop ("MUTRACK_PARAM::GoodBox"), and the green boxes show the standard fiducial volume used for filling lifetime histograms ("MUTRACK_PARAM::BetterBox"). Left: Y_Z vs. (z,y). Middle: Y_Z vs. (x,y). Right: Y_Z vs. (z,x).

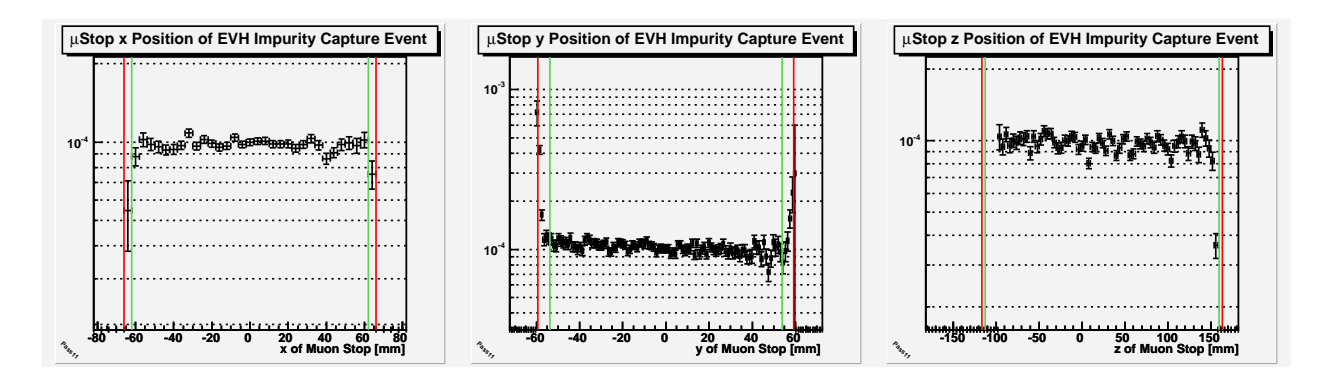


Figure 11.13: Impurity Capture Yield (Y_Z) Requiring EVH-Threshold vs. 1D Muon Stop Position, CalibD2 μ^- Data. In each view, events near the walls in the dimensions perpendicular to the displayed axis are removed before projection of the 3D distribution; thus, subsequent division by the normalization histogram of all μ -stops (projected onto the same axis) gives the capture yield untainted by stops near the edges in the projected-out dimensions. The red lines show the boundaries of the largest fiducial volume in the analysis to detect a muon stop ("MUTRACK_PARAM::GoodBox"), and the green lines show the standard fiducial volume used for filling lifetime histograms ("MUTRACK_PARAM::BetterBox"). Left: Y_Z vs. x. Middle: Y_Z vs. y. Right: Y_Z vs. z.

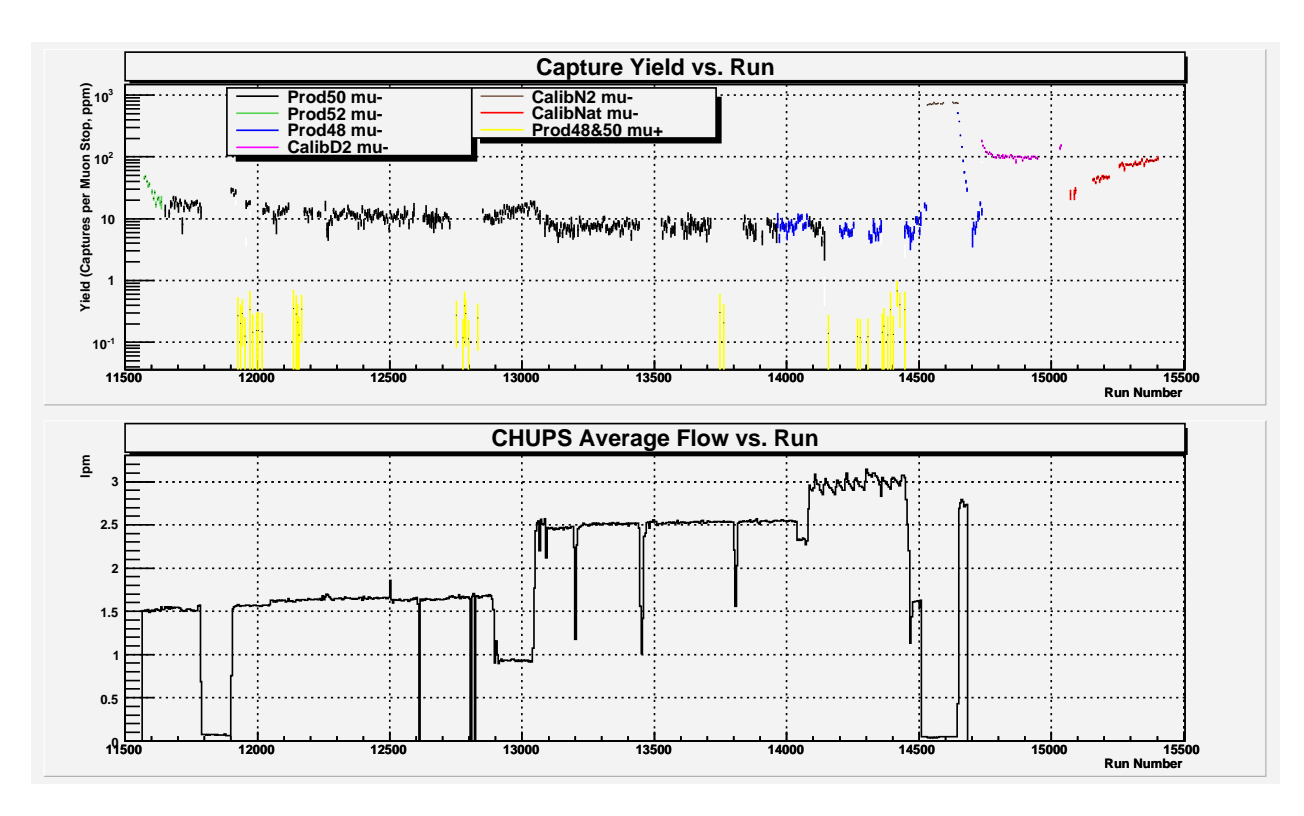


Figure 11.14: Top: Capture Yield vs. Run Number. Bottom: Average CHUPS Flow Rate vs. Run Number. In both plots the quantities are averaged over five runs.

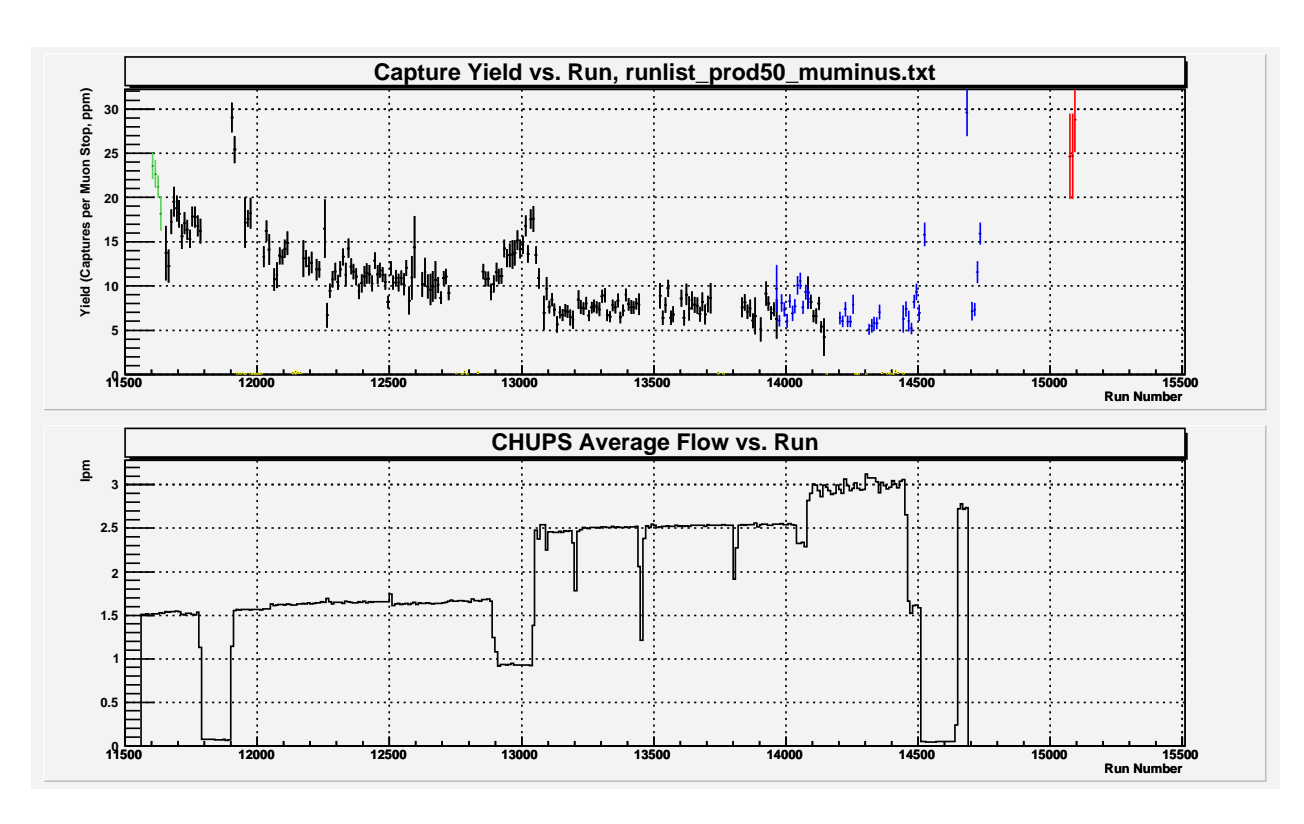


Figure 11.15: Top: Capture Yield vs. Run Number, Linear Scale and Zoomed in on Prod50 (Black Points). Bottom: Average CHUPS Flow Rate vs. Run Number. In both plots the quantities are averaged over ten runs.

Data Set	Yield [ppm]	$\lambda - \lambda_{Prod50} [\mathrm{s}^{-1}]$	ϵ_N	$\delta \lambda_{Correction} [\mathrm{s}^{-1}]$	$c_N[ppm]$
Prod50	10.670 ± 0.075	_	_	13.9	0.17
CalibN2	728.847 ± 2.745	936.4 ± 54.3	0.64	950.3	11.61
NaturalH2	67.462 ± 0.561	1037.7 ± 37.5	_	88.0	1.07
CalibD2	105.762 ± 0.664	283.0 ± 35.5		137.9	1.68

Table 11.2: Difference in Electron Lifetime Fit Results (120 mm Impact Parameter Cut Spectra) from that for the Prod50 Data, and EVH Capture Yields for Different Data Sets. To get an idea of the size of the impurity corrections, columns 4 through 6 are calculated assuming the only impurity present is nitrogen in all data sets. The efficiency for nitrogen capture detection ϵ_N (fourth column) is calculated using $\alpha_N \equiv \delta \lambda/Y_{\epsilon=1} = 1.819\lambda_0$, from Peter's recent Mathematica studies, http://www.npl.uiuc.edu/twiki/bin/view/Main/ImpurityFormalismPK, and $\epsilon_N = \alpha_N(Y_{CalibN2} - Y_{Prod50})/(\lambda_{CalibN2} - \lambda_{Prod50})$. The factor of λ_0 , the free muon decay rate, in the expression for α_N is necessary to convert Peter's results using rates in ppm to the rates in s⁻¹ shown in the table. Column 5, the impurity correction to the lifetime, is calculated with $\delta\lambda = \alpha_N Y/\epsilon_N$, where Y is the yield of column 2. Finally, in column 6 the nitrogen concentration consistent with the observed capture yield and ϵ_N is calculated with $c_N = (Y/\epsilon_N)/98.8$.

μp and μd Diffusion

The presence of deuterium in the target gas leads to a systematic shift of the lifetime measurement. While the somewhat different capture rate of μ d compared to μ p is not important at MuCap deuterium concentration, the effect of μ d diffusion out of μ -e vertex cuts, perhaps into wall material, can be severe. Our approach to correct for this is an extrapolation procedure, assuming the effect on the lifetime is linear with deuterium concentration c_D . In addition to the main production data with deuterium-depleted hydrogen, with $c_D(Prod) \sim$ a few ppm, data with higher c_D were taken: CalibD2 with $c_D(CalibD2) \approx 17$ ppm, and NatH2 with $c_D(NatH2) = 126.7$ ppm.¹

The deuterium extrapolation procedure turns out not to be completely straightforward. As shown in fig. 12.1, the c_D ratio appears to depend on which impact parameter cut is taken. The problem is resolved by first accounting for μp diffusion. A calculation of the effect on the rate due to μp diffusion and the procedure to find the deuterium concentration ratio of different data sets are described in a MuCap Note ² and will not be repeated here. Rather, some updated plots are shown in figures 12.2 to 12.5. An improvement in these updates is the elimination of the possibly not well-motivated "offset" parameter in the model fit: by taking the rate differences with respect to the wide impact parameter cut of 150 mm, instead of the infinite cut as before, the offset parameter is no longer necessary. Perhaps the large difference in background level with the infinite cut spectrum could be blamed for the previous offset; regardless, the μp diffusion model requires only one free parameter, k, describing the rate of thermal diffusion, and the results are not changed significantly from those of the Note.

The deuterium extrapolation procedure can be done with either the NatH2 or CalibD2 data sets. Results for the c_D ratios are shown in table 12.1; the important column is the second, with values for $c_D(Prod50)/c_D(calib) = \tilde{c}^{-1}$, where "calib" is either NatH2 or CalibD2. The value of k is chosen that gives the best χ^2 to a constant fit to \tilde{c}^{-1} vs. impact parameter annulus cut; the value and error for k indicated in the table are as reported by MINUIT (MIGRAD), where the minimization is on the χ^2 of the constant fit, and \tilde{c}^{-1} in the table is the value from the same constant fit.

¹The value quoted for $c_D(NatH2)$ is from Saurer's April 4, 2006 measurement (what about the earlier measurement of 117.6 ppm?). The CalibD2 target was prepared by mixing in some of the NatH2 gas into the Prod gas; the value quoted for $c_D(CalibD2)$ is from Claude and Malte, based on $c_D(NatH2)$ and volumetric considerations (we should check that 17 ppm results from the most recent c_D measurements).

²MuCap Note #40: "µp Diffusion and Impact Parameter Cuts in MuCap," available at http://ten.npl.uiuc.edu:8085/MuCap+Notes/40 and also in the source tree of this report, Doc/mup_bcut_calcs.pdf

The correction to the rate is

$$\delta\lambda = \frac{-\tilde{c}^{-1}}{1 - \tilde{c}^{-1}} (\lambda_{calib} - \lambda_{Prod}), \tag{12.1}$$

where the λ have first been corrected for Z > 1 impurities. The correlation between the error on \tilde{c}^{-1} , from the data-analytic technique, and the error on the λ may require more thought. It could be that since the \tilde{c}^{-1} quoted in the table are based on relatively small subsets of the statistics (impact parameter annulus cuts), the error correlations are small. Alternatively, the external measurements can be used with their completely independent errors, calculating \tilde{c}^{-1} and applying equation 12.1.

In addition the μ d correction of equation 12.1, we should also consider correcting for μ p diffusion, depending on which impact parameter cut is used for the final result. The expected rate shift from μ p diffusion is shown in table 12.2 along with the shift attributed to μ d diffusion. For an impact parameter cut of 120 mm, the μ p diffusion correction is $\approx 3 \text{ s}^{-1}$.

Data Sets	Fitted \tilde{c}^{-1}	χ^2/NDF	c_{calib} (Meas.)	$c_{prod} = \tilde{c}^{-1} c_{calib}$
Prod50/NatH2	0.0122 ± 0.0010	8.0/9	126.7 ppm	$1.545 \pm 0.129 \text{ ppm}$
Prod50/CalibD2	0.0890 ± 0.0077	7.3/9	17.8 ppm	$1.581 \pm 0.136 \text{ ppm}$
CalibD2/NatH2	0.1360 ± 0.0028	7.5/9	126.7 ppm	$17.235 \pm 0.357 \text{ ppm}$

 $\mu p \ Diffusion \ Parameter \ k = 0.4911 \pm 0.0070 \ mm/\sqrt{\mu s}$

Table 12.1: Results of constant fits as in fig. 12.3(middle) are shown in columns 2 and 3. Column 4, c_{calib} , is from an external measurement of the calibration gas, Saurers April 4, 2006, measurement of the 2004 natural hydrogen bottle (there was an earlier measurement of 117.6 ppm D — which should we use?). Column 5 is the deuterium concentration of the production gas (or CalibD2 gas, in the last row) derived from the columns 2 and 4 by the formula indicated in the column label. These c_{prod} thus derived agree, at the 1σ level, with external ETH tandem accelerator measurements of $c_D(prod2004) = 1.44 \pm 0.13$ ppm D (measured May 18, 2006) and $c_D(prod2005) = 1.45 \pm 0.14$ ppm D (measured April 25, 2006); the same production gas as in 2004 was used in 2005.

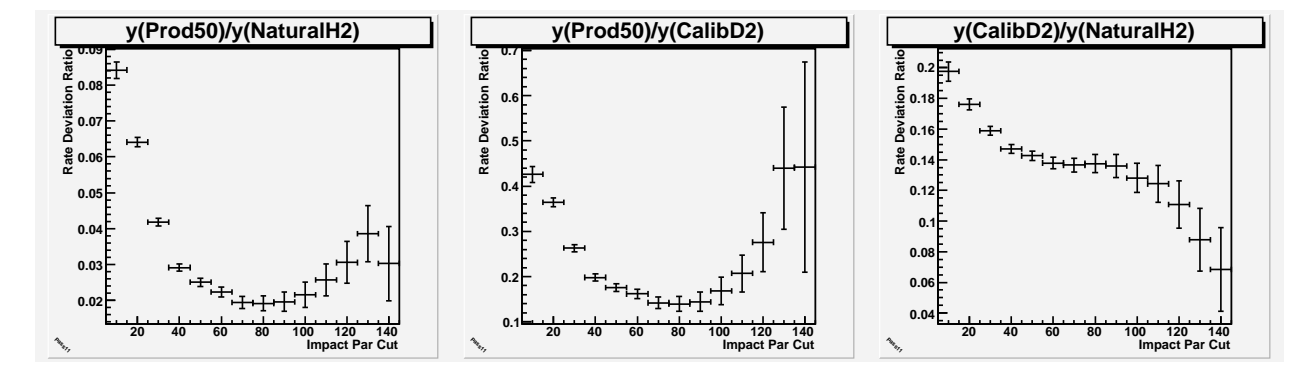


Figure 12.1: Ratio between different data sets of the change in fitted rate due to the impact parameter disc cut indicated on the x-axis. $y = \lambda_{fit}(b_{cut}) - \lambda_{fit}(150)$; that is, y is the difference in fitted rate from making a tighter impact parameter cut compared to the 150 mm cut.

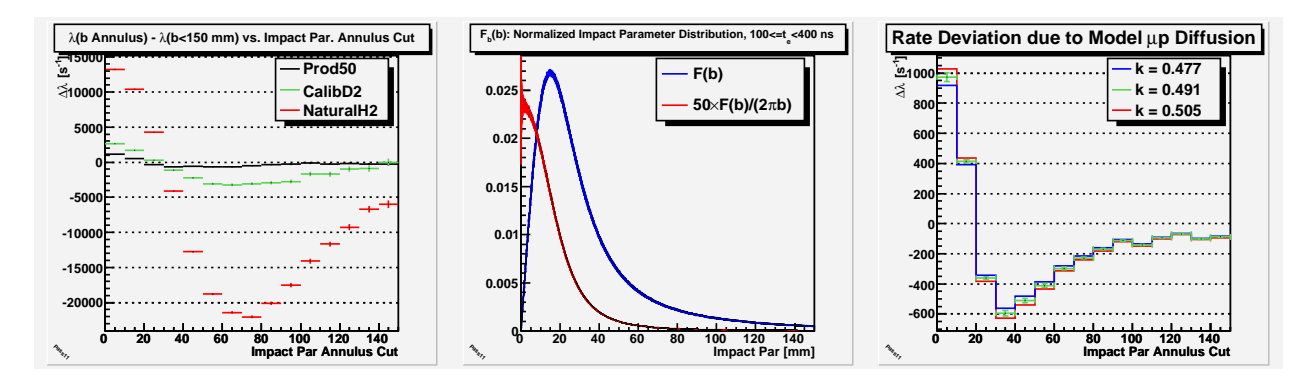


Figure 12.2: Left: rate deviations of impact parameter annulus cuts compared to the 150 mm disc cut. The impact parameter annulus cuts are indicated on the x-axis: the low edge of a bin indicates b_{cut1} of the cut, the up edge b_{cut2} . Middle: impact parameter distribution. Right: calculated rate deviations of impact parameter annulus cuts due to μ p diffusion, assuming thermal diffusion. The μ p are assumed to move from the stop position according to a 3D gaussian distribution with $\sigma = k\sqrt{t}$, where t is the time after the muon stop. Three different values of k are shown, with the green points corresponding to the optimal value (see right panel in fig. 12.3).

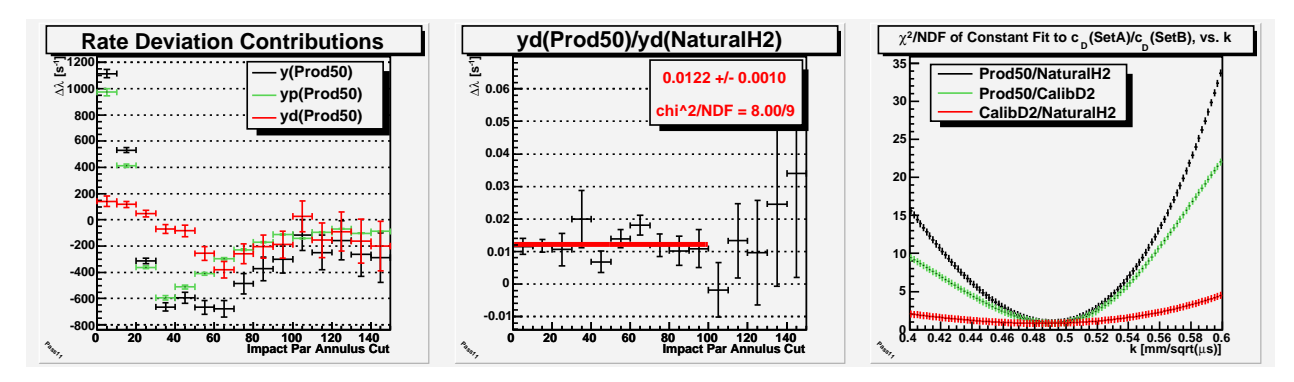


Figure 12.3: Left: rate deviations of impact parameter annulus cuts are shown by the black points (actual Prod50 data, same as the black points in fig. 12.2:left); calculated rate deviation due to μp diffusion (same as the green points in fig. 12.2:right); and the differences between the black and green points, shown in red, are attributed to μd diffusion. Middle: ratio of rate deviations attributed to μd diffusion for different data sets, in this case Prod50 and NatH2; that is, $y_d(Prod50)/y_d(NatH2)$ is shown. A constant fit to the ratios from the first 10 annulus cuts is shown in red. Right: χ^2/NDF of constant fits to the y_d ratios, as in the middle panel, for different values of the diffusion parameter k. All pairs of data sets are consistent with the same optimal value of k.

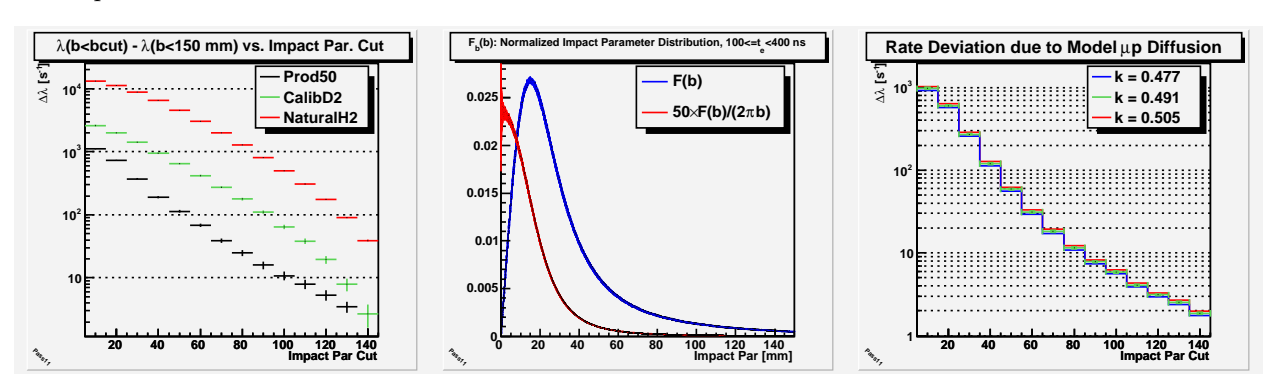


Figure 12.4: The same plots as in fig. 12.2, but with impact parameter disc cuts.

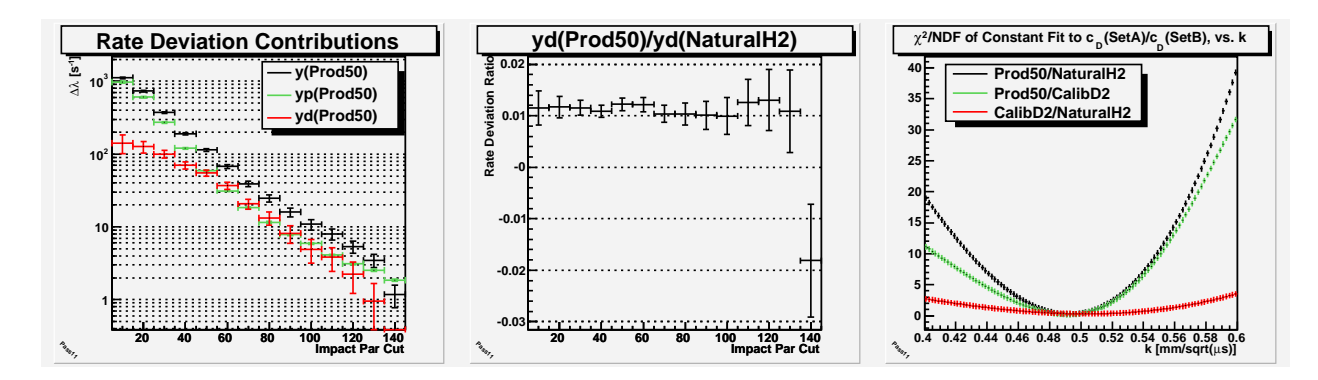


Figure 12.5: The same plots as in fig. 12.3, but with impact parameter disc cuts. The leftmost plot here is useful to read off the systematic effect due to μp diffusion of taking an impact parameter cut. For example, we see that the a cut of 120 mm leads to a rate deviation of $\approx 3 \text{ s}^{-1}$, not corrected by the deuterium extrapolation procedure because it is common to all data sets.

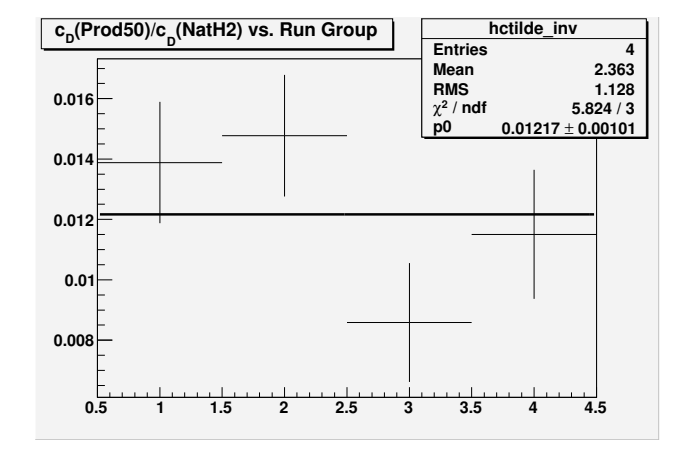


Figure 12.6: Prod50/NatH2 Diffusion concentration ratio \tilde{c}^{-1} vs. Prod50 run group. The runs groups are in chronological order, formed arbitrarily by dividing the data file list evenly (by number of files) into four groups. The diffusion parameter k is set to the value found from optimization over all Prod50 data. There was some concern that the c_D concentration in the production gas may have increased in the course of the run when more gas was produced from the same light water, but no evidence of an increase is observed in this study.

b_{cut} [mm]	$y(b_{cut})$ [s ⁻¹]	$y_p(b_{cut}) [s^{-1}]$	$y_d(b_{cut}) [s^{-1}]$
10	1115.0 ± 29.8	973.9 ± 27.7	141.2 ± 40.7
20	729.3 ± 14.3	603.4 ± 17.2	125.9 ± 22.3
30	371.6 ± 9.2	272.1 ± 7.8	99.6 ± 12.0
40	190.0 ± 6.7	120.2 ± 3.4	69.8 ± 7.5
50	113.5 ± 5.1	58.9 ± 1.7	54.6 ± 5.4
60	67.9 ± 4.1	31.2 ± 0.9	36.7 ± 4.2
70	39.0 ± 3.3	18.3 ± 0.5	20.7 ± 3.4
80	24.7 ± 2.7	11.5 ± 0.3	13.2 ± 2.7
90	16.0 ± 2.2	7.8 ± 0.2	8.2 ± 2.2
100	10.8 ± 1.7	5.9 ± 0.2	4.9 ± 1.8
110	7.9 ± 1.4	4.1 ± 0.1	3.8 ± 1.4
120	5.4 ± 1.0	3.1 ± 0.1	2.2 ± 1.0
130	3.5 ± 0.7	2.5 ± 0.1	1.0 ± 0.7
140	1.2 ± 0.4	1.9 ± 0.1	-0.7 ± 0.4

 $\mu p \ Diffusion \ Parameter \ k = 0.4911 \pm 0.0070 \ mm/\sqrt{\mu s}$

Table 12.2: Contribution to the rate deviation due to an impact parameter disc cut. The y-column is from Prod50 data, $y(b_{cut}) = \lambda(b_{cut}) - \lambda(150mm)$. $y_p(b_{cut})$ is the expected rate shift due to μ p diffusion, where the uncertainty in the values are from the error in the diffusion parameter k. $y_d(b_{cut}) = y(b_{cut}) - y_p(b_{cut})$ is attributed to μ d diffusion and should not be taken to be the total rate shift, due to deuterium, of a lifetime spectrum subject to a given impact parameter cut: y_d is the rate deviation with respect to the 150 mm cut, which may itself be shifted from the "true" lifetime. These values in this table are plotted in the left panel of figure 12.5.

12.1 Sensitivity of \tilde{c}^{-1} to Impact Parameter Distribution

The impact parameter distribution function, $F_b(b)$ (shown in the middle panel of figure 12.4), is of critical importance in the calculation of $y_p(b)$. For a given impact parameter cut b_{cut} , the approximate region $b_{cut} - \delta b < b < b_{cut} + \delta b$ of $F_b(b)$ is relavent, where $\delta b \sim k/\lambda \approx 1$ mm. An undiffused $F_b(b)$ is required.

The results shown in this chapter approximate $F_b(b)$ with a histogram of impact parameters for electrons within 100 ns to 400 ns of good muon stops. In the original MuCap Note #40, electrons within 0 ns to 100 ns are used. Other acceptance time intervals were tried, but the first 100 ns gave best results based on χ^2 of the constant fit to \tilde{c}^{-1} . In the updates of this chapter, though, excellent χ^2 is achieved with the slightly later time interval, and the results are consistent with those using other intervals, including 0 ns to 100 ns. There is some theoretical preference to using decays starting at the lifetime fit start time ($\approx 100 \text{ ns}$) to construct $F_b(b)$: by this time many of the epithermal μ p have thermalized, and the spreading of μ p stop position is folded into $F_b(b)$ and automatically accounted for in the y_p calculation. The time acceptance interval should not extend too late, however, because then F_b would already be somewhat spread by thermal diffusion and possibly μ d diffusion.

The change of the impact parameter distribution for later decay times can be seen almost directly. Figure 12.7 shows $F_b(b)$ based on different electron appearance times (left panel) and rebinned to have 1 mm bin widths. Dividing the later-decay-time $F_b(b)$ by the earliest highlights the depopulation of low impact parameter bins in favor of larger impact parameters.

To see how different choices of decay time intervals affects the result \tilde{c}^{-1} , the entire

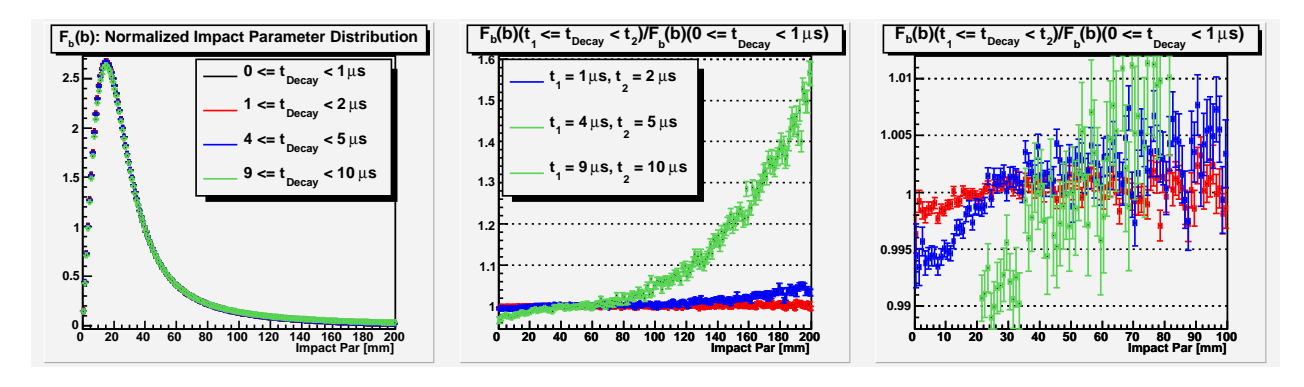


Figure 12.7: Left: Impact parameter distribution functions $F_b(b)$ based on different electron appearance time intervals. Middle: Division of the histograms of the left panel by the $F_b(b)$ based on the earliest decays. Right: zoomed view of the middle panel.

procedure was repeated for $F_b(b)$ based on successively later electron appearance times. Figure 12.8 shows the optimal value of k, χ^2 of the constant fit across impact parameter annuli, and the resultant \tilde{c}^{-1} for F_b from 1 μ s decay time intervals; Figure 12.9 is the same but with the F_b based on narrower time intervals of 100 ns.

In figure 12.10, the impact parameter distribution and lifetime spectra are drawn from different data sets: Prod50, subgroups of Prod50, and Prod50 μ^+ (the last uses Prod50 μ^- for lifetimes). The electron appearance time used for F_b is 0 to 1 μ s for each data set.

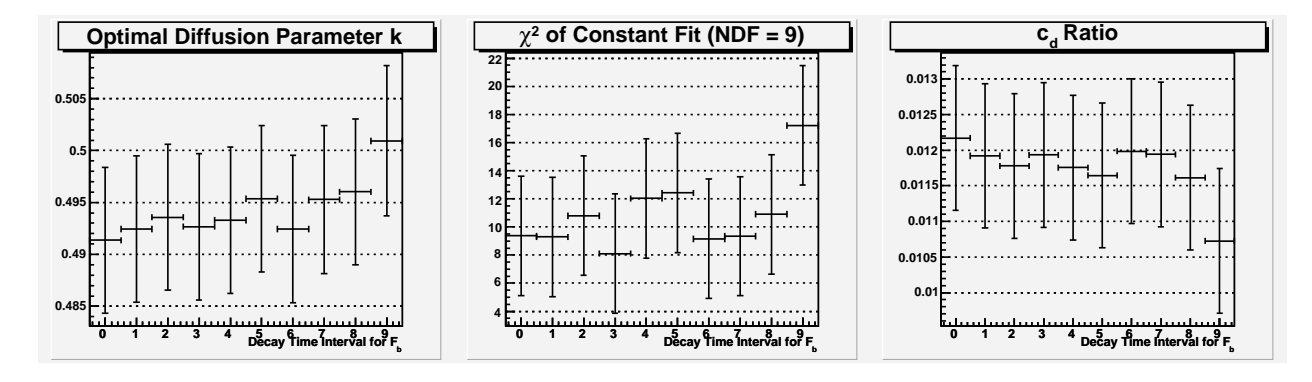


Figure 12.8: Left: Optimal diffusion parameter k resulting from impact parameter distribution functions $F_b(b)$ based on successive 1 μ s electron appearance time intervals. The intervals are the indicated by the x-axis of the plots: $x \leq t_{Decay} < x + 1$, in units of μ s. Middle: χ^2 of the constant fit to \tilde{c}^{-1} vs. impact parameter annulus, starting with the $F_b(b)$, k of the left panel. Right: \tilde{c}^{-1} from the constant fits of the middle panel. The results are consistent within the error bars except for the rightmost point, which corresponds to rather late decays from 9 μ s to 10 μ s.

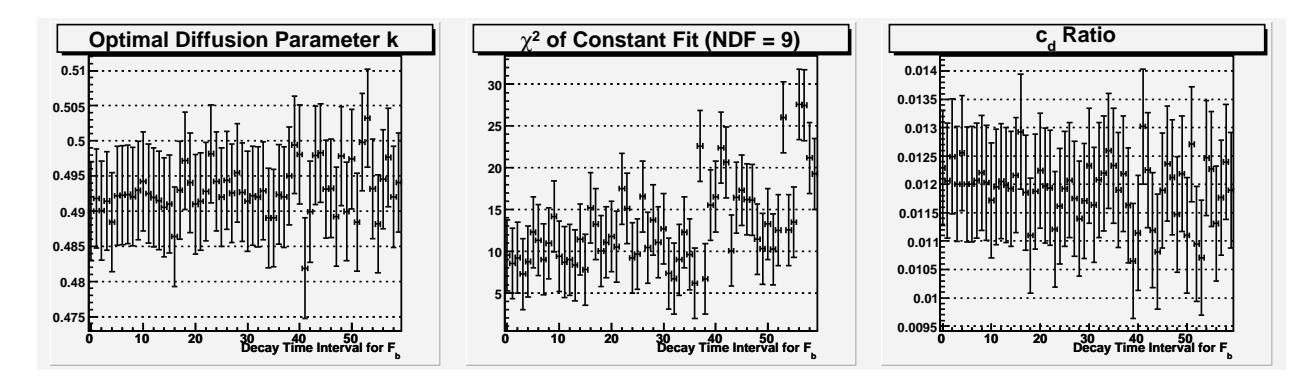


Figure 12.9: Left: Optimal diffusion parameter k resulting from impact parameter distribution functions $F_b(b)$ based on successive 100 ns electron appearance time intervals. The intervals are the indicated by the x-axis of the plots: $100x \le t_{Decay} < 100(x+1)$, in units of ns. Middle: χ^2 of the constant fit to \tilde{c}^{-1} vs. impact parameter annulus, starting with the $F_b(b)$, k of the left panel. Right: \tilde{c}^{-1} from the constant fits of the middle panel. The results are consistent within the error bars.

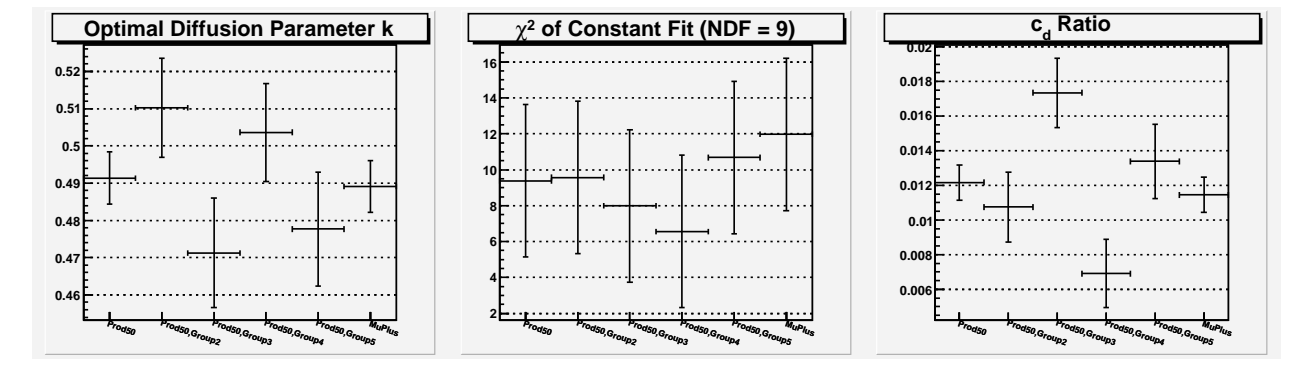


Figure 12.10: Left: Optimal diffusion parameter k resulting from impact parameter distribution functions $F_b(b)$ drawn from different data sets, electron appearance time interval $0 \le 1 \mu s$. The data set is used for the impact parameter distribution is labeled on the x-axis. Lifetime fits are taken from NatH2 and the data set indicated, except for the MuPlus bin which uses NatH2 and Prod50. Middle: χ^2 of the constant fit to \tilde{c}^{-1} vs. impact parameter annulus, starting with the lifetimes, $F_b(b)$, k of the left panel. Right: \tilde{c}^{-1} from the constant fits of the middle panel.

Part III Simulations

Numerical Studies

show some of the quick ROOT macro studies regarding statistical consistency of lifetimes, vs. rebinning. Kinetics.

13.1 χ^2 vs. Lifetime Histogram Binning Phase

I presented this in the May 9, 2006 teleconference: http://www.npl.uiuc.edu/exp/mucapture/coll/mucap/smclayto/TeleConf09May2006/teleconf.html. The simulation results are at http://www.npl.uiuc.edu/exp/mucapture/coll/mucap/smclayto/TeleConf09May2006/simfit_rebins.html. Conclusion: the observed variation in χ^2 of fits to the real data vs. rebinning phase is consistent with expectations.

13.2 χ^2 vs. Impurity Concentration

http://www.npl.uiuc.edu/exp/mucapture/coll/mucap/smclayto/TeleConf02May2006/teleconf.html.

Conclusion: the distortion of the lifetime spectrum due to impurities is not reflected in the χ^2 of the lifetime fit for reasonable c_Z (or capture yield Y_Z less than several hundred ppm).

13.3 Allowed Rate Deviation of Fit to Subset with Different Background Level

http://www.npl.uiuc.edu/exp/mucapture/coll/mucap/smclayto/TeleConf16May2006/teleconf.html.

Part IV Conclusions

Results

The results of lifetime fits, corrected for impurities, extrapolated to zero deuterium concentration, and then with the μ p diffusion effect correction subtracted off, are shown in table 14.3, for the D extrapolation using the natural hydrogen data, and table 14.4, for the D extrapolation using CalibD2 data. Tables 14.1 and 14.2 summarize fit results and corrections.

	Prod50		NatH2	
	Value $[s^{-1}]$	Error $[s^{-1}]$	Value $[s^{-1}]$	Error $[s^{-1}]$
λ_{fit} from Lifetime Spectrum ^a	455433.98	± 12.11	456471.71	± 35.51
Z > 1 Impurities	-13.90	± 5.00	0.00	± 5.00
$\delta\lambda$ from D-Extrapolation ^b	-11.90	± 1.08		
μ p Diffusion ^c	-3.11	± 0.09		
Seen $\mu + p$ Scatters	-1.10			
Unseen $\mu + p$ Scatters	-2.00?			
10 ns MuSC Deadtime	-0.06			
MuPCXorY Inefficiency	1.10?			
Corrected λ	455403.91	± 13.14		

 $[^]a\mathrm{CathodeOR},\,120~\mathrm{mm}$ Impact Parameter Cut

Table 14.1: Analysis Results and Corrections with Deuterium Extrapolation Based on CalibNat Data Set. Entries tagged with question marks are not included in the net result shown in the last row.

Other corrections, such as due to molecular formation and transitions, time dialation (factor of $0.5\alpha^2$), and possible radiative corrections should also be applied.

^bUsing $\tilde{c}^{-1} = 0.0122 \pm 0.0010$

^cUsing Model Diffusion Parameter $k = 0.4911 \pm 0.0070 \text{ mm}/\sqrt{\mu s}$

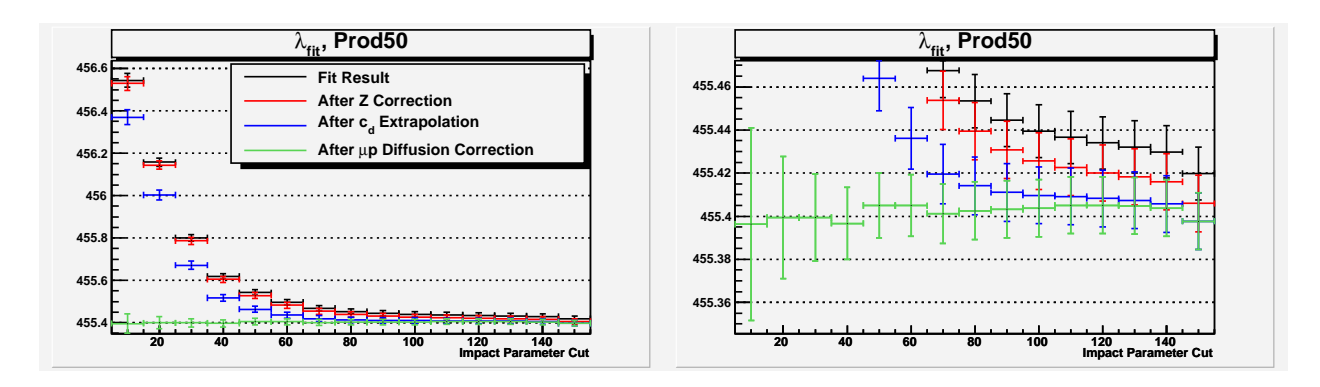


Figure 14.1: Prod50 Rates Corrected for Impurities, μ d Diffusion (using NatH2) and μ p Diffusion (using calculation based on a thermal diffusion model and the observed impact parameter distribution). These are also listed in table 14.3. The rightmost bin is for no impact parameter cut, not 150 mm as labeled.

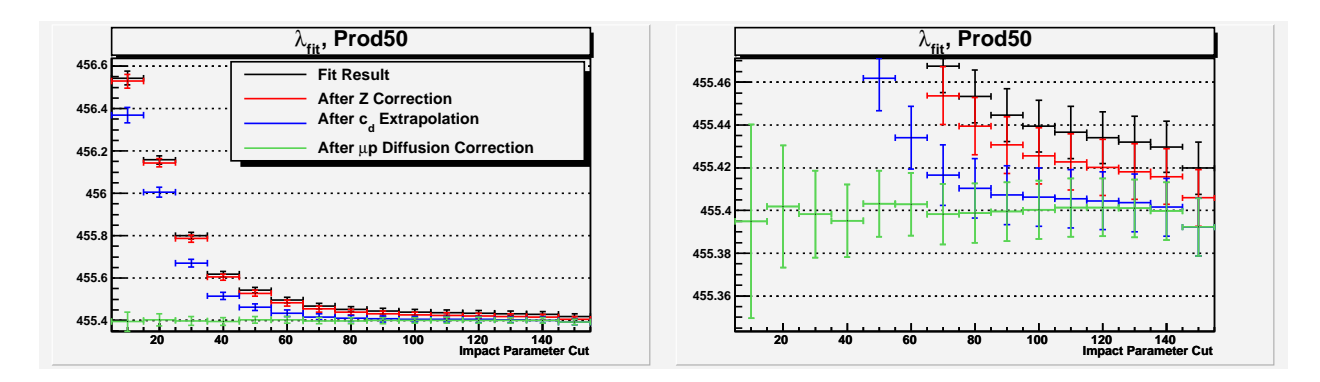


Figure 14.2: Prod50 Rates Corrected for Impurities, μ d Diffusion (using CalibD2) and μ p Diffusion (using calculation based on a thermal diffusion model and the observed impact parameter distribution). These are also listed in table 14.4. The rightmost bin is for no impact parameter cut, not 150 mm as labeled.

Impact Parameter Cut	N	$\lambda [\mathrm{s}^{-1}]$	В	B/N	χ^2/DOF
10	2.962×10^{7}	458314.2 ± 88.6	0.8 ± 0.4	2.664×10^{-8}	1.06 ± 0.06
20	8.736×10^{7}	457701.1 ± 51.6	7.1 ± 0.8	8.115×10^{-8}	0.99 ± 0.06
30	1.329×10^{8}	457110.0 ± 41.8	17.7 ± 1.0	1.331×10^{-7}	1.07 ± 0.06
40	1.612×10^{8}	456656.5 ± 38.0	31.8 ± 1.2	1.974×10^{-7}	1.07 ± 0.06
50	1.785×10^{8}	456343.2 ± 36.1	51.0 ± 1.3	2.859×10^{-7}	1.09 ± 0.06
60	1.898×10^{8}	456116.8 ± 35.1	74.1 ± 1.4	3.906×10^{-7}	1.05 ± 0.06
70	1.975×10^{8}	455971.9 ± 34.5	102.6 ± 1.6	5.193×10^{-7}	1.03 ± 0.06
80	2.032×10^{8}	455875.0 ± 34.1	135.7 ± 1.7	6.678×10^{-7}	1.05 ± 0.06
90	2.074×10^{8}	455808.3 ± 33.8	172.7 ± 1.8	8.325×10^{-7}	1.04 ± 0.06
100	2.107×10^{8}	455761.9 ± 33.6	213.7 ± 1.9	1.014×10^{-6}	1.04 ± 0.06
110	2.133×10^{8}	455735.8 ± 33.4	259.0 ± 2.0	1.214×10^{-6}	1.03 ± 0.06
120	2.155×10^{8}	455717.0 ± 33.4	309.2 ± 2.1	1.435×10^{-6}	1.03 ± 0.06
130	2.172×10^{8}	455705.5 ± 33.3	362.2 ± 2.2	1.667×10^{-6}	1.05 ± 0.06
140	2.186×10^{8}	455700.3 ± 33.3	419.4 ± 2.3	1.918×10^{-6}	1.05 ± 0.06
150	2.257×10^{8}	455683.7 ± 33.6	1425.8 ± 3.6	6.317×10^{-6}	1.08 ± 0.06

Pass11

Figure 14.3: Fit Results to CalibD2 Data. The bin errors of lifetime histograms have been corrected for double counting with a factor m = 0.5 (see chapter 9). The last row is for no impact parameter cut, not 150 mm as labeled.

	Prod50		Cali	bD2
	Value $[s^{-1}]$	Error $[s^{-1}]$	Value $[s^{-1}]$	Error $[s^{-1}]$
λ_{fit} from Lifetime Spectrum ^a	455433.98	± 12.11	455716.99	± 33.36
Z > 1 Impurities	-13.90	± 5.00	0.00	± 5.00
$\delta\lambda$ from D-Extrapolation ^b	-15.54	± 3.45		
μ p Diffusion ^c	-3.11	± 0.09		
Seen $\mu + p$ Scatters	-1.10			
Unseen $\mu + p$ Scatters	-2.00?			
10 ns MuSC Deadtime	-0.06			
MuPCXorY Inefficiency	1.10?			
Corrected λ	455400.27	± 13.55		

 $[^]a$ CathodeOR, 120 mm Impact Parameter Cut

Table 14.2: Analysis Results and Corrections with Deuterium Extrapolation Based on CalibD2 Data Set. Entries tagged with question marks are not included in the net result shown in the last row.

b_{cut}	y_p	Prod50 λ_{fit} [s ⁻¹]	NatH2 λ_{fit} [s ⁻¹]	Prod50 λ_{fit} [s ⁻¹]	Prod50 λ_{fit} [s ⁻¹]
mm	$[s^{-1}]$	Z Corrected ^{a}	Z Corrected ^{b}	D Corrected c	y_p Subtracted ^d
10	973.9	456529.8 ± 32.5	469453.3 ± 97.5	456370.2 ± 35.1	455396.3 ± 44.7
20	603.4	456144.1 ± 19.4	467584.5 ± 56.6	456002.8 ± 22.6	455399.4 ± 28.4
30	272.1	455786.3 ± 16.0	465092.9 ± 45.6	455671.4 ± 18.6	455399.4 ± 20.1
40	120.2	455604.7 ± 14.7	462726.5 ± 41.3	455516.8 ± 16.4	455396.6 ± 16.7
50	58.9	455528.2 ± 14.0	460735.7 ± 39.1	455463.9 ± 15.0	455405.0 ± 15.1
60	31.2	455482.6 ± 13.7	459249.8 ± 37.9	455436.1 ± 14.2	455404.9 ± 14.2
70	18.3	455453.7 ± 13.5	458218.1 ± 37.1	455419.6 ± 13.8	455401.3 ± 13.8
80	11.5	455439.5 ± 13.3	457498.7 ± 36.6	455414.0 ± 13.5	455402.5 ± 13.5
90	7.8	455430.7 ± 13.2	457023.2 ± 36.3	455411.0 ± 13.3	455403.2 ± 13.4
100	5.9	455425.6 ± 13.2	456710.8 ± 36.1	455409.7 ± 13.2	455403.8 ± 13.3
110	4.1	455422.6 ± 13.1	456516.1 ± 36.0	455409.1 ± 13.2	455405.1 ± 13.2
120	3.1	455420.1 ± 13.1	456383.7 ± 35.9	455408.2 ± 13.1	455405.1 ± 13.1
130	2.5	455418.2 ± 13.1	456298.7 ± 35.8	455407.3 ± 13.1	455404.8 ± 13.1
140	1.9	455415.9 ± 13.1	456247.5 ± 35.8	455405.6 ± 13.1	455403.8 ± 13.1
∞	1.4	455405.9 ± 13.2	456071.0 ± 36.1	455397.7 ± 13.2	455397.7 ± 13.2

Table 14.3: Prod50 Rates Corrected for Impurities, μd Diffusion (using NatH2) and μp Diffusion (using calculation based on a thermal diffusion model and the observed impact parameter distribution). The corrected rates are also plotted in figure 14.1.

 $^{^{}b}$ Using $\tilde{c}^{-1} = 0.0890 \pm 0.0077$

 $[^]c \text{Using Model Diffusion Parameter} \; k = 0.4911 \pm 0.0070 \; \text{mm} / \sqrt{\mu s}$

^aUsing impurity correction of $\delta\lambda=13.9~[{\rm s}^{-1}]$ subtracted for each b_{cut} ^bUsing impurity correction of $\delta\lambda=-0.0~[{\rm s}^{-1}]$ subtracted for each b_{cut}

^cStarting with the Z-corrected rates, then using $\tilde{c}^{-1} = 0.0122 \pm 0.0010$

 $[^]d$ Starting with the Z- and D-corrected rates, then subtracting the y_p value in the second column

b_{cut}	y_p	Prod50 λ_{fit} [s ⁻¹]	CalibD2 λ_{fit} [s ⁻¹]	Prod50 λ_{fit} [s ⁻¹]	Prod50 λ_{fit} [s ⁻¹]
mm	$[s^{-1}]$	Z Corrected a	Z Corrected ^{b}	D Corrected c	y_p Subtracted ^d
10	973.9	456529.8 ± 32.5	458176.3 ± 88.8	456368.8 ± 35.9	455394.9 ± 45.4
20	603.4	456144.1 ± 19.4	457563.2 ± 51.8	456005.3 ± 22.7	455401.9 ± 28.5
30	272.1	455786.3 ± 16.0	456972.1 ± 42.1	455670.4 ± 18.8	455398.4 ± 20.4
40	120.2	455604.7 ± 14.7	456518.6 ± 38.3	455515.4 ± 16.7	455395.2 ± 17.0
50	58.9	455528.2 ± 14.0	456205.3 ± 36.5	455462.0 ± 15.4	455403.1 ± 15.5
60	31.2	455482.6 ± 13.7	455978.9 ± 35.5	455434.1 ± 14.6	455402.9 ± 14.6
70	18.3	455453.7 ± 13.5	455834.0 ± 34.8	455416.5 ± 14.2	455398.2 ± 14.2
80	11.5	455439.5 ± 13.3	455737.1 ± 34.4	455410.4 ± 13.9	455398.9 ± 13.9
90	7.8	455430.7 ± 13.2	455670.4 ± 34.1	455407.3 ± 13.8	455399.5 ± 13.8
100	5.9	455425.6 ± 13.2	455624.0 ± 34.0	455406.2 ± 13.7	455400.3 ± 13.7
110	4.1	455422.6 ± 13.1	455597.9 ± 33.8	455405.5 ± 13.6	455401.4 ± 13.6
120	3.1	455420.1 ± 13.1	455579.1 ± 33.7	455404.5 ± 13.5	455401.4 ± 13.5
130	2.5	455418.2 ± 13.1	455567.6 ± 33.7	455403.6 ± 13.5	455401.1 ± 13.5
140	1.9	455415.9 ± 13.1	455562.4 ± 33.6	455401.6 ± 13.5	455399.7 ± 13.5
∞	1.4	455405.9 ± 13.2	455545.8 ± 34.0	455392.2 ± 13.6	455392.2 ± 13.6

^aUsing impurity correction of $\delta\lambda = 13.9 \text{ [s}^{-1}\text{]}$ subtracted for each b_{cut}

Table 14.4: Prod50 Rates Corrected for Impurities, μd Diffusion (using CalibD2) and μp Diffusion (using calculation based on a thermal diffusion model and the observed impact parameter distribution). The corrected rates are also plotted in figure 14.2.

Impact Parameter Cut	N	$\lambda [\mathrm{s}^{-1}]$	В	B/N	χ^2/DOF
10	2.243×10^{8}	456543.7 ± 32.1	15.5 ± 1.3	6.905×10^{-8}	1.00 ± 0.06
20	6.622×10^{8}	456158.0 ± 18.7	60.9 ± 2.2	9.198×10^{-8}	1.00 ± 0.06
30	1.008×10^9	455800.2 ± 15.2	133.4 ± 2.8	1.324×10^{-7}	0.99 ± 0.06
40	1.222×10^9	455618.6 ± 13.8	241.8 ± 3.3	1.979×10^{-7}	0.99 ± 0.06
50	1.353×10^{9}	455542.1 ± 13.1	382.0 ± 3.6	2.822×10^{-7}	0.99 ± 0.06
60	1.438×10^9	455496.5 ± 12.7	550.3 ± 4.0	3.826×10^{-7}	1.00 ± 0.06
70	1.497×10^9	455467.6 ± 12.5	749.5 ± 4.3	5.007×10^{-7}	1.01 ± 0.06
80	1.539×10^{9}	455453.4 ± 12.4	980.1 ± 4.6	6.367×10^{-7}	1.02 ± 0.06
90	1.571×10^{9}	455444.6 ± 12.3	1240.0 ± 4.9	7.891×10^{-7}	1.02 ± 0.06
100	1.596×10^{9}	455439.5 ± 12.2	1528.4 ± 5.1	9.575×10^{-7}	1.01 ± 0.06
110	1.616×10^{9}	455436.5 ± 12.1	1844.8 ± 5.4	1.141×10^{-6}	0.99 ± 0.06
120	1.632×10^{9}	455434.0 ± 12.1	2191.4 ± 5.7	1.343×10^{-6}	0.97 ± 0.06
130	1.645×10^{9}	455432.1 ± 12.1	2566.7 ± 6.0	1.560×10^{-6}	0.98 ± 0.06
140	1.656×10^{9}	455429.8 ± 12.1	2964.7 ± 6.3	1.790×10^{-6}	0.98 ± 0.06
150	1.710×10^9	455419.8 ± 12.2	10105.3 ± 9.5	5.911×10^{-6}	1.09 ± 0.06

Table 14.5: Fit Results to Prod50 Data. The bin errors of lifetime histograms have been corrected for double counting with a factor m = 0.5 (see chapter 9). The last row is for no impact parameter cut, not 150 mm as labeled.

bUsing impurity correction of $\delta\lambda=10.5$ [s⁻¹] subtracted for each b_{cut} cStarting with the Z-corrected rates, then using $\tilde{c}^{-1}=0.0890\pm0.0077$

dStarting with the Z- and D-corrected rates, then subtracting the y_p value in the second column

Impact Parameter Cut	N	$\lambda [\mathrm{s}^{-1}]$	В	B/N	χ^2/DOF
10	2.561×10^{7}	469541.3 ± 97.4	2.0 ± 0.4	7.923×10^{-8}	1.26 ± 0.06
20	7.597×10^{7}	467672.5 ± 56.4	9.0 ± 0.7	1.187×10^{-7}	1.75 ± 0.06
30	1.162×10^{8}	465180.9 ± 45.4	18.2 ± 0.9	1.569×10^{-7}	2.44 ± 0.06
40	1.414×10^{8}	462814.5 ± 40.9	30.0 ± 1.1	2.118×10^{-7}	2.98 ± 0.06
50	1.571×10^{8}	460823.7 ± 38.8	45.4 ± 1.2	2.889×10^{-7}	2.95 ± 0.06
60	1.673×10^{8}	459337.8 ± 37.5	65.5 ± 1.3	3.914×10^{-7}	2.64 ± 0.06
70	1.744×10^{8}	458306.1 ± 36.8	91.5 ± 1.5	5.246×10^{-7}	2.29 ± 0.06
80	1.795×10^{8}	457586.7 ± 36.3	120.9 ± 1.6	6.736×10^{-7}	1.97 ± 0.06
90	1.833×10^{8}	457111.2 ± 36.0	154.0 ± 1.7	8.402×10^{-7}	1.73 ± 0.06
100	1.863×10^{8}	456798.8 ± 35.8	192.1 ± 1.8	1.031×10^{-6}	1.56 ± 0.06
110	1.886×10^{8}	456604.1 ± 35.6	234.0 ± 1.9	1.241×10^{-6}	1.47 ± 0.06
120	1.905×10^{8}	456471.7 ± 35.5	279.7 ± 2.0	1.468×10^{-6}	1.41 ± 0.06
130	1.921×10^{8}	456386.7 ± 35.4	328.3 ± 2.1	1.709×10^{-6}	1.35 ± 0.06
140	1.933×10^{8}	456335.5 ± 35.4	380.7 ± 2.2	1.969×10^{-6}	1.31 ± 0.06
150	1.996×10^{8}	456159.0 ± 35.8	1296.0 ± 3.4	6.491×10^{-6}	1.21 ± 0.06
90 100 110 120 130 140	$\begin{array}{c} 1.833 \times 10^{8} \\ 1.863 \times 10^{8} \\ 1.886 \times 10^{8} \\ 1.905 \times 10^{8} \\ 1.921 \times 10^{8} \\ 1.933 \times 10^{8} \end{array}$	457111.2 ± 36.0 456798.8 ± 35.8 456604.1 ± 35.6 456471.7 ± 35.5 456386.7 ± 35.4 456335.5 ± 35.4	154.0 ± 1.7 192.1 ± 1.8 234.0 ± 1.9 279.7 ± 2.0 328.3 ± 2.1 380.7 ± 2.2	8.402×10^{-7} 1.031×10^{-6} 1.241×10^{-6} 1.468×10^{-6} 1.709×10^{-6} 1.969×10^{-6}	1.73 ± 0.06 1.56 ± 0.06 1.47 ± 0.06 1.41 ± 0.06 1.35 ± 0.06 1.31 ± 0.06

Table 14.6: Fit Results to NatH2 Data. The bin errors of lifetime histograms have been corrected for double counting with a factor m=0.5 (see chapter 9). The last row is for no impact parameter cut, not 150 mm as labeled.

Further Work

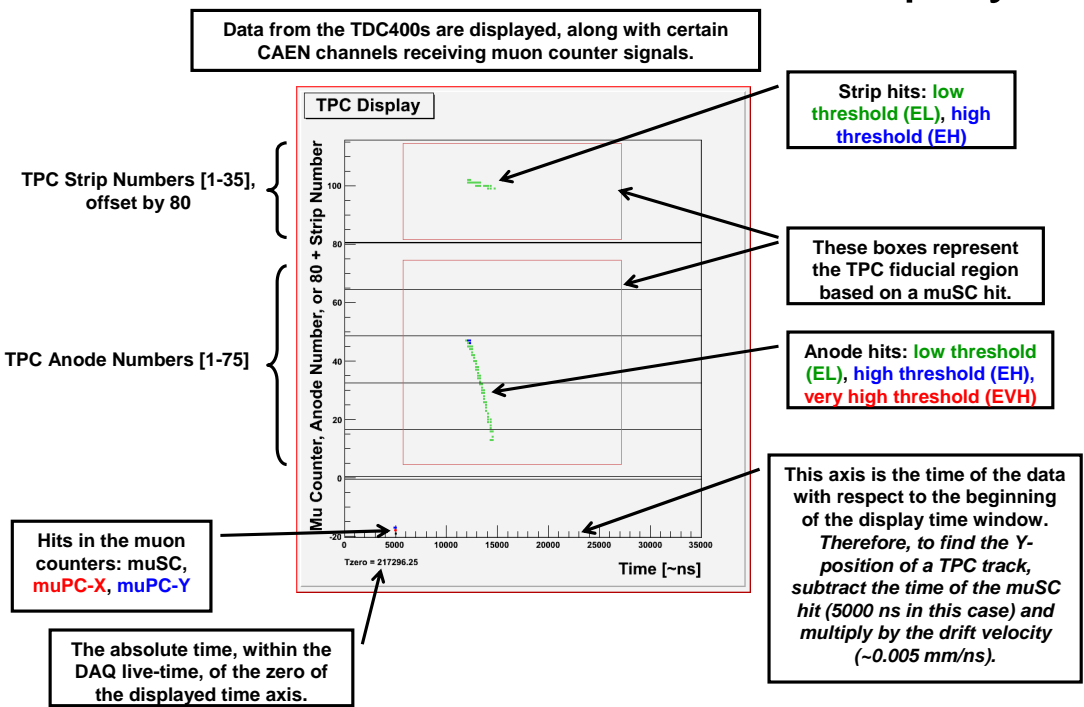
- Improve $\mu + p$ scatter finding in the UIUC analysis.
- Do another pass over the raw data (skimmed okay) to fill lifetime histograms of individual electron detector elements and simpler combinations than EpcTracks. These are in previous passes, but I hadn't specified muon->IsTrack(), so TPC background events are included, making detailed comparison with the usual lifetime histograms difficult.
- Impurities: check if the EVH capture yield changes in the Prod-48 data compared to the Prod-50. CalibN2 data were taken with the TPC at 4.8 kV, so we should make sure the impurity finder efficiency estimate is reasonable. Calculate the lifetime correction assuming different impurity species and combinations.
- Lifetime vs. slow control parameters?

$\begin{array}{c} {\rm Part~V} \\ {\bf Appendix} \end{array}$

Appendix A

UIUC Event Display

How to read the Mu Event Display



Appendix B

Description of ROOT Macros

Describe the ROOT macros used in the preparation of this document.

Several C++ classes were developed for this report to ease in the creation of the figures and to organize the studies. They are compiled into the shared library report2006.so in the "Macros" directory, and the source files are in "Macros/src." To use the library, cd to the "Macros" directory and run make. If successful, the shared library should be created, and will be available in ROOT CINT. The following ROOT CINT session demonstrates how the report2006 classes can be used, in this case to display some of the ePC1 raw data histograms. Comments are added with "// ..." on some lines and were not actually present in the terminal output.

```
smclayto@mu05:~/mucap/run8/Analysis/Report2006/Macros$ root
```

FreeType Engine v2.1.3 used to render TrueType fonts. Compiled for linuxdeb with thread support.

```
CINT/ROOT C/C++ Interpreter version 5.15.169, Mar 14 2005
Type ? for help. Commands must be C++ statements.
Enclose multiple statements between { }.
root [0] .L report2006.so
root [1] TFile f("/data/25/mucap/smclayto/ncsa/Pass10/pass10muminProd50RawHists.root")
root [2] TEpcHistsDisplay epc1( // pressed tab to see function declaration
TEpcHistsDisplay TEpcHistsDisplay(int id, TFile* fptr = 0, TCanvas* can = 0)
TEpcHistsDisplay TEpcHistsDisplay(const TEpcHistsDisplay&)
```

```
root [2] TEpcHistsDisplay epc1(1, &f)
root [3] epc1.Show // pressed tab to see list of methods beginning with Show
ShowClusteringCuts
ShowAnodeCathodeCuts
ShowHitCluAutocorr
ShowPhiZDist
ShowWireDist
ShowWgapDist
ShowClusterSizeDist
ShowAnodeWireVsCathodeWire
ShowHitCluZdiff
ShowMembers
root [3] epc1.ShowWireDist( // pressed tab
TCanvas* ShowWireDist()
root [3] epc1.ShowAnodeWireVsCathodeWire( // pressed tab
TCanvas* ShowAnodeWireVsCathodeWire()
root [3] epc1.ShowWireDist()
(class TCanvas*)0x8f27d88 // canvas is displayed with the hists
root [4] TCanvas c1 // new canvas pops up
root [5] epc1.draw // pressed tab
drawWgapDist
drawWireDist
drawHitCluAutoTdiff
drawAnodeCathTdiff
drawClusterSizeDist
drawAnodeWireVsCathodeWire
root [5] epc1.drawWgapDist( // pressed tab
TH1* drawWgapDist(TVirtualPad* pad, int epc_plane)
root [5] epc1.drawWgapDist(gPad, TEpcHistsDisplay::kAnodes)
(class TH1*)0x9389450 // histogram displayed in canvas c1
```

Here are the report 2006 macros.

- TBaseHistsDisplay is the histogram display base class, designed for this report, to create a canvas, display histograms in a standard style, and add drawing objects, such as vertical lines to indicate cuts. Many of the derived classes described below provide "Show..." methods, which are used directly to create the figures in this document. Individual panels of many of the figures can be created with the "draw..." methods, which take a TVirtualPad as the first argument and return a pointer to the histogram displayed; in CINT, you can for example create a canvas on the command line, then pass the ROOT global variable gPad to the "draw..." methods.
- TEpcHistsDisplay, which derives from TBaseHistsDisplay, displays many histograms from the raw analysis of ePCn data (n = 1, 2). An instance of this class should be created for each ePC. The figures in section 3.2 were created with the "Show..." methods.
- TGondHistsDisplay, which derives from TBaseHistsDisplay, displays histograms from the raw analysis of eSC data. The figures of section 3.3 were created with the "Show..."

- methods. An argument of the constructor allows one to specify either CAEN data (default) or Compressor data.
- TEpc1Epc2HistsDisplay, which derives from TBaseHistsDisplay, displays the ePC1×ePC2 histograms of section 3.4.
- TEpcTrackHistsDisplay, which derives from TBaseHistsDisplay, displays the ePC1×ePC2×eSC histograms of section 3.5.
- TEpcGondHistsDisplay, which derives from TBaseHistsDisplay, displays ePCn×eSC histograms (n = 1, 2). These histograms are not shown in the document.
- TLifetimeFit, which derives from TObject, handles fitting a lifetime histogram. An instance of this class should be created for each histogram to be fit. Fitting is accomplished by calling the "Set(...)" method, which takes a pointer to the histogram. Before Set(...) is called, the method SetmFactor(double m) can be called to specify the fraction of the flat background due to doubly-counted cosmics; then when Set(...) is called the bin errors are accordingly corrected. By default no bin error correction is performed.
- TLifetimeStudy, a base class for some of the specific studies, organizes the fitting of several histograms. Histograms are specified by calling SetLifetimeHist(...). Fits of all the histograms are done by calling Set(...). Fit results are displayed with Display(...).
- TExtraELStudy, which derives from TBaseHistsDisplay, creates the figures of chapter 7.
- TCosmicsStudy, which derives from TBaseHistsDisplay, creates the figures of chapter 9.
- TLifetimeStudyVsFiducialV derives from TLifetimeStudy. The method dofits(...) sets the histograms and fits them. Use Display(...) to show the fit results.
- TLifetimeStudyVsGond derives from TLifetimeStudy. The method dofits(...) sets the histograms and fits them. Use Display(...) to show the fit results.
- TLifetimeStudyVsMuscDT derives from TLifetimeStudy. Specify either "b120mm" (default) or "nocut" in the constructor, referring to impact parameter cuts. The method dofits(...) sets the histograms and fits them. Use Display(...) to show the fit results.
- TLifetimeStudyVsb (lifetime vs. impact parameter cut) derives from TLifetimeStudy. The method dofits(...) sets the histograms and fits them. Use Display(...) to show the fit results.
- TZCapHists, which derives from TBaseHistsDisplay, has methods to show the impurity capture yield. The methods GetTotalYield(...) return the total capture yield over the fiducial volume.
- TZCapStudy organizes the study of impurity capture yields and lifetimes over different data sets (Prod50, CalibN2, NaturalH2, CalibD2). The method SetFiles(...) or SetFilePtrs(...) should be called before dofits(...).